The Dissertation Committee for Jasmine Mason Certifies that this is the approved version of the following Dissertation:

Sediment transport and the geomorphic evolution of the coastal Trinity River, TX

Committee:

David Mohrig, Supervisor

Joel Johnson

Wonsuck Kim

Gary Parker

Paola Passalacqua

Sediment transport and the geomorphic evolution of the coastal Trinity River, TX

by

Jasmine Mason

Dissertation

Presented to the Faculty of the Graduate School of

The University of Texas at Austin

in Partial Fulfillment

of the Requirements

for the Degree of

Doctor of Philosophy

The University of Texas at Austin

December 2018

Abstract

Sediment transport and the geomorphic evolution of the coastal Trinity River, TX

Jasmine Mason, PhD

The University of Texas at Austin, 2018

Supervisor: David Mohrig

This dissertation uses field observations to understand how changes in sediment transport affect the geomorphic evolution of the coastal Trinity River in Texas. I focus on the main channel of the river along the transition from quasi-uniform flow conditions into gradually varying flow. To begin, I will use elevation data in conjunction with stratigraphic analysis to suggest that scroll bars represent levee deposition along the inner bank of the river channel (Chapter 2). Because their channel-ward edge marks the transition from bed-material transport processes that are associated with the point bar and the proximal overbank deposits of the floodplain, they can be considered the geomorphic edge of the active channel form. Chapters three and four then focus on changes within the active channel through a range of time scales. Separate measurements of inner and outer bank volumetric change and migration show that river banks are capable of migrating independently over short time scales, but migrate compensationally over longer periods. The fifth chapter discusses the observation of a new scale of self-organization in bed topography that occurred along the base of the channel during a historic flood in 2015 (which was captured by the time-lapse lidar used in chapters 3 and 4). Repeat depth surveys show that 12 km long wavelength trains of dunes, spread out over an average of 12 river

bends, advected and deformed downstream throughout the 55 day flood. These bedform groups are interpreted as an expression of prolonged washout that occurred over an initially spatially variable bedform field. Remaining questions and suggestions for future research directions are provided in the final chapter. Altogether, this dissertation represents a body of work that spans multiple temporal and spatial scales, and provides the community with a better understanding of how gradually varied flow affects sediment transport and geomorphology. In addition, it provides a foundation for future research that can illuminate important details about fluvial processes in general.

Table of Contents

List of Figures

Chapter 1: Introduction

As a river nears its outlet into a standing body of water, the flow conditions within the channel begin to vary (Chow 1959). During low discharge conditions on the Trinity River in Texas, the wetted cross sectional area of the channel increases with distance downstream (Smith 2012), leading to a spatial deceleration in flow and an associated decrease in predicted sediment transport conditions. During large enough flooding events, however, the wetted cross sectional area of the channel decreases towards the coastline, leading to flow accelerations and an increase in the predicted rate of sediment transport. The reach of the river that undergoes this spatial and temporal variability in flow conditions is referred to as the backwater zone.

In low-sloped, sand-bedded meandering rivers this hydraulic transition into backwater flow is correlated with a marked shift in the geomorphology of the system (Hudson and Kesel 2000; Smith 2012; Fernandes et al. 2017). On the Trinity River, point bars become smaller, finer grained, and take up a smaller fraction of the total channel width within the backwater zone (Smith 2012). Associated with the reduction in point bar size is a decrease in the amount of lateral migration of the channel. River bends within the backwater zone tend to migrate less laterally compared to their normal flow counterparts. This is true for most other major low sloped river systems as well, including the Mississippi River.

The hydraulics of backwater flow have been well-understood by civil engineers and hydrologists for many decades (Chow 1959). In addition, the correlated changes in the geomorphology of these river systems have been noted on several river systems by a variety of authors (Hudson and Kesel 2000; Smith 2012; Fernandes et al. 2017). However, in order to better understand how the backwater effect causes the geomorphic shifts, we

need to understand the spatial and temporal variability in sediment transport through this dynamic zone. While predictions have been made about the transport conditions based on changes in flow (Nittrouer et al. 2011; Lamb et al. 2012; Nittrouer et al. 2012), we have no direct observations of them occurring in natural systems. One goal of my dissertation was to make field observations of changes in sediment transport within the transition between normal flow and backwater flow in order to connect the changes in the flow conditions with the shift in the geomorphology and kinematics of the river system.

Another important motivation for my research has been the desire to better understand how sediment is moved through the coastal portions of rivers and subsequently into deltaic systems. Deltas are incredibly sensitive to small changes in relative sea level rise (Blum and Roberts 2009; Wassmann et al. 2004). Because they tend to have low surface gradients, any small change in sea level causes a large area to become submerged. Additionally, compaction of the deltaic sediments causes the surface to subside through time. The combination of subsidence and sea level rise (which is predicted to increase in the future due to climate change; Hay et al. 2015) make these areas extremely vulnerable. In order to understand how we can better design infrastructure and possibly engineer a solution to this issue, we need to better understand how and when sediment is delivered into these systems. This means that we first need to have an understanding of the spatiotemporal changes in sediment transport conditions within the portion of the river system that is just upstream of the river mouth. The observations and interpretations provided in this dissertation are a first step towards achieving this goal.

This dissertation will provide you with data and interpretations that span a range of temporal and spatial scales. In order to observe how the channel changes through time, I first need to define the spatial extent of the active channel form. The erosional outer bank of meandering river bends is typically nearly vertical and easy to demarcate. However,

defining the edge of the inner bank is more complex due to the presence of the point bar. In Chapter 2, I will discuss the topographic form and stratigraphic architecture of scroll bars. These features related to the migration of the inner banks of river bends (Nanson and Hickin 1983; Rodnight et al. 2005) are constructed almost entirely out of fine-grained, reworked suspended sediment. Their crestal elevations are similar to the levee crest elevations on the outer bank, across the channel. I conclude that scroll bars are representative of proximal overbank deposition, and are inconsistent with the bed material transport that one would expect to see within the channel itself (e.g., dune-scale cross stratification in coarser sand; Allen 1985). Scroll bars are levees that are deposited along the inner banks of rivers, and thus their channel-ward edge represents the geomorphic edge of the inner bank.

Chapter 3 will then focus on analyzing the changes that occur within the edges of the channel at the scale of a single extreme event. In this chapter, I use time-lapse lidar data to examine volumes of deposited and eroded material from the inner and outer banks of 55 consecutive river bends of the Trinity River. I discuss how volumes of change correlate between the inner and outer bank of individual river bends, as well as examine spatial trends in volumes along the study reach that are due to the backwater effect. Results from this research are important for understanding how river banks migrate as well as for understanding how changes in sediment transport conditions due to the backwater effect alter the larger-scale geomorphology of the system.

In Chapter 4, I discuss time-averaged bank changes spanning multiple events. A second time-lapse lidar data set covering a portion of the channel that is discussed in the previous chapter is used to understand how differential bank migration occurs through time. Observations show that while the inner and outer banks of river bends migrate independently from each other at the event scale, they tend to migrate compensationally

over periods of 2-3 years. In other words, bends that experience narrowing during an initial time interval are more likely to experience widening during the next time period and vice versa. This is likely due to the spatial accelerations and decelerations in flow that are associated with channel narrowing or widening (e.g., a wider channel will cause flow to decelerate, favoring subsequent deposition). Results from this research suggest that while width changes can be significant over the event or annual timescale, compensational adjustments by the river banks can lead to invariant channel widths at the decadal scale.

Chapter 5 will then examine changes in bed material transport within the channel before, throughout, and following the single extreme flooding event captured by the time-lapse lidar data set referenced in Chapters 3 and 4. Repeat depth surveys of the channel provide information on bedform size and coverage. Groups of similarly sized bedforms 12 km in wavelength (spanning an average of 12 river bends) are seen advecting along the length of the 25 km long survey reach throughout the flood. I interpret these groups of bedforms to be a result of preferential wash out of smaller dunes during flood. Spatial trends along the survey reach in the bedform group peak height are related to differences in sediment availability from eroded cut banks, as noted in the third chapter. These groups of bedforms are a novel field observation that illustrate a new scale of self-organizational behavior of the channel bed topography. In addition, results suggest that the practice of using measurements of bedform metrics as a way to interpret flow conditions should be approached with caution.

The final chapter will conclude the dissertation by addressing any lingering questions related to the completed research projects. I will suggest future research directions that would be beneficial undertake in order to better understand the processes and forms I have documented. In this way, the dissertation will begin at the largest spatial scale and gradually zoom in to finer and finer spatial resolution. Results will span time

scales as short as within a single event, but will also have implications for how to interpret deposits that might represent hundreds of thousands of years. In addition, results will be pertinent for validating numerical models and for aiding in the design of future modelling efforts.

REFERENCES

Allen, J. R. L. (1985). Principles of physical sedimentology (272 pp.). London: Allen&Unwin.

Blum, M. D., & Roberts, H. H. (2009). Drowning of the Mississippi Delta due to insufficient sediment supply and global sea-level rise. Nature Geoscience, 2(7), 488.

Te Chow, V. (1959). Open-channel hydraulics (Vol. 1). New York: McGraw-Hill.

Hay, C. C., Morrow, E., Kopp, R. E., & Mitrovica, J. X. (2015). Probabilistic reanalysis of twentieth-century sea-level rise. Nature, 517(7535), 481.

Hudson, P. F., & Kesel, R. H. (2000). Channel migration and meander-bend curvature in the lower Mississippi River prior to major human modification. Geology, 28(6), 531-534.

Fernandes, A. M., Törnqvist, T. E., Straub, K. M., & Mohrig, D. (2016). Connecting the backwater hydraulics of coastal rivers to fluvio-deltaic sedimentology and stratigraphy. Geology, 44(12), 979-982.

Lamb, M. P., Nittrouer, J. A., Mohrig, D., & Shaw, J. (2012). Backwater and river plume controls on scour upstream of river mouths: Implications for fluvio-deltaic morphodynamics. Journal of Geophysical Research: Earth Surface, 117(F1).

Nanson, G. C., & Hickin, E. J. (1983). Channel migration and incision on the Beatton 694 River. Journal of Hydraulic Engineering, 109(3), 327-337.

Nittrouer, J. A., Mohrig, D., & Allison, M. (2011). Punctuated sand transport in the lowermost Mississippi River. Journal of Geophysical Research: Earth Surface, 116(F4).

Nittrouer, J. A., Shaw, J., Lamb, M. P., & Mohrig, D. (2012). Spatial and temporal trends for water-flow velocity and bed-material sediment transport in the lower Mississippi River. Bulletin, 124(3-4), 400-414.

Rodnight, H., Duller, G. A. T., Tooth, S., & Wintle, A. G. (2005). Optical dating of a 710 scroll-bar sequence on the Klip River, South Africa, to derive the lateral migration rate of 711 a meander bend. The Holocene, 15(6), 802-811.

Smith, V. B. (2012). Geomorphology of a coastal sand-bed river: Lower Trinity River, Texas. PhD dissertation.

Wassmann, R., Hien, N. X., Hoanh, C. T., & Tuong, T. P. (2004). Sea level rise affecting the Vietnamese Mekong Delta: water elevation in the flood season and implications for rice production. Climatic Change, 66(1-2), 89-107.

Chapter 2: Scroll bars are inner bank levees along bends in meandering channels[1]

ABSTRACT

Scroll bars across a 65-kilometer stretch of the Trinity River in Texas, USA, were studied using lidar data as well as with a series of 11 trenches spread out across the survey area. We conclude that scroll bars are levees that are deposited along the inner banks of these meandering river bends. Scroll bar crests were found to have similar elevations to those of outer bank levee crests, implying that they are constructional features that create positive topographic relief above the elevation of the floodplain. Trenches reveal that scroll bars are built from reworked suspended sediment, with common ripple-scale cross stratification, planar laminations, and muddy bioturbated layers—characteristics that are often associated with levee sedimentation in other systems. Lidar observation of the erosion of scroll bars by bed material transport during flood implies that scroll bar spacing is an imperfect proxy for estimating overall channel migration rates. In addition, interspersed lenses of coarser sediment with dune-scale cross stratification represent the stratigraphic record of these erosional events and suggest that erosion of the channel-ward edge of the scroll bar is not uncommon. Preservation of scroll bars is unlikely given that they are responsible for an average of only the uppermost 12% of the total inner bank relief. We suggest that misidentification of point bar lateral accretion surfaces as scroll bars is

---

[1] This chapter was submitted for publication to Earth Surface Processes and Landforms by authors Jasmine Mason and David Mohrig on September 8, 2018. As first author, I was responsible for designing the project, collecting the field data, data processing and analysis, and writing and submitting the paper. David Mohrig provided project guidance and edits.

common and can lead to issues with reconstructing channel properties due to systematic differences between point bar and scroll bar planform geometries.

INTRODUCTION AND BACKGROUND

Scroll bars are responsible for some of the most striking patterns on Earth's surface. These arcuate topographic features present on the inner banks of migrating river bends are widely recognized as a distinct component of fluvial systems despite being incompletely understood. Published explanations for scroll bar formation are varied, with even their production by constructional or erosional processes not universally agreed upon. Scroll bars are alternately described as simply the top of a point bar behind which deposition is dampened (Hickin 1974; Nanson 1980; Van de Lageweg 2014), the result of enhanced sedimentation at the leading edge of inner bank vegetation or in the shadow of woody debris (Jackson 1976; Nanson 1981; Zen et al. 2017), topography built from longitudinal bars migrating up and out of the channel during flood (Sundborg 1956; Nilsson and Martval 1972; Jackson 1976; Ielpi and Ghinassi 2014), the result of depositional patterns produced by a bimodal distribution of grain sizes (Nanson 1980), the result of suspended sediment deposition due to flow separation over a point bar (Nanson 1980), or the product of chute channel erosion between the point bar and inner bank (McGowen and Garner 1970; Nanson and Croke 1992). Even with an ambiguous formative process, for decades scientists have understood scroll bars to be intimately related to river channel migration, even using scroll bar age and spacing to estimate lateral migration rates (Hickin 1974; Hickin and Nanson 1975; Nanson and Hickin 1983; Rodnight et al. 2005). Their occurrence is reported in ancient riverine deposits exposed at Earth's surface (Ielpi and Ghinassi 2014; Durkin et al. 2015; Wang and Battacharya 2017), in seismically imaged subsurface deposits (Durkin et

al. 2017), and even in remote sensing studies of strata on other planets (Moore et al. 2003; Moore and Howard 2005; Schon et al. 2012; Burr et al. 2009), where they have been used to estimate paleochannel position, wavelength, and curvature.

This paper presents a comprehensive survey of modern scroll bars along the lower Trinity River in east Texas, USA, describing their form and stratigraphy and inferring processes required for their formation. The Trinity River at Romayor, Texas (Figure 2.1), has an average annual discharge of around 200 cubic meters per second. This project uses an airborne lidar survey that was flown in 2015 in conjunction with focused trenching of five scroll bars to determine the nature of scroll bar deposition, stratigraphy, and evolution along the Trinity River. The area covered by the survey is 65 river kilometers long and includes data from 45 river bends. Our results have implications for using scroll bars as a measure for migration rate on modern rivers and highlight the systematic differences between scroll bars and their adjacent point bars. In addition, results suggest that lateral accretion surfaces associated with point bar growth are commonly misidentified as scroll bars along modern rivers, in outcrop, in subsurface data, and on other planets.

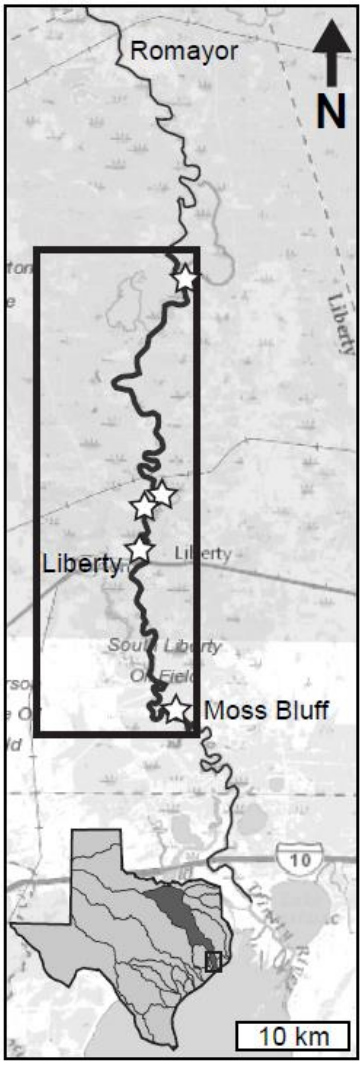

Figure 2.1: Location map of the lower Trinity River

Study area defined by the black rectangle. Flow is from north to south. Trinity Bay is located at southern end of the map extent. Locations of the Romayor, Liberty, and Moss Bluff USGS gaging stations (IDs 08066500, 08067000 and 08067100, respectively) are labeled. The five river bends chosen for trenching are marked with stars. Inset state of Texas shows the Trinity River watershed in dark grey, with the lower Trinity River circumscribed by the small black box.

METHODS

A bare-earth lidar data set collected in August of 2015 by the National Center for Airborne Laser Mapping was used to measure elevations and planform curvatures of scroll bars (Figure 2.2). The lidar dataset was collected at low discharge conditions using an Optech Titan with a reported vertical accuracy within 5-15 cm of the known elevation and rasterized to 1-meter horizontal resolution. In addition, we will discuss scroll bar change based on previously published results by Mason and Mohrig in 2018 that utilized timelapse lidar covering the same survey area. Every topographic ridge along the inner bank of a river bend that had a planform geometry that mimicked that of the channel bend was considered a scroll bar. Bends were selected for measurement if there was an obvious associated point bar and at least one well-defined scroll bar. Ten bends that did not have obvious scroll or point bars associated with them (either due to recent cutoff or minimal migration) were left out of the study as well as two bends whose geometry was altered by the presence of human infrastructure. The transition from uniform flow into backwater flow occurs about halfway along the survey area and is accompanied by distinct changes in channel morphology and kinematics (Smith 2012, Mason and Mohrig 2018). This transition approximately begins where the mean elevation of the channel bottom drops below mean sea level, and is accompanied by a decrease in the sub-aerial exposure of the channel with distance downstream.

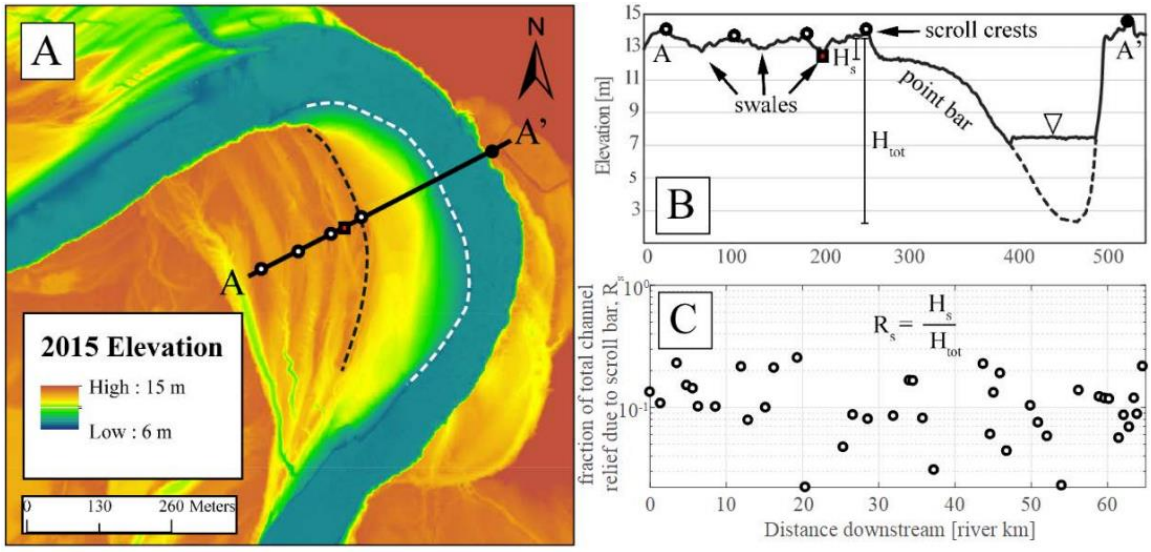

Figure 2.2: Studied river bend showing lidar measurement scheme

A) Topographic map of the most upstream starred bend in Figure 2.1 with a single transect oriented perpendicular to the local channel centerline (black line, A to A', total length = 540 m). Measurement points along the transect are marked by symbols located at the outer bank levee crest (filled circle), at the highest point of each consecutive scroll bar (open circles), and within the swale behind the youngest scroll (red square). The crestline of the youngest scroll bar and the point bar shoreline are marked by the black and white dashed lines. The radius of curvature was calculated for each scroll- and point- bar in every channel bend. B) Elevation profile for the transect A to A'. The solid line demarcates data from the airborne lidar survey used in this study. The dashed line defines merged bathymetric data from a boat-based acoustic survey running up and down the Trinity River. Note that the broad, convex-up top of the point bar is lower than the elevations of the crests of scroll bars, and that the elevations associated with scroll bar peaks are similar to the elevation of the outer bank levee crest. The height of the youngest scroll bar, Hs, and the height of the inner bank, Htot, are denoted by the vertical lines. C) Fraction of total inner bank relief associated with the scroll bar topography, Rs= Hs/Htot, for each bend in the survey area. On average, scroll bars are responsible for only the uppermost 12% of the total inner bank relief.

A channel centerline was created in Esri's ArcMap 10.3 geographic information system by collapsing the manually mapped positions of the inner and outer river banks (demarcated by the landward edge of the point bar and the vertical cut bank, respectively). Transects perpendicular to the centerline were created every 100 meters along channel

bends with scroll bars. The elevation of the edge of the outer bank (i.e. the outer bank levee crest), the highest elevations associated with each consecutive scroll bar ridge, and the elevation of the swale behind the youngest scroll bar (defined as the one closest to the point bar) were measured along each of these perpendicular transects (Figure 2.2A, 2.2B). The planform shape of the youngest scroll bar was mapped (Figure 2.2A) and its radius of curvature was estimated by fitting a circle to the data points using the Pratt method (Pratt 1987). To determine any systematic difference in planform geometry between scrolls and their adjacent point bars, the shorelines on point bars were mapped and these close-to-horizontal surfaces were used to estimate the radius of curvature for each bar using the same method (Figure 2.2A). In the zone of quasi-uniform flow these horizontal surfaces were on average at 57% of the total point bar height, while in the downstream backwater zone these surfaces moved up to an average position of 71% of the total point bar height. While there is undoubtedly a trend in point bar radius of curvature with the height at which the measurement is taken, our analysis is meant only to ascertain if there is any systematic difference between scroll and point bar planform geometries, and not intended to quantify the exact magnitude of the difference.

Along each transect, the steep channel-ward slope of the most recent scroll bar rises above the broad, relatively flat top of the point bar (Figure 2.2B). Relief of the youngest scroll bar, H_s, was measured by subtracting the average elevation of the flattened top of the adjacent point bar from the average elevation of the scroll crest for each bend. Bathymetry data collected by the Texas Parks and Wildlife Department (TPWD) in 2009 – 2010 was used to measure the average thalweg elevation for each river bend. The total height of the inner bank, H_{tot}, was measured by subtracting the average thalweg elevation from the average elevation of the scroll bar crest for each bend. H_s and H_{tot} were then used to

calculate fraction of total relief of the inner bank that was due to scroll bar topography, $R_s = H_s/H_{tot}$ (Figure 2.2C).

To complement the measurements taken from the lidar data, five separate point/scroll bar complexes were chosen for trenching (Figure 1, starred river bends). A total of eleven trenches were dug. These trenches were generally ~1m deep and 10+ m long, and several captured the point bar to scroll bar transition. Trenches were inspected, photosurveyed, and mapped in order to determine the depositional character of the scroll bars as well as the stratigraphic character of the transition from point bar to scroll bar. The bends associated with the trenched sections are spread out across the entire length of the survey. Trenches were oriented both parallel and perpendicular to the transport direction for each bend. Sediment samples were collected from each trench to define the change in grain size associated with the transition from point bar to scroll bar. If sediment samples contained no visible mud, they were run on a Retsch Camsizer P4 particle analyzer, which uses dynamic image analysis to determine grain size. Samples containing a substantial mud fraction were run on a Malvern Panalytical Mastersizer 3000, which estimates grain size from the laser-diffraction pattern produced by a dispersed suspended sample. Grain size results were reported using the Wentworth grain size classes.

RESULTS

Lidar data

Results from timelapse lidar data published by Mason and Mohrig in 2018 show that the edges of the youngest scroll bars along the same portion of the Trinity River are actively moving. Figure 2.3 shows an example of a river channel bend where the position of the scroll bar moved landward away from the channel as a result of erosion due to a

historically large flood on the river in 2015. All of the river bends studied in Mason and Mohrig's previous survey show a change in the position of the edge of the youngest scroll bar (either moving away from the channel, as in Figure 2.3, or moving in the same direction as the erosion of the outer bank).

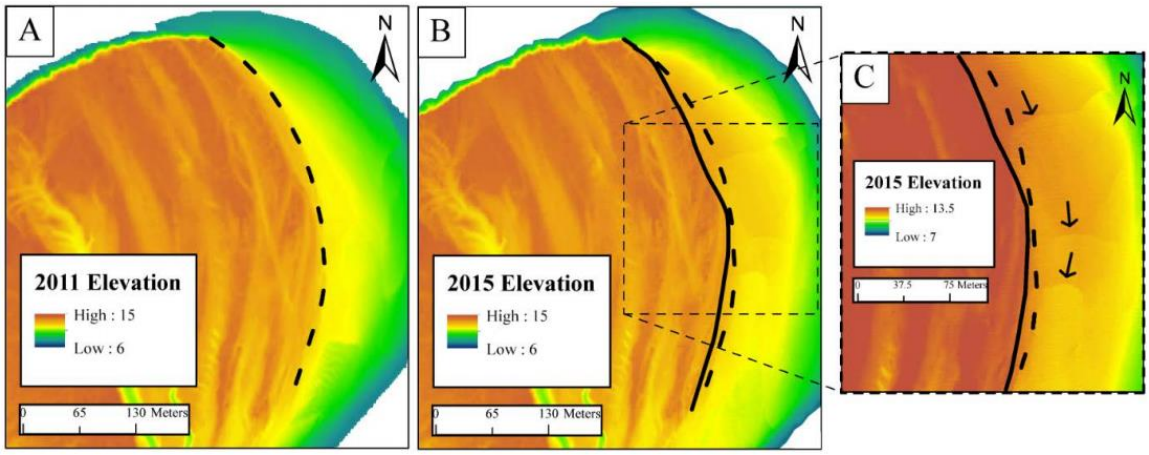

Figure 2.3: Time-lapse elevation data showing the erosion and lateral movement of the edge of the youngest scroll bar

A) Scroll and point bar associated with a Trinity River bend in 2011 (same bend as in Figure 2). The edge of the scroll bar is marked by the bold dashed line. B) The same bend in 2015, with the previous position of the scroll marked by the dashed line and its new position by the solid black line. Note that the new position of the scroll bar has moved landward, not channel-ward. C) A zoomed in portion of the 2015 scroll/point bar complex highlighting the presence of large bed forms mantling the uppermost point bar at the position of the 2011 scroll bar.

Measurements from scroll bars and adjacent point bars highlight consistent differences in their plan-form size and shape. First, the arc-length for a scroll bar is less than that of the adjacent point bar. Second, the radius of curvature for scroll bars is consistently greater than the radius of curvature of the associated point bar shoreline (Figure 2.2A, Figure 2.4). No significant trend in the relationship between the radii of

curvature of the point and scroll bars is found moving from the upstream to downstream ends of the survey area despite the change in point bar measurement height with distance downstream due to the backwater effect. A Wilcoxon rank-sum test shows that the distributions of ratios of scroll bar to point bar radii of curvature for the uniform and backwater zones are indistinguishable at the 99% confidence level.

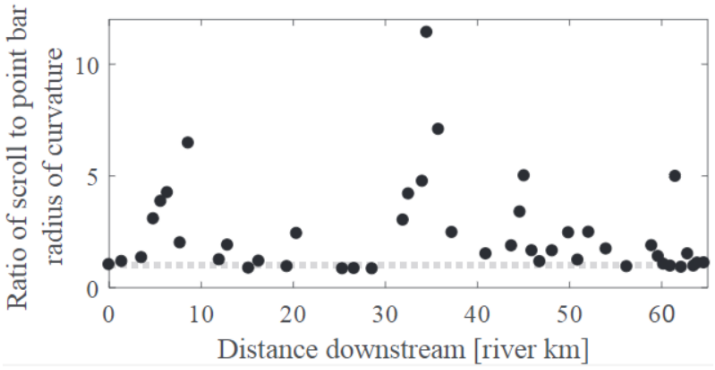

Figure 2.4: Ratio of the active scroll bar radius of curvature to the point bar shoreline radius of curvature

Scroll and point bar radii of curvature were measured from the 2015 lidar data. Dashed grey line represents a ratio of 1. 80% of the youngest measured scroll bars have a radius of curvature that is larger than that of their associated point bars. Bends where scroll and point bars have similar radii of curvature are young, short amplitude bends. There is no significant trend in the relationship between the two as the river transitions into the backwater zone.

Figure 2.2B shows a representative channel cross section from the outer bank levee crest to the oldest scroll bar. On the inner bank, the top of the point bar, defined by a relatively flat but still convex-upward surface is positioned well below the elevation of the outer bank. The scroll bars rise several meters above the top of the point bar and are positioned only slightly below the elevation of the outer bank levee crest on average. This relationship holds true for the majority of transects measured across the survey reach.

Figure 2.5A shows a histogram of the difference in elevation between all measured scroll bars and the associated outer bank levee crests. The majority of scroll bar elevations are on the order of decimeters below the elevations of the outer banks (mean difference is -0.4 m with a standard deviation of 0.7 m). 82% of measured scroll crests were within one meter of the outer bank in elevation. A fourth of the measured scroll bar crests are higher than their associated outer banks.

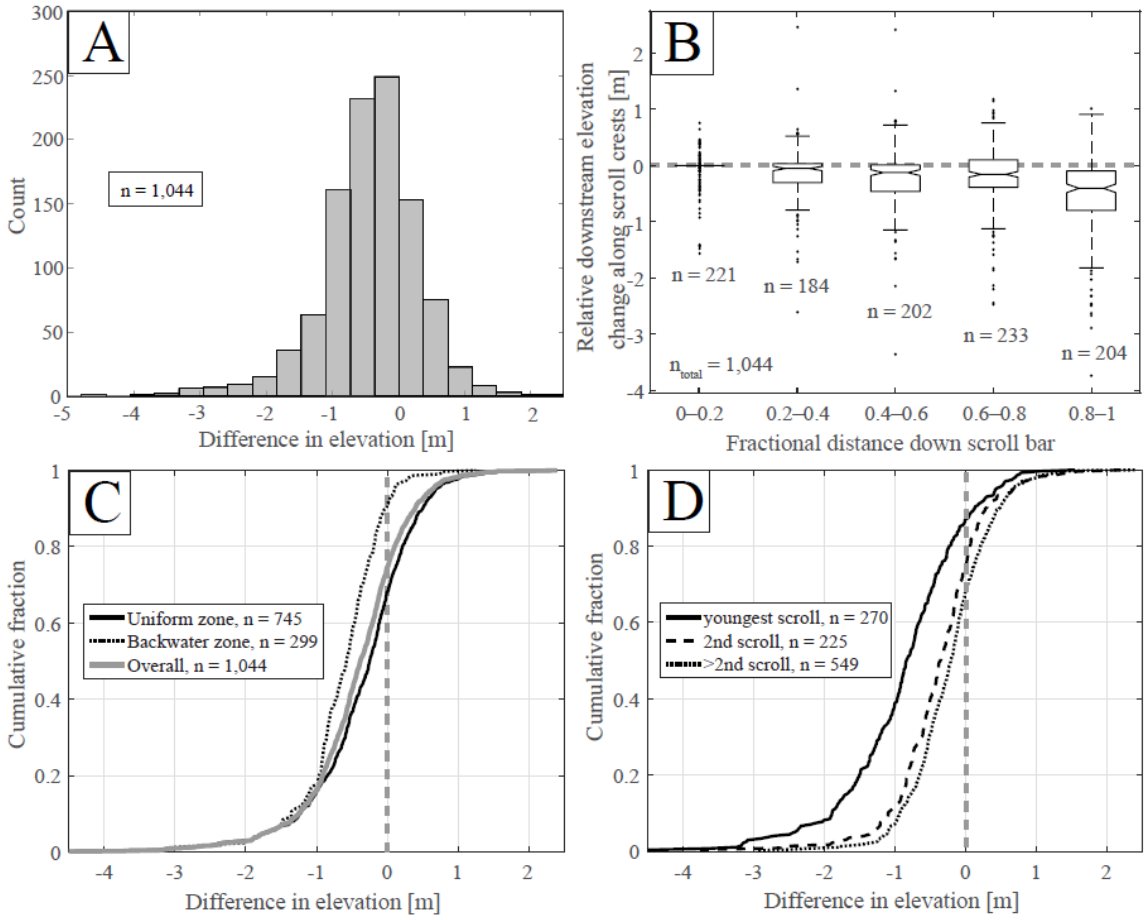

Figure 2.5: Trends in scroll bar crestal elevations

Figure 2.5: Trends in scroll bar crestal elevations
A) Histogram of measured elevation differences between the scroll bar crest and the outer-bank levee crest for all transects within the study area (n=1044, bin width = 35 cm). Negative values indicate the scroll crest is lower than the outer bank. Elevation differences are centered just below zero and are negatively skewed. The mean elevation difference is -0.4 m with a standard deviation of 0.7 m. B) Box plots showing the relative downstream elevation change for all of the measured scroll bar crests as a function of fractional distance down the river bend. On each plot, the central line indicates the median, the bottom and top edges of the box represent the 25th and 75th percentiles, the whiskers indicate the range of the data and the points are considered outliers. On average, scroll crests tend to decrease in elevation with distance down the river bend. C) Cumulative distributions of elevation differences between measured scroll bar crests and the outer bank levee crests. Dashed grey vertical line represents equal elevation for measured scroll crests and outer bank levee crests. The scroll bars forming in the zone of quasi-uniform flow are shown in the solid line, and backwater-zone scrolls in the dotted line. There are fewer measured scroll bars present in the backwater zone, and they are less likely to be higher than the associated outer bank levee crest. D) Cumulative distributions for elevation differences between measured scroll bar crests and their outer bank organized by distance away from channel. Dashed grey vertical line represents equal elevation for measured scroll crests and outer bank levee crests. The youngest scroll bar (the one closest to the channel centerline) is on average 0.6 m lower than the subsequent scrolls. The second scroll bar is higher. All remaining older scroll bars are still slightly higher in elevation.

In general, the crest of a given scroll bar is highest at its upstream end and gradually decreases in elevation downstream (Figure 2.5B). Only 16% of the measured scroll bar crests are more than 1 meter below the outer bank in elevation. Of these 169 measured points, 115 (68%) were located along the downstream half of the scroll bar. Of the 30 measured scroll bar crests that were more than 2 meters below the outer bank (3% of all measurements), 27 were located along the downstream half of the scroll. The youngest scroll bar crest is on average 0.6 m lower than more landward scrolls, while the second scroll bar is just 0.1 m lower than all older scrolls on average (Figure 2.5D). Beyond the second scroll bar, there is no significant trend in crestal elevation with distance away from the channel.

The crestal elevations for scroll bars change character from the zone of uniform flow into the backwater zone (Figure 2.5C). In the backwater zone there are fewer scroll bars present (n=299 for the backwater zone versus n=745 upstream). The bends that were sampled in the backwater zone reveal a tighter distribution of elevation differences between scrolls and outer banks due to a decrease in the number of positive differences.

Figure 2.6 shows the character of the swales associated with the active scroll bars. In general, the difference in elevation between the scroll crest and the adjacent swale increases down the length of the bend (Figure 2.6A).

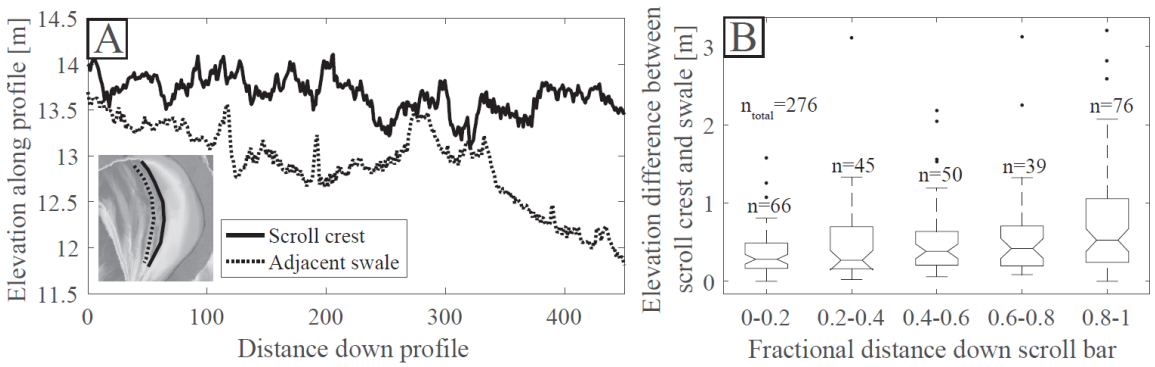

Figure 2.6: Trends in scroll bar swale elevations

A) Elevation profiles along the crest of the youngest scroll bar (black line) and its adjacent swale (dotted line) for the river bend shown in Figure 2. The difference in elevation between the two increases downstream. B) Box plots showing the distribution of elevation differences between the active scroll bar crest and its adjacent swale with fractional distance down the scroll bar for the youngest scrolls along each bend within the survey area. On each plot, the central line indicates the median, the bottom and top edges of the box represent the 25th and 75th percentiles, the whiskers indicate the range of the data and the points are considered outliers. The swale becomes progressively lower relative to the scroll crest farther along the scroll.

Stratigraphy

Eleven trenches dug along five separate scroll bars show similarities in stratigraphic architecture across the entire survey reach. Three characteristic trenches are shown as Figures 2.7, 2.8, and 2.9. The majority of trench walls were composed of ripple-scale cross strata that showed a variety of transport directions (away from the channel, downstream, and towards the channel; Figure 2.9 shows an example of multiple ripple migration directions within a single package of sediment). Boundaries between sets of rippled cross strata generally dip towards the channel, but can dip away from the channel as well (Figure 2.7). These deposits were composed of very fine and fine sand. Often, dune-scale cross strata were dominant at the base of the trench (Figure 2.8) and lenses of coarser dune-scale

strata were seen interspersed within rippled strata (white colored deposits in Figures 2.8, 2.9). These deposits were most often composed of medium and coarse sand. Mud-rich intervals are common and these contained the highest densities of roots and bioturbation. Even so, organic-rich deposits were relatively sparse; if present they were in the form of isolated root zones, buried branches, or detrital leaf material.

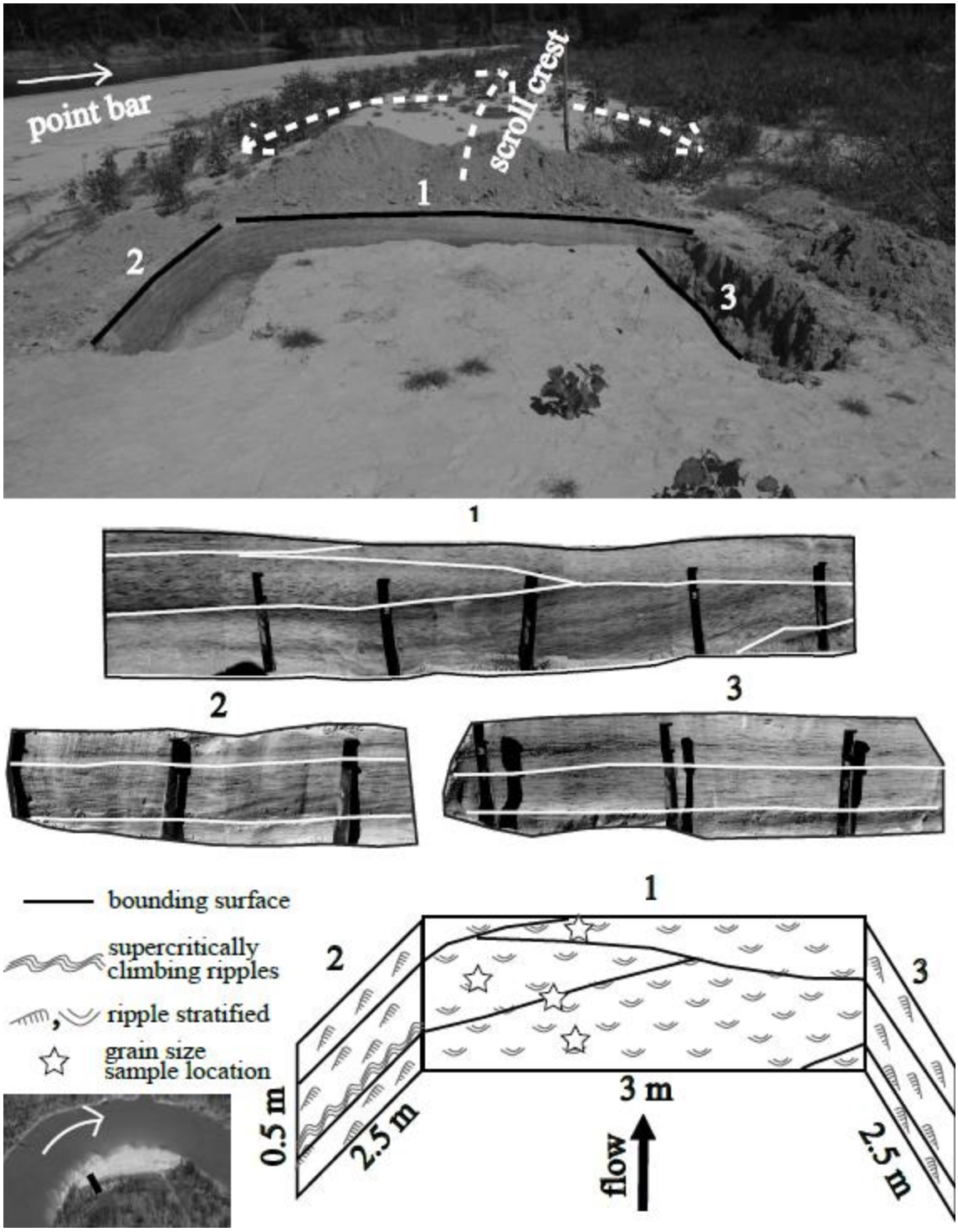

Figure 2.7: Scroll bar stratigraphy, trench 1

Figure 2.7: Scroll bar stratigraphy, trench 1
Photos and line drawing of a U-shaped trench that was centered on the crest of a scroll bar. This scroll bar is located at the most downstream star in Figure 2.1. Its positioning in the river bend is marked on the inset lower left aerial image. The upper photograph looks downstream along the crest of the scroll bar and captures the 3 trench faces, with the associated point bar and main channel visible to the left. Dotted white lines on the photo mark the position of the scroll crest and highlight the curvature of the scroll bar in the cross-channel direction. The 3 trench walls were entirely composed of ripple-stratified deposits. All of these climbing ripples were migrating the downstream direction during scroll bar construction. Bounding surfaces separating the packages of rippled sediment dip both towards the channel and away from the channel, indicating alternating growth of both lateral slopes of the scroll bar.

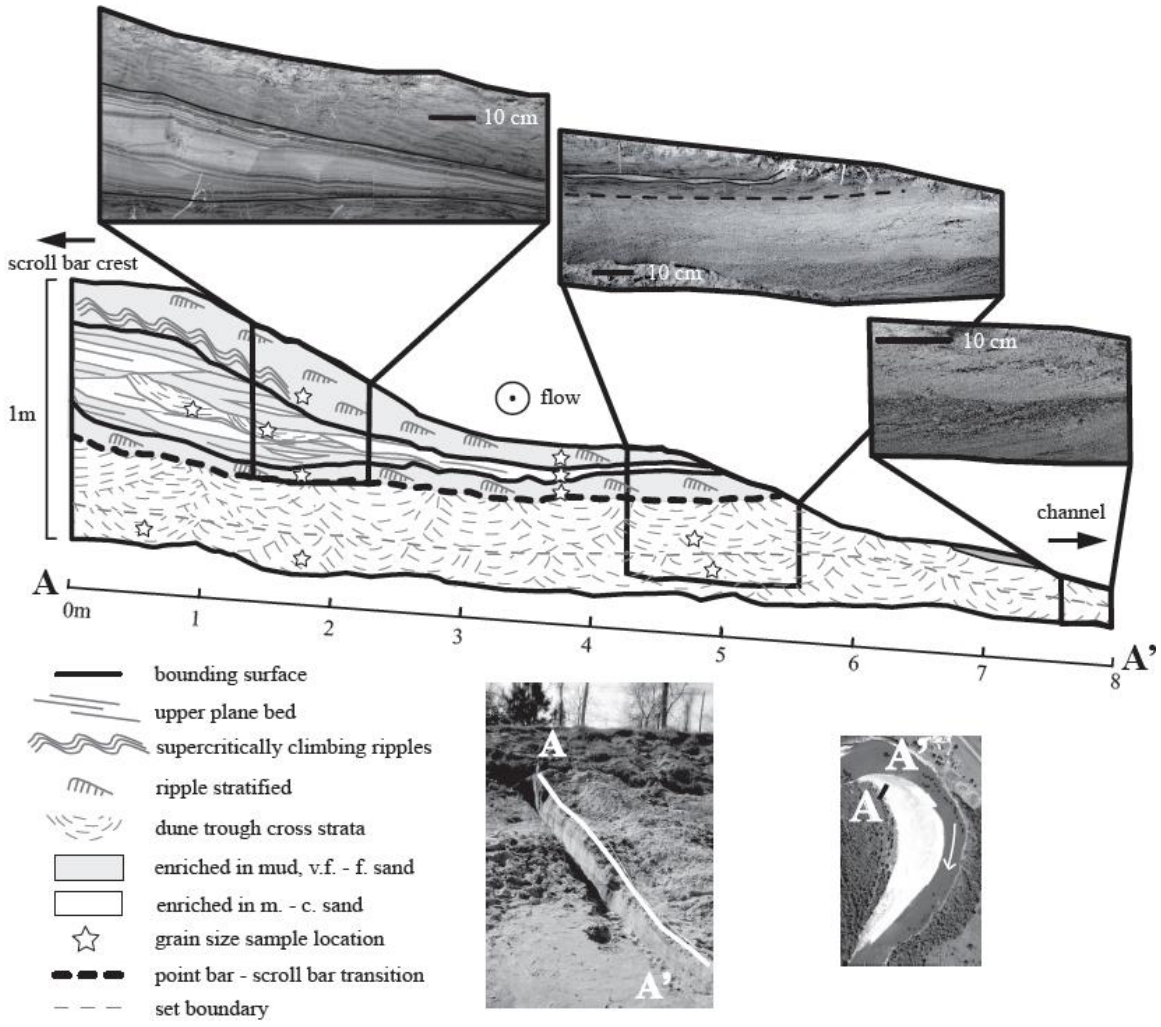

Figure 2.8: Scroll bar stratigraphy, trench 2

Figure 2.8: Scroll bar stratigraphy, trench 2
Photos and line drawing of an 8 m long trench (2x VE) oriented perpendicular to the channel centerline on the channel-ward side of the youngest scroll bar in the bend (see inset aerial image for relative location). Most upstream star in Figure 2.1 marks the position of this river bend. Surface context is provided by small bottom-center image looking at the trench and up to the scroll-bar crest from the top of the point bar. The crest of the scroll bar is ~ 3 m beyond the left end of the line drawing, and the trench dips towards the channel. Flow within the main channel is moving out of the page. Darker colored deposits indicate finer grain sizes. The base of the trench is composed of pebbly sand with dune trough cross-stratification indicating bed material transport out of the page and interpreted as deposition connected to a previous position of the point bar. The transition into deposits composed of reworked suspended material (indicated by the thick dashed line) is abrupt. Ripple cross-stratification makes up the majority of the scroll bar deposit, with some plane bed stratification and lenses of coarser bed material interspersed within the rippled sediment.

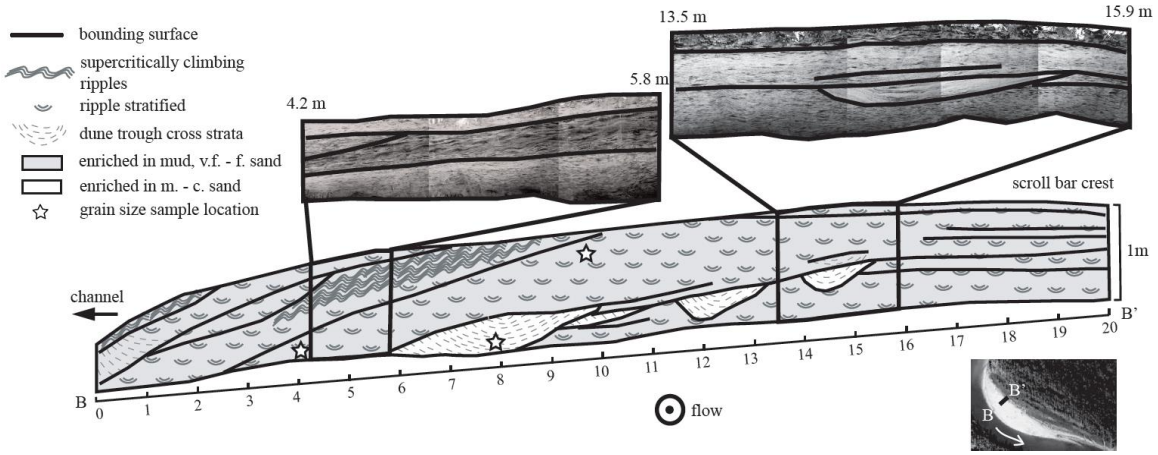

Figure 2.9: Scroll bar stratigraphy, trench 3

Photos and line drawing of a 20 m long trench (2x VE) that was positioned perpendicular to the channel centerline on the channel-ward slope of a scroll bar (fourth starred bend near Liberty, Figure 2.1). The right-hand edge of the trench is at the position of the scroll-bar crest (see aerial image for the relative location of trench). Flow within the main channel is moving out of the page. Trench is dipping towards the channel. Darker colored deposits indicate finer grain sizes. This trench is primarily composed of deposits with ripple cross-strata with some supercritically climbing ripples indicating transport out of the channel. Lenses of dune-scale cross stratification are interspersed within with the finer-grained rippled beds associated with scroll bar deposition. Surfaces between packages of rippled sediment are subtle and are often unable to be followed laterally (see right side of trench), and likely reflect local variability in deposition rate.

The modern scroll bar topography was overwhelmingly composed of rippled very fine to fine sand deposits that were interspersed with lenses of coarser, dune-scale cross stratified sands and mud-rich intervals. If a base of coarser dune-scale cross stratified sands was present in a trench, it was below the elevation associated with the modern scroll bar topography and was instead consistent with the elevation of the adjacent point bar.

A total of eighty-five sediment samples were taken from representative locations along each trench (35 from dune-scale cross strata, 50 from rippled and/or mud-rich locations) and analyzed for grain size (Figure 2.10). The mean value for D50 from the 50

rippled/muddy samples was 0.17 mm (lower fine sand; all grain size classifications correspond to the Wentworth classes). 25 out of the 50 rippled samples contained more than 20% medium sand. The coarsest rippled sample was composed of 60% medium sand or coarser. This sample was taken from the trench in Figure 2.8, just above the transition from coarser, cross stratified sands to the rippled deposit (the bottom star near meter 4). The 35 samples with dune-scale cross-strata were measurably coarser than the rippled samples, with a mean D10 of 0.19 mm (upper fine sand, coarser than the D50 for the rippled samples) and mean D50 of 0.36 mm (upper medium sand). 8 out of the 35 dune scale cross-stratified samples were composed of more than 20% coarse sand or above. The largest measured grain sizes are within the lower fine pebble range (5 mm) and are present only within the dune scale cross-stratified basal portions of trenches (see top right inset photo in Figure 2.8). A Kruskal-Wallis test done on the two groups of grain size distributions confirmed that they are statistically different at the 1% significance level.

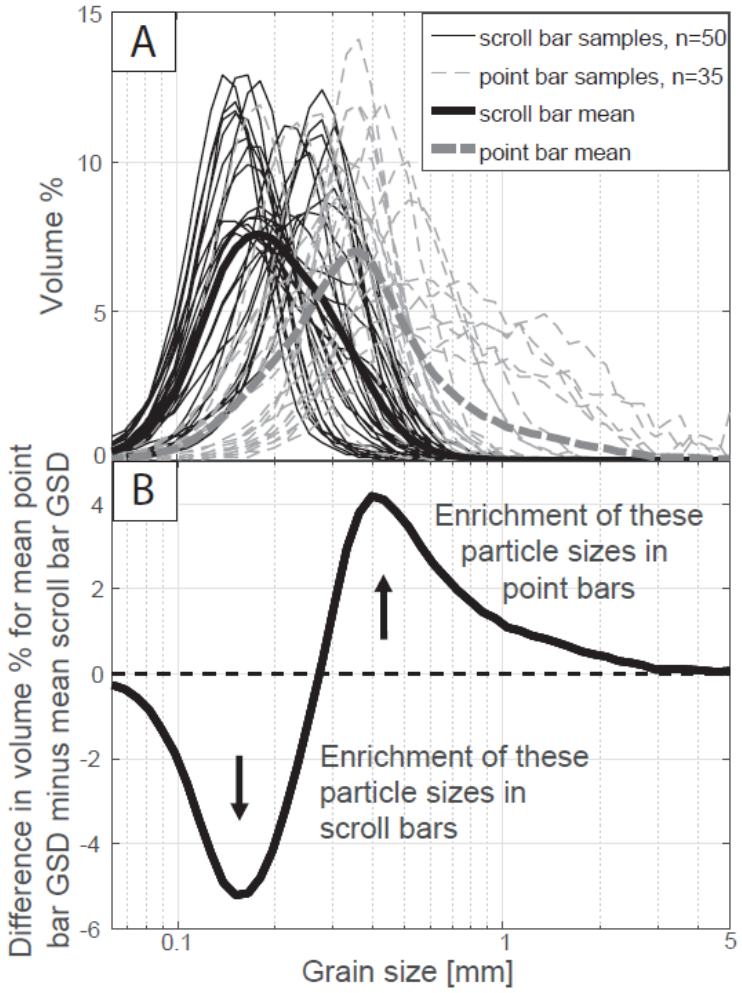

Figure 2.10: Scroll bar grain size data

A) Grain size distributions for point bar samples labeled in thin, grey, dotted lines and scroll bar samples in thin black lines. Mean distributions for the scroll and point bars are shown by the thick black and grey dashed lines, respectively. B) Difference between the mean grain size distribution (GSD) for the scroll bar samples and point bar samples. Positive values indicate point bar deposits are relatively enriched in those grain sizes, and negative values indicate relative enrichment in scroll bars. Point bars are relatively enriched in all grain sizes greater than 0.27 mm (where the line crosses zero), which is close to the boundary value separating fine and medium sand (0.25 mm). Scroll bars are relatively enriched in fine sand and smaller sizes.

DISCUSSION

The trend of increasing scroll bar crestal elevation with orthogonal distance away from the channel (Figure 2.5D) is only significant for the first two scroll bars. Beyond the second scroll bar, the crestal elevations appear to stabilize. This is likely due to the amount of time that each scroll has had to aggrade. The youngest scroll bar has experienced the fewest overbank flooding events and is likely lower as a result of the relatively limited sediment delivery. The maximum elevation that a scroll bar crest can reach is capped by the elevation of the free surface of the overbank flow, which cannot exceed a certain depth as the flow is no longer confined within the channel. An alternative interpretation to explain the lower elevation of the youngest scroll bar requires that the channel is actively incising into the floodplain. However, several depth profiles taken along a 27 km stretch of the river preceding, during, and following a historically large flooding event on the Trinity show no net aggradation or erosion (Mason and Mohrig, 2018), implying that active vertical incision is not an important factor dictating scroll bar crestal elevations in this system.

On the average scroll bar, the crestal elevation tends to decrease with distance down the river bend (Figure 2.5B). In addition, the swales behind the active scroll bars become increasingly lower farther downstream (Figure 2.6). This is likely due to the direction of the sediment source responsible for the growth of the scroll bars and infilling of the swales. During prolonged overbank flood conditions, flow is supplied to the floodplain not only from the orthogonally adjacent channel but also from the upstream bends (which is also evidenced by the dominance of downstream-migrating ripple cross strata present in scroll bar trench walls; see Figures 2.7 and 2.9). The sediment within the flow is deposited quickly upon exiting the channel, leading to preferential deposition along the upstream portions of the scroll bars and swales. In other words, the rate of growth for a single scroll bar decreases downstream.

Scroll bars within the backwater zone exhibit slightly different characteristics than their uniform flow counterparts. Lateral migration of the channel is dampened within the backwater zone (Hudson and Kesel 2000; Lamb et al. 2012; Nittrouer et al. 2012; Smith 2012; Fernandes et al. 2016), leading to fewer total scroll bars (Figure 2.5C). The scroll bars that are present in the backwater zone are less likely to have crest elevations that are higher than the outer bank levee crests. The reason behind this remains unclear; future research aimed at understanding why scroll bars appear to behave slightly differently within the backwater zone would be beneficial.

The existing literature about scroll bars has been inconsistent on their identification as constructional or erosional features. Some authors suggest that focused erosion between bars is what creates the topography associated with scrolls, making them a negative relief feature (McGowen and Garner 1970; Nanson and Croke 1992; Lewin and Ashworth 2014). In Figure 2.2B it is clear that the swales between successive scroll ridges are not lower than the top of the point bar. While the swales between scrolls do tend to focus overbank flow and drainage once a succession of scroll bars has been established (see the downstream portion of Figure 2.2A for an example of swales between older scrolls focusing drainage), our data suggest that at least on the Trinity River, scrolls are primarily formed through preferential and focused deposition on top of the point bar surface.

The Trinity River has extensive, mature levees associated with overbank deposition along the outer banks of most bends. The mean levee height above the adjacent floodplain on the studied reach of the Trinity River is 1.3 m (Hassenruck-Gudipati et al., 2017). Levees are highest at the edge of the main channel, where the outer bank elevation measurements used in this study were taken. While the nature of levee deposition and growth is not perfectly understood, they are universally recognized as features that create positive relief above the elevation of the floodplain (Leopold et al., 1964). Because the

crests of scroll bars are on average only 0.4 m below the outer bank levee crests (Figure 2.5A), scroll bars can also be considered constructional features of positive relief 0.9 m above the floodplain, on average.

The constructional nature of scroll bars has implications for their identification in the sedimentary record. We suggest that unless a feature can be definitively identified as having positive relief above the elevation of the associated point bar or floodplain, it should not be interpreted as a scroll bar. There are several likely examples of misinterpretation of features as scroll bars. For example, planetary geomorphologists often interpret curved strata within preserved channel belts on Mars as scroll bars (Moore and Howard 2005; Schon et al. 2012; Burr et al. 2009). These features are much more likely to represent the lateral accretion surfaces associated with point bar growth and bend migration, as the likelihood of preserving a scroll bar is low considering that they are confined to the upper portion of the deposit and the average scroll bar is responsible for only 12% of the total inner bank relief (Figure 2.2C). Without clues indicating that scroll-like features are topographically higher than the point bars or floodplain they are associated with, the definitive identification of these features as scroll bars would be difficult.

While we believe the misidentification of point bar lateral accretion surfaces as scroll bars is common, it doesn't greatly alter most interpretations because both scrolls and point bar surfaces are indicative of deposition associated with meandering river channels. However, the misidentification becomes problematic if the deposits are subsequently used to reconstruct paleochannel properties. Point bars consistently have a lower radius of curvature than their associated scroll bars (Figure 2.4). The few bends that have scroll bars and point bars with similar curvature are low amplitude young bends affected by recent cutoffs or bends with narrow point bars. Reconstructions of river bend length and amplitude based on a set of point bar surfaces misinterpreted as scroll bars would therefore

be overestimates. In addition, the reconstructed centerline would have a higher sinuosity than one reconstructed from a set of actual scroll bars.

Trench walls show the volumetric majority of sediment associated with scroll bars was deposited by grains that settled out of suspension and were subsequently reworked as a low transport stage bedload (i.e. ripples; Figures 2.7, 2.8, and 2.9). Because of their association with the modern scroll bar topography, we interpret these deposits to represent the construction of the scrolls. Ripple cross stratification records a variety of transport directions that are consistent with flow out of the channel, down the channel, and back into the channel. These ripples are interpreted to record multiple stages of the flood duration, i.e. flood stage as it begins to flow overbank, sustained overbank flow, and drainage of the floodplain following recession of the flood, respectively. Planar laminations in the form of lower plane bed are also fairly common, as well as mud-rich layers. All of these observed depositional structures are commonly used as stratigraphic indicators of levee deposition in modern and ancient channel belts (Bridge 2009; Brierly et al. 1997). The coarser, dune-scale cross strata often present along the bases of trenches are interpreted as deposition associated with earlier point bar growth. Scrolls are relatively enriched compared to point bars in all grain sizes smaller than fine sand, the largest grain size that is commonly moved in coastal fluvial systems as both bedload and in suspension (Nittrouer et al., 2008). Based on the stratigraphic evidence, scroll bar depositional style and grain size appear to be comparable to proximal overbank deposition, i.e. fluvial levees.

The relative scarcity of organic-rich deposits within the observed trench walls implies that the sedimentation associated with scroll bar growth is not necessarily linked with the presence of vegetation. While there certainly tends to be a correlation between the position of scroll bars and the presence of vegetation in many modern rivers, causation

can't be applied to one or the other; especially as many plant species likely preferentially colonize areas characterized by finer grain sizes and less frequent inundation.

Since point bar deposition is consistent with bed material transport within the channel, and the stratigraphy of the scroll bar is more consistent with proximal overbank deposition, it can be inferred that the edge of the scroll bar marks the geomorphic edge or inner bank of the channel. Time-lapse lidar data that cover the same extent of the Trinity River as the lidar data discussed here show that landward movement of the inner bank occurred in 32 out of 55 measured bends as a result of a flood in early 2015 (Mason and Mohrig 2018; that length of overbank flood had not previously been measured on the Trinity since the installation of the Liberty flood gage in 1938). Figure 2.3 (Figure 11 from Mason and Mohrig 2018) shows a single bend where the antecedent scroll bar position has been eroded and subsequently covered with large bed forms after the sustained flooding event. The observation of bed material depositing over the position of an antecedent scroll can also account for the lenses of coarser grained material with larger scale cross stratification present in scroll bar trench walls (Figures 2.8 and 2.9). Lenses of point bar material encapsulated within scroll bar deposits were present within trenches in 3 of the 5 sampled scroll bars, implying that the process of scroll bar erosion by point bar widening is not uncommon.

Scroll bar growth and migration isn't necessarily unidirectional, as our trenches and the data from Mason and Mohrig 2018 suggest (Figures 2.3, 2.7, 2.8, 2.9). Packages of rippled sediment defining the growth of scroll bars mostly dip towards the channel, consistent with growth of the scroll bar to follow the overall outward migration of the river bend. However, some packages do dip away from the channel along the landward slope of the scroll (see Figure 2.7). These packages imply that scroll bars can widen both channel-ward and in the landward direction as well, reducing the spacing between consecutive

scroll bars. These observations should induce caution when attempting to use the spacing between scroll bars as a proxy for overall channel migration. However, it is clear that on average, scroll bars tend to track the outward migration of the river bend.

For a given flood discharge, the formation of a new scroll bar in a more channel-ward position is likely not favored until the river bend has migrated out some threshold distance dictated by the geometry of the bend and point bar. When the bend migrates less than that threshold distance, suspended material is still preferentially deposited on the antecedent scroll bar. When the river bend migrates more than the threshold distance, the widening of the point bar top (assuming the point bar is laterally accreting to more or less keep pace with the erosion of the outer bank) causes the flow to decelerate sufficiently to induce deposition of suspended sediment in a new, more channel-ward position. Because the top of the point bar is typically meters below the elevation of the floodplain (Figure 2.2B), scrolls must vertically aggrade much more than an outer bank levee to reach an equivalent crestal elevation. As a result, they tend to be lower than their associated outer bank levees.

Proposing that there exists a genetic distinction between scroll bars and outer bank levees is a difficult argument to support. The crestal elevations of scrolls and outer bank levees are quite similar, implying they are both constructional features that create positive relief above the adjacent floodplain (Figures 2.2, 2.5). In addition, they have similar stratigraphic architectures and sedimentary structures (Figures 2.7, 2.8, and 2.9). Lastly, scroll bars and levees tend to demarcate the inner and outer edges of the channel, respectively. Thus, we interpret scroll bars as levees that have been deposited along the inner banks of these meandering river bends.

CONCLUSIONS

We posit that scroll bars on the Trinity River are analogous to outer bank levees that have instead been deposited along the inner banks of the river. We draw the analogy between scroll bars and levees based on their similar crestal elevations (Figures 2.2, 2.5), comparable stratigraphic architectures (Figures 2.7, 2.8, and 2.9), and ability to demarcate the edge of the channel (i.e. the transition from bed load deposition to suspended sediment deposition, Figure 2.3). While it is undoubtedly true that the presence of a number of scroll bars in other systems is likely due to other factors (e.g. flood debris or vegetation inducing fall out of suspended sediment), our hypothesis implies that the presence of scroll bars in rivers can occur without significant vegetation (on Mars, for example). Future modelling efforts to determine when and where flow decelerates enough along the tops of point bars to induce suspended sediment deposition will be immensely helpful for understanding why scroll bars form where they do.

Because the position of preferred scroll bar deposition continues to move as the channel itself migrates, scroll bars are likely representative of the initial stages of levee development. It is interesting then to consider the transition from a young levee (i.e. scroll bar) to a larger mature levee. Using scroll bars as a proxy for early levee growth would be hugely beneficial for learning more about levee sedimentation, a process that is still relatively understudied.

The results presented here should promote the use of caution when attempting to identify scroll bars preserved in the stratigraphic record. Positive topographic relief above the tops of the associated flood plain or point bar as well as structures consistent with proximal overbank deposition should be used as distinguishing characteristics before a feature can be recognized as a scroll bar. Point bar lateral accretion surfaces may at first appear qualitatively similar to scroll bars but represent a different process with markedly

different geometries (Figure 2.4) and stratigraphic architectures (Figure 2.8). If one accepts the interpretation of scroll bars as inner bank levees, then they should be considered the geomorphic edge of the channel. The point bar, by definition, is fixed within the channel; meaning that its upstream and downstream limits must converge with the position of the inner bank. Therefore, if the point bar extrudes into the channel at all, its curvature will be exaggerated compared to that of the scroll bar. Misidentification of a point bar lateral accretion surface as a scroll bar can thereby lead to errors in bend length and amplitude estimates, as well as estimations of the channel centerline position. It should be noted as well that preservation of scroll bars in the rock record is unlikely given that their relief is small compared to the total relief of the channel (Figure 2.2C), and many features identified as scroll bars in the rock record may instead be point bar lateral accretion surfaces.

ACKNOWLEDGEMENTS

The authors would like to thank Hima Hassenruck-Gudipati, Timothy Goudge, Paola Passalacqua, Ben Cardenas, and the remaining members of the Mohrig Research Group. We acknowledge and thank James Pizzuto and the Earth Surface Processes and Landforms reviewers and editors for their helpful suggestions. Support was provided by the Jackson School of Geosciences and the NSF through the OCE 1135427 and EAR 1547200.

REFERENCES

Bridge, J. S. (2009). Rivers and floodplains: forms, processes, and sedimentary record. John Wiley & Sons.

Brierley, G. J., Ferguson, R. J., & Woolfe, K. J. (1997). What is a fluvial levee? Sedimentary Geology, 114(1-4), 1-9.

Burr, D. M., Enga, M. T., Williams, R. M., Zimbelman, J. R., Howard, A. D., & Brennand, T. A. (2009). Pervasive aqueous paleoflow features in the Aeolis/Zephyria Plana region, Mars. Icarus, 200(1), 52-76.

Durkin, P. R., Hubbard, S. M., Boyd, R. L., & Leckie, D. A. (2015). Stratigraphic expression of intra-point-bar erosion and rotation. Journal of Sedimentary Research, 85(10), 1238-1257.

Durkin, P. R., Hubbard, S. M., Holbrook, J., & Boyd, R. (2017). Evolution of fluvial meander-belt deposits and implications for the completeness of the stratigraphic record. Geological Society of America Bulletin.

Fernandes, A. M., Törnqvist, T. E., Straub, K. M., & Mohrig, D. (2016). Connecting the backwater hydraulics of coastal rivers to fluvio-deltaic sedimentology and stratigraphy. Geology, 44(12), 979-982.

Hassenruck-Gudipati, H.J., Mohrig, D.C., and Passalacqua, P. Characterizing natural levee morphology for a sand-bed coastal river. Abstract 202-4, Geological Society of America Annual Meeting, Seattle, WA. October 22-25, 2017.

Hickin, E. J. (1974). The development of meanders in natural river-channels. American journal of science, 274(4), 414-442.

Hickin, E. J., & Nanson, G. C. (1975). The character of channel migration on the Beatton River, northeast British Columbia, Canada. Geological Society of America Bulletin, 86(4), 487-494.

Hudson, P. F., & Kesel, R. H. (2000). Channel migration and meander-bend curvature in the lower Mississippi River prior to major human modification. Geology, 28(6), 531-534.

Ielpi, A., & Ghinassi, M. (2014). Planform architecture, stratigraphic signature and morphodynamics of an exhumed Jurassic meander plain (Scalby Formation, Yorkshire, UK). Sedimentology, 61(7), 1923-1960.

Jackson, R.G. (1976) Large scale ripples of the lower Wabash River. Sedimentology, 23, 593-623.

Lamb, M. P., Nittrouer, J. A., Mohrig, D., & Shaw, J. (2012). Backwater and river plume controls on scour upstream of river mouths: Implications for fluvio-deltaic morphodynamics. Journal of Geophysical Research: Earth Surface, 117(F1).

Leopold, L. B., Wolman, M. G., and Miller P. (1964). Fluvial processes in geomorphology. Dover Publications.

Lewin, J., & Ashworth, P. J. (2014). The negative relief of large river floodplains. Earth-Science Reviews, 129, 1-23.

Mason, J. & Mohrig, D. (2018). Using time-lapse lidar to quantify river bend evolution on the meandering coastal Trinity River, Texas, USA. Journal of Geophysical Research: Earth Surface, 123. https://doi.org/10.1029/2017JF004492

McGowan, J. H., and L. E. Garner (1970), Physiographic features and stratification types of coarse-grained point bars: Modern and ancient examples, Sedimentology, 14, 77–111.

Moore, J. M., & Howard, A. D. (2005). Large alluvial fans on Mars. Journal of Geophysical Research: Planets, 110(E4).

Moore, J. M., A. D. Howard, W. E. Dietrich, and P. M. Schenk (2003), Martian Layered Fluvial Deposits: Implications for Noachian Climate Scenarios, Geophys. Res. Lett., 30, 2292, doi:10.1029/2003GL019002, 24.

Nanson, G. C. (1980). Point bar and floodplain formation of the meandering Beatton River, northeastern British Columbia, Canada. Sedimentology, 27(1), 3-29.

Nanson, G. C. (1981). New evidence of scroll-bar formation on the Beatton River. Sedimentology, 28(6), 889-891.

Nanson, G. C., & Croke, J. C. (1992). A genetic classification of floodplains. Geomorphology, 4(6), 459-486.

Nanson, G. C., & Hickin, E. J. (1983). Channel migration and incision on the Beatton River. Journal of Hydraulic Engineering, 109(3), 327-337.

Nilsson, G. and Martvall, S. (1972) The Ore River and its Meanders. Uppsala Univ., Dept. phys. Geugr. Urgi. Rep. 19.

Nittrouer, J. A., Allison, M. A., & Campanella, R. (2008). Bedform transport rates for the lowermost Mississippi River. Journal of Geophysical Research: Earth Surface, 113(F3).

Nittrouer, J. A., Shaw, J., Lamb, M. P., & Mohrig, D. (2012). Spatial and temporal trends for water-flow velocity and bed-material sediment transport in the lower Mississippi River. Geological Society of America Bulletin, 124(3-4), 400-414.

Pratt, V. (1987). Direct least-squares fitting of algebraic surfaces. In ACM SIGGRAPH computer graphics (Vol. 21, No. 4, pp. 145-152). ACM.

Rodnight, H., Duller, G. A. T., Tooth, S., & Wintle, A. G. (2005). Optical dating of a scroll-bar sequence on the Klip River, South Africa, to derive the lateral migration rate of a meander bend. The Holocene, 15(6), 802-811.

Schon, S. C., Head, J. W., & Fassett, C. I. (2012). An overfilled lacustrine system and progradational delta in Jezero crater, Mars: Implications for Noachian climate. Planetary and Space Science, 67(1), 28-45.

Smith, V. B. (2012). Geomorphology of a coastal sand-bed river: Lower Trinity River, Texas. PhD dissertation.

Sundborg, A. (1956). The River Klaralven, a study of fluvial processes. Geogr. Annlr, 38, 127-316.

van de Lageweg, W. I., van Dijk, W. M., Baar, A. W., Rutten, J., & Kleinhans, M. G. (2014). Bank pull or bar push: What drives scroll-bar formation in meandering rivers?. Geology, 42(4), 319-322.

Wang, J, and Bhattacharya J.P. (2017). Plan-view Paleochannel Reconstruction of Amalgamated Meander Belts, Cretaceous Ferron Sandstone, Notom Delta, South-central Utah, U.s.a.. Journal of Sedimentary Research; 88 (1): 58–74. doi: https://doi-org.ezproxy.lib.utexas.edu/10.2110/jsr.2017.77

Zen, S., Gurnell, A. M., Zolezzi, G., & Surian, N. (2017). Exploring the role of trees in the evolution of meander bends: The Tagliamento River, Italy. Water Resources Research.

Chapter 3: Using time-lapse lidar to quantify channel bend evolution[2]

ABSTRACT

Time-lapse airborne lidar on the coastal Trinity River in Texas, USA, shows profound downstream variability in point bar growth and cut bank erosion resulting from a historically large flood that occurred in 2015. The difference map generated from two surveys covers 55 river bends and captures the transition from quasi-uniform flow into backwater flow. In the upstream portion of the survey, reach-averaged deposition is greater than erosion, with high local variability between the two due to the occurrence of bend cutoffs. Point bars shift laterally up to 3 times as much as cut bank retreat in this area. In the backwater zone, cut bank erosion consistently outpaces deposition on point bars and cut bank retreat exceeds the lateral shift of the point bar. Edge-to-edge channel width, measured from active scroll bar to outer bank, increases for all bends. This widening is often partially due to point bar widening and movement of the scroll bar away from the channel. The combination of net erosion and limited lateral movement of point bars within the backwater zone implies that during large sustained floods, bank pull instigates channel migration in this area. Farther upstream, net deposition and the high ratio of point bar to cut bank lateral motion imply bar push is more important. Patterns of deposition and erosion within a single bend suggest that channel migration was dominated by downstream

---

[2] This chapter was published by authors Jasmine Mason and David Mohrig in the Journal of Geophysical Research: Earth Surface in 2018. https://doi.org/10.1029/2017JF004492. As first author, I was responsible for designing the project, collecting the field data, data processing and analysis, and writing and submitting the paper. David Mohrig provided project guidance and edits.

bend translation with little bend deformation. Results from this study help to deepen the understanding of coastal river system morphodynamics by connecting changes in the geomorphology to changes in river bend kinematics, hydraulics, and sediment transport.

INTRODUCTION

The coevolution of point bars and cut banks in the channel bends of meandering rivers is incompletely understood. While we have long recognized the basic transport physics governing point bar development (Allen 1985; Engelund 1974; Kikkawa et al. 1976), as of yet we do not understand specifics about what controls their geometry and growth in natural channel bends. Point bars are linked to bend migration, acting as topographic obstructions to flow that steer water toward the outer bank, enhancing outer bank erosion (Dietrich & Smith, 1983; Eke et al., 2014). Conversely, experiments have shown that erosion along the outer banks of bends and an associated local widening of the channel can promote sedimentation on point bars (Eke et al., 2014; van de Lageweg et al., 2014). Recent modeling efforts have moved away from centerline descriptions of bend kinematics and have begun to decouple the inner and outer channel banks in an attempt to distinguish how their independent motions lead to bend migration and deformation (Eke et al., 2014; Parker et al., 2011). The case where erosion at the outer bank is forced by a more rapidly accreting point bar is referred to as bar push, while deposition at the point bar being forced by a more rapidly eroding outer bank is called bank pull.

While this new generation of models provides results that hugely impact how we think about river systems, they are in desperate need of validation from field data sets that independently measure change to the inner and outer banks of channel bends. Difference maps created from time-lapse airborne lidar data provide a unique opportunity to observe

how bends within natural channels evolve through time. However, lidar data sets only resolve the subaerial portions of channels. The incorporation of bathymetry data is necessary to fully estimate the total changes to deposition or erosion along the inner and outer banks.

While the most distal tail of point bars is often built from suspended sediment deposition in a hydraulic separation zone (Ghinassi et al., 2016; Leeder & Bridges, 1975; Smith et al., 2009), the volumetric majority of a point bar is typically built from deposition of bed-material load (Allen, 1985) as shown by dune-scale cross stratification that is directly observed in point bar trench walls and geophysically imaged using ground-penetrating radar (Allen, 1963; Bridge et al., 1995; Frazier & Osanik, 1961). Point bar growth is therefore considered sediment deposition within the channel along the inner bank of the river. Scroll bars are the arcuate topographic ridges formed at the landward edges of point bars. They are often used to interpret the previous positions of inner banks and to reconstruct historic bend migration patterns. While there are few studies on the conditions necessary for scroll bar formation, a leading hypothesis cites flow separation over the point bar as a potential cause for the preferential deposition of suspended sediment (Nanson, 1980). In this case, the scroll bar marks the edge of bed-material deposition and thus the landward edge of the point bar and the transition to floodplain or overbank along the inner bank of river bends.

The gradually varied flow in rivers nearing their outlets is well understood by engineers and hydrologists (Chow, 1959; Lane, 1957) and is commonly referred to as the backwater effect. Recent research has begun to focus on how the downstream hydraulic transition from quasi-uniform flow to backwater flow might influence river avulsion sites (Chatanantavet et al., 2012; Edmonds et al., 2009; Hoyal & Sheets, 2009), as well as shifts in river channel geometry and river bend migration rate (Fernandes et al., 2016; Hudson &

Kesel, 2000; Lamb et al., 2012; Nittrouer et al., 2012; Smith, 2012). Results show unambiguous spatial changes in large-scale channel geomorphology as well as inferred temporal shifts in sediment transport (Nittrouer et al., 2011).

The Trinity River in east Texas, USA, has a drainage basin of 40,000 km2 and an average annual discharge of about 200 m^3/s at Romayor, TX (Figure 3.1). This project uses time-lapse airborne lidar data (from 2011 to 2015) together with bathymetric measurements to measure erosion and deposition within channel bends of the coastal Trinity River. For 55 days in 2015, the Trinity River was above the National Weather Service flood stage (defined by a discharge of 850 m3/s at Liberty, TX; Figure 3.1). Throughout the remainder of the time period covered by the lidar, the river was in an extended period of drought, reaching flood stage for a total of only 14 days spread out over multiple events. The 65 river kilometers covered in the two surveys encompass an upstream portion of quasi-uniform flow and the complete transition into backwater flow. The results document patterns and amounts of sediment added to point bars and removed from the outer banks of 55 successive river bends. Differences in the channel before and after the flood (both in individual bends as well as throughout the entire survey reach) were measured to observe the effect of the prolonged high discharge on the river's geomorphology. Trends and correlations in measured variables reveal interesting details about how the backwater effect changes point bar and cut bank shapes and growth and deepens the understanding of river bend kinematics.

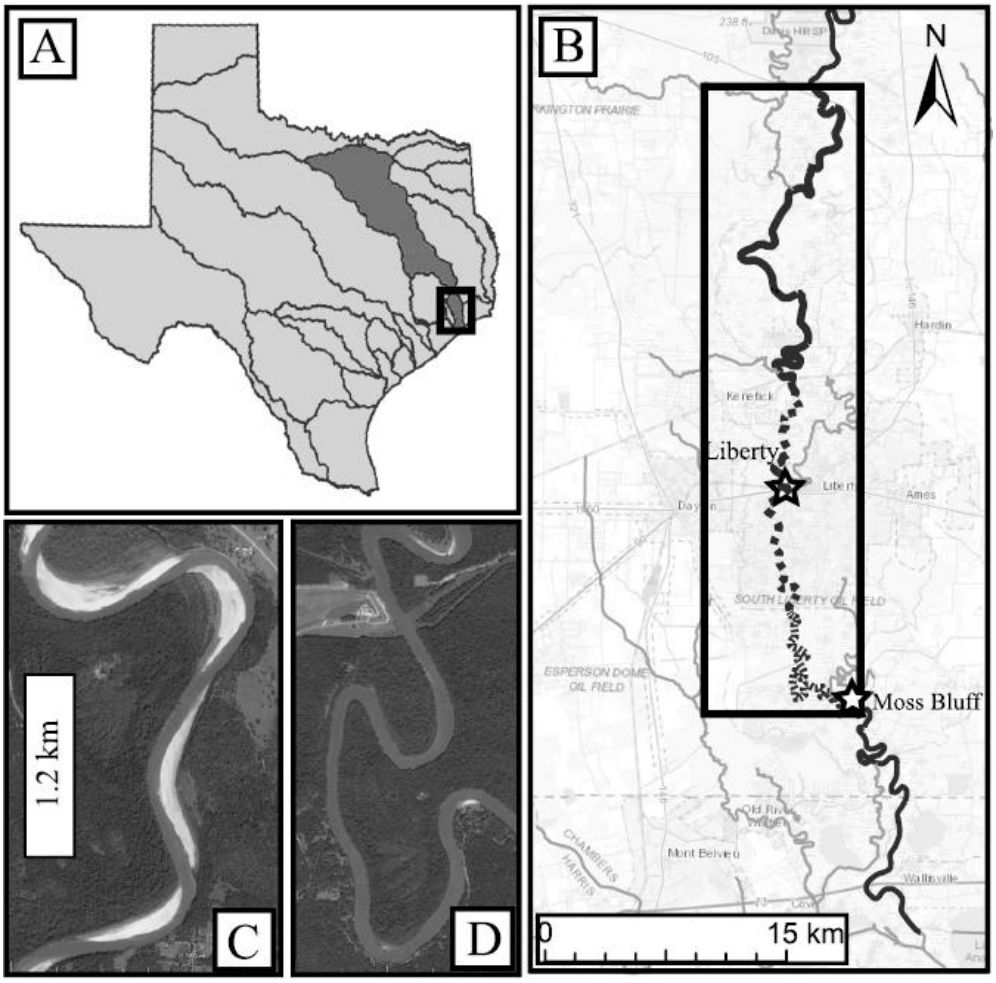

Figure 3.1: Map of the study area

A) The state of Texas with the Trinity River watershed filled in dark gray. Bold black box indicates the lower Trinity River. B) Map showing the 55-channel bends included in this study within the long black rectangle. Bold, dashed, and dotted lines represent the quasi-uniform, transitional, and backwater reaches, respectively. Liberty and Moss bluff USGS stations are marked and labeled with stars. The Romayor USGS station is located 30 km upstream of the survey start. C) Aerial photograph of several bends from the quasi-uniform portion of the river, exhibiting large sandy point bars. D) Aerial photograph of several bends from the backwater portion of the river with much little to no subaerial point bars. Figures 1c and 1d are at the same scale and were taken on the same day, so water discharge between the two sites is ~ equal. USGS = U. S. Geological Survey.

DATA AND METHODS

Two bare-Earth lidar data sets were used for this study. The first was collected by the Federal Emergency Management Agency in January of 2011 using a Leica ALS60 lidar system with a reported vertical accuracy within 15 cm of the known elevation and 1-m horizontal resolution. The second was collected in August 2015 by the National Center for Airborne Laser Mapping using an Optech Titan with a reported vertical accuracy within 5–15 cm of the known elevation and rasterized to 1-m horizontal resolution. These data sets were differenced in ArcMap 10.3 to observe areas of elevation change associated with sediment deposition or erosion. Zero net change on widely distributed engineering structures was used to confirm the accuracy of the difference map.

Two United States Geological Survey gaging stations are located within the survey area (one at Liberty, TX 08067000 and the other at Moss Bluff, TX 08067100) and provided stage and discharge data. Water levels at the upstream end of the reach of interest during the 2015 survey were about a half a meter higher than the 2011 survey. During the 4.4 years prior to the late spring-early summer flood of 2015, the Trinity River at Liberty had been in an extended period of drought, reaching flood stage for a total of only 14 days. Differences observed in the lidar surveys are therefore proposed to be primarily the consequence of the 55 consecutive days of flooding experienced from May to July of 2015, an unprecedented event since the installation of the Liberty gage station in 1938.

Fifty-five bends covering 65 river kilometers were included in this study (Figure 3.1). Two bends whose geometry was noticeably altered by human infrastructure were intentionally left out of the study as they are not representative of the behavior of an unperturbed system. While bends are traditionally defined as the channel segments between successive points of centerline inflection, the lidar data clearly show that the paired sites of inner bank deposition and outer bank erosion are lagged downstream by an

average of 30% of a bend length. This downstream shift in the foci of deposition and erosion tied to characteristic bends is shown in Figure 3.2. The spatial lag in deposition on point bars and erosion of the outer bank was sufficient so that both typically extended beyond the downstream inflection point defining their associated channel bend (Figure 3.2). On average, the combined length of the deposition and erosion zones equaled 85% of the associated bend length. The channel segments associated with the combined lengths of inner and outer bank change are hereby termed the operational bends.

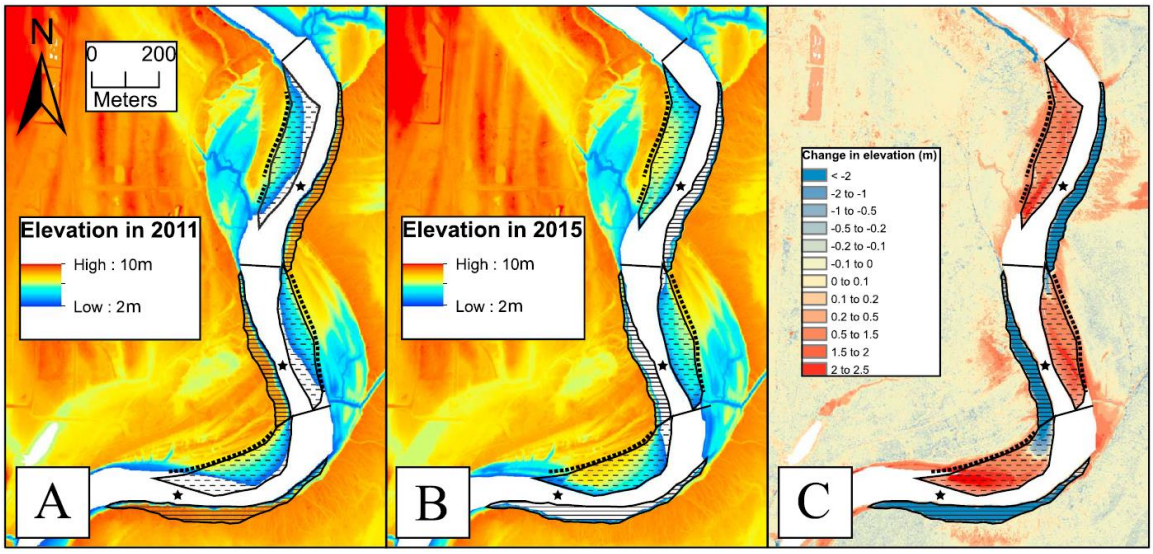

Figure 3.2: Example map showing the measurement scheme

Bends 22, 23, and 24 (river kilometer 31–33). Flow is from top to bottom. A) 2011 lidar survey, A) 2015 lidar survey, and C) 2015 minus 2011. Point bar polygons are outlined and filled with dashed lines, and cut bank polygons are outlined and filled with horizontal lines. Sites of enhanced deposition of suspended sediment defining the 2015 scroll bars are marked with a bold dashed line. Landward point bar edges are defined by the position of the 2015 scroll bars and on the outer edge by the maximum extent of the subaerial point bar between the two surveys. Centerline inflection points are marked with black stars, and operational bend limits are marked with solid black lines. Notice that operational bend limits lag downstream of inflection points. In Figure 3.2c, notice that the cut bank width increases downstream and that point bar deposition is thickest at the downstream edge of each bar. Bends 23 and 24 are two of the most erosive bends and include significant removal of the point bar by the upstream cut bank. In addition, these bends are unusually short compared to others in the survey reach because a recent cutoff occurred immediately upstream of bend 22.

The landward edge for the inner bank of every channel bend was defined by the scroll bar, an arcuate and elongate ridge that repeated trenching has revealed is constructed of sediment primarily deposited from suspension. Growth of the scroll bar is therefore considered proximal overbank deposition as opposed to bed material deposition inside the active channel. Vegetation line was not used to demarcate the inner bank as the presence of vegetation is too dependent on the season, recent precipitation, and the amount of time

that has passed since the last flood. Scroll bars represent the geomorphic channel edge and were considered more appropriate for use in this study. The position of the most channelward scroll bar was used to define the landward edge of the subaerial point bar polygon (Figure 3.2). The channelward edge of the subaerial point bar polygon was defined by the channel-most extent of either the 2011 or the 2015 bar form (Figure 3.2). These areas represent the combined area of change between 2011 and 2015 and thus are likely larger than the planform area of the subaerial point bar from either individual survey. The cut bank erosion was defined as the area separating the outer edge of the channel in 2011 and the outer edge of the channel in 2015. Widths associated with cut bank erosion were measured every 100 m perpendicular to the 2015 channel centerline. Cut bank erosion occasionally extended into the upstream ends of point bars in subsequent bends, and in these cases the cut bank erosional area was terminated at the upstream extent of the antecedent point bar. Areas were calculated by counting the number of 1 m pixels within each polygon. Subaerial volumes of eroded or deposited topography were calculated in ArcGIS by summing the z values on the difference map for every 1 × 1 m pixel within each point bar or cut bank polygon. Edge-to-edge channel width was measured from inner scroll bar to outer bank. Horizontal movement of the point bar and cut bank was evaluated by measuring their change in position between the two surveys at an elevation not more than 1.5 m above the 2015 water surface for each bend. Measurements were made every 100 m perpendicular to the 2015 channel centerline.

The lidar data used to measure areas and volumes are limited to the subaerial portions of point bars and cut banks. Fortunately, the bathymetry of the river channel is well known from data collected by the Texas Parks and Wildlife Department in 2009–2010. The resulting subaqueous digital elevation model was used in conjunction with the lidar data to estimate the relative subaqueous fractions of the inner and outer bank within

each river bend. Elevations used to calculate these fractions were averaged over three points collected at upstream, central, and downstream portions of each operational bend. Water depth (representing the subaqueous fraction, H) was measured by subtracting the mean elevation of the channel thalweg from the mean elevation of the 2015 water surface for each bend. The subaerial point bar and cut bank fractions (h_{pb} and h_{cb}) were measured by subtracting the mean water surface elevation from the mean elevation of the top of the point bar or cut bank. H and h were then used to calculate the relative subaqueous portion of the channel form, $k_{pb} = (H + h_{pb})/h_{pb}$ and $k_{cb} = (H + h_{cb})/h_{cb}$, at each bend (Figure 3). This modifier was then applied to subaerial volumes of accretion and erosion taken from the lidar difference map in order to estimate the total subaerial plus subaqueous change values. The use of k assumes channel-form motion with little change in point bar or cut bank shape or channel bottom elevation. Seven depth surveys covering 27 river kilometers of the survey area that were collected before, throughout, and following the duration of the flood show no net change in channel bottom elevation. A subset of 29 point bars within the survey shows an average of only 1% change in surface slope, further supporting the use of k in this study. In order to estimate the error associated with the k values, a second-order polynomial was fit to the long profiles of the cut bank tops, point bar tops, water surface, and thalweg elevations. The total error associated with each k value was estimated by calculating the root-mean-square error associated with each long profile and combining and propagating them based on the structure of the algebraic equation defining the k value, assuming the covariance between variables was zero (Bevington, 1969).

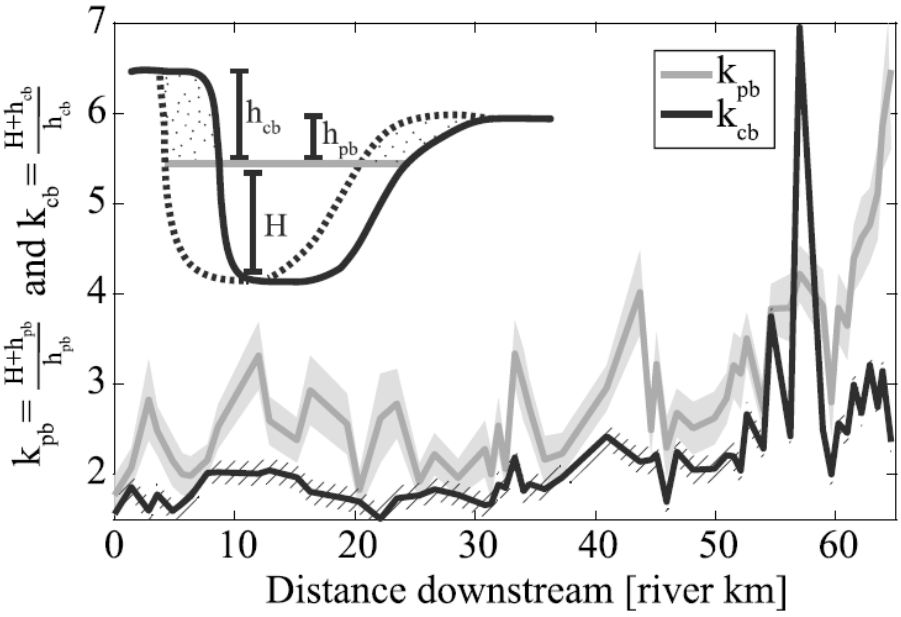

Figure 3.3: Relative sub-aqueous portions (k values) of cut banks and point bars

The relative subaqueous portions of the cut bank (k_{cb}, black line with error highlighted in the hatched background) and the point bar (k_{pb}, dark gray line with error highlighted in light gray) for each bend, calculated using the joined 2009–2010 bathymetric and 2015 lidar digital elevation models. H is the subaqueous height of the channel and h_{cb} or h_{pb} is the subaerial height of the cut bank or point bar. The k values increase toward the coast as the subaerial fraction for each channel cross section decreases moving into the backwater zone. Error associated with these k values decreases with distance downstream as the long profiles for the thalweg, water surface, and cut bank and point bar tops flatten out and spatial variability in elevation decreases. The single bend where k_{cb} is greater than k_{pb} (at river kilometer 57) is due to migration of the bend into the location of a partially filled paleochannel that left the cut bank elevation unusually low.

RESULTS

Individual point bars and cut banks show consistent patterns of deposition and erosion throughout the entire survey reach. The onset of measurable outer bank erosion typically lags downstream of the onset of deposition on the point bar (Figure 3.2c). The downstream end of the point bar regularly has the thickest layer of sediment added to it (Figure 3.2c). In addition, the greatest amount of outer bank retreat is generally located on

its downstream half, directly across the channel from the highly depositional section of the point bar (Figures 3.2c and 3.4). Cut bank widths are never at their maximum value within the first fifth of the bend (Figure 3.4). On average throughout the entire survey, maximum outer bank migration occurred at about 60% of the total operational bend length (Figure 3.4). The most net erosive bends are those where the upstream ends of point bars were partially eroded by the cut banks of bends positioned immediately upstream (Figure 3.2). In addition, 69% of cut banks have a streamwise length of bank erosion that is greater than the streamwise length of the lidar-defined, affiliated point bar deposition.

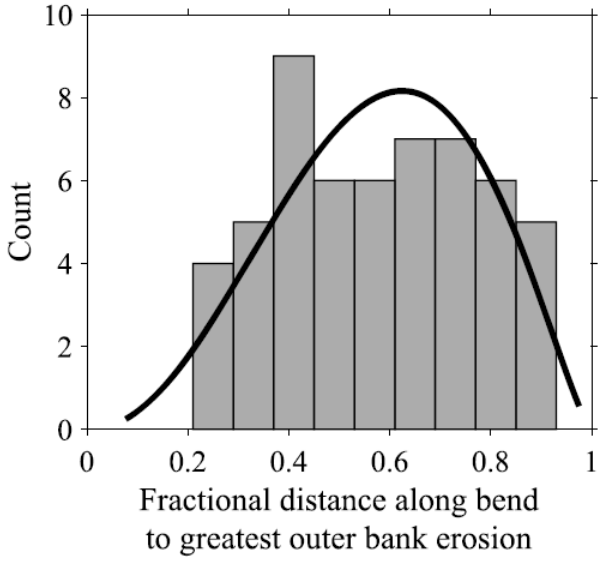

Figure 3.4: Cut bank erosional pattern

Histogram (n = 55, 9 bins) showing fractional bend distance to greatest cut bank erosion between 2011 and 2015 for 55 channel bends on Trinity River. Black line represents a best fit beta distribution to the data, with $\alpha = 3.25$ and $\beta = 2.36$. Downstream measurements were taken every 100 m perpendicular to the 2015 channel centerline. Notice that no bends have a maximum cut bank width that occurs within the first 20% of the total bend length, and the fitted distribution is at a maximum at about 60% of the total bend length.

Spatial change in the hydraulics of the Trinity River throughout the survey area motivated dividing the survey into three separate reaches for thorough analysis. The average elevation for the channel bottom drops below sea level at around river kilometer 30 or bend number 21, defining the maximum backwater extent. Marked downstream change in the pattern of sediment accretion and erosion began at about bend number 22 or river kilometer 31 (Figures 3.3 and 3.5–3.10). Upstream of river km 31, values tend to be large and highly variable. Downstream of that point, magnitudes decrease gradually over 19 km (15 bends) until they reach consistently low values for the last 14 river kilometers (18 bends). For the remainder of this paper, these three reaches will be referred to as the quasi-uniform, transitional, and backwater regions, respectively.

The subaerial volume of material deposited within or eroded from each point bar or cut bank polygon is shown in Figure 3.5. These volumes (for both point bars and cut banks) decrease as the river nears the coast. In addition, the standard deviation for volume measurements in each reach decreases systematically as the river transitions into the backwater zone. The correlation between the point bars and cut bank volumes is further explored by separating the subaerial volume of each polygon into its respective area (Figure 3.6) and its associated average elevation change (Figure 3.7).

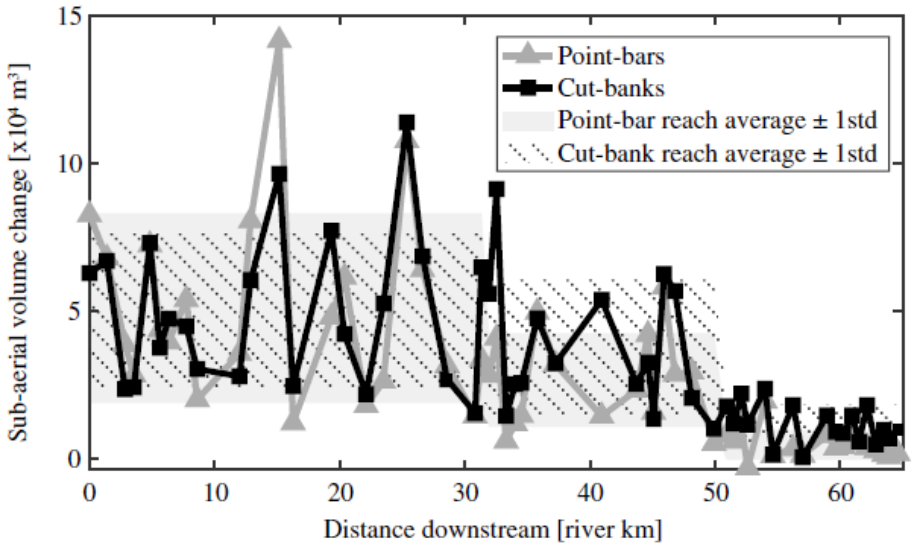

Figure 3.5: Sub-aerial volume change for point bars and cut banks

Point bar (dark gray line and triangles, reach average ± 1 standard deviation shown in the light gray area) and absolute cut bank subaerial volume change (black line and squares, reach average ± 1 standard deviation shown in the hatched area) for each bend. Volumes were measured by summing elevation change values for each point within individual polygons. Absolute values for cut bank volume change are shown to highlight correlation with point bars. Subaerial point bar volume averages for the quasi-uniform, transitional, and backwater reaches are 5.1 × 10^4 m^3 (std = 3.2 × 10^4 m^3), 2.6 × 10^4 m^3 (std = 1.6 × 10^4 m^3), and 4.5 × 10^3 m^3 (std = 5.0 × 10^3 m^3), respectively. Averages for cut banks are 5 × 10^4 m^3 (std = 2.6 × 10^4 m^3), 3.8 × 10^4 m^3 (std = 2.3 × 10^4 m^3), and 1.1 × 10^4 m^3 (std = 6.6 × 10^3 m^3). Wilcoxon rank-sum tests show that the cut bank and point bar volumes for each zone come from distinct distributions at the 2% significance level (except for the comparison of cut bank erosional volumes between the quasi-uniform and transitional zones, which were deemed distinct at the 15% significance level).

Subaerial point bar polygon area decreases by more than an order of magnitude within the region covered by the survey (Figure 3.6). The mean point bar area for the quasi-uniform bends is 7.6 × $10^4$$m^2$, decreasing by 67% to a mean value of 2.5 × 10^4 m^2 for the transitional bends before decreasing an additional 74% to a mean value of 6.7 × 10^3 m^2 for the backwater bends. Standard deviations between reaches also decrease (Figure 3.6). In addition, the streamwise length of point bar deposition equals or exceeds the streamwise

length of cut bank erosion in only 17% of bends within the backwater zone, compared to half of bends in the quasi-uniform flow reach. Aerial photography shows that immediately downstream of the survey reach, the subaerial point bar area decreases to essentially zero as temporal variability in river stage becomes small enough that bars remain subaqueous throughout the year. In spite of this dramatic decrease in subaerial point bar area, the mean elevation change over a single bar stays relatively constant at about 0.8 m of deposition on average throughout the entire reach (with a standard deviation of 0.4 m, Figure 3.7). The single bar that has a negative value for mean elevation change (located in the backwater zone) was significantly eroded into by its upstream cut bank, a phenomenon that affected six other point bars that still managed to be net depositional. Because no systematic trend in deposit thickness was observed (Figure 3.7), the trend in subaerial volume of accumulated deposit on point bars (Figure 3.5) is similar to the subaerial trend in point bar area (Figure 3.6), large volumes upstream (a mean of 5.1×10^4 m^3 in the upstream bends), dropping by 48% to lower values in the transitional area (a mean of 2.6×10^4 m^3) and a further 83% in the backwater zone (at a mean of 4.5×10^3 m^3).

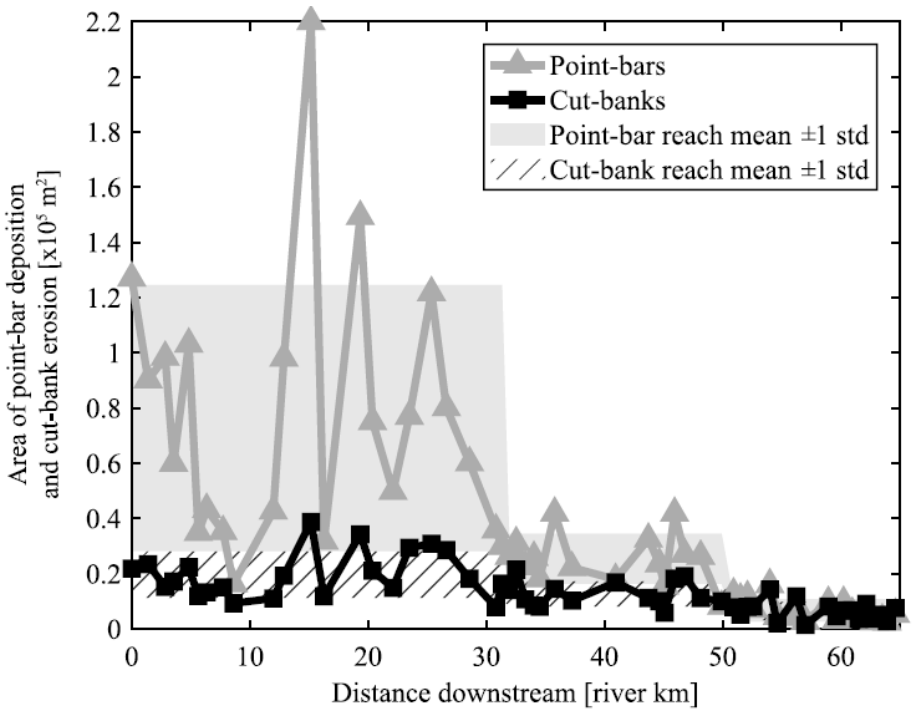

Figure 3.6: Sub-aerial depositional or erosional areas

Areas mapped on the lidar difference map (Figure 3.2c) defining the subaerial point bar deposition (gray triangles) and the area associated with cut bank erosion (black squares). Reach averages ±1 standard deviation are shown in the light gray and hatched areas for the point bars and cut banks, respectively. Point bar area averages for the quasi-uniform, transitional, and backwater reaches are 7.6 × 10^4 m^2 (std = 4.8 × 10^4), 2.5 × 10^4 m^2 (std = 9.1 × 10^3), and 6.7 × $10^3$$m^2$ (std = 4.1 × 10^3), respectively. Averages for cut banks are 2.0 × 10^4 m^2 (std = 8.4 × 10^3), 1.3 × 10^4 m^2 (std = 4.5 × 10^3), and 6.5 × 10^3 m^2 (std = 3.3 × 10^3). Point bar and cut bank areas decrease toward the coast, with the difference between the two decreasing as well. Wilcoxon rank-sum tests done on the reach averages show that each zone is composed of statistically distinct values at the 2% significance level.

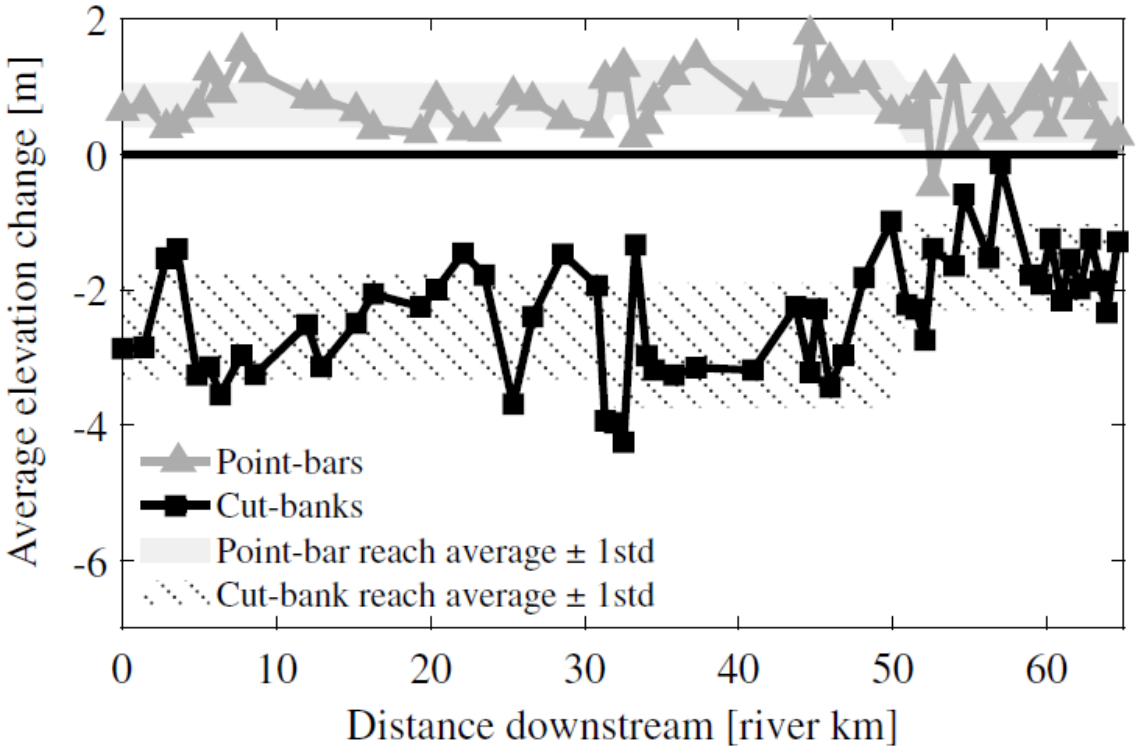

Figure 3.7: Average elevation change for point bars and cut banks

Average change in surface elevation associated with sediment either deposited or eroded from each point bar (gray triangles) and cut bank polygon (black squares) for all 55 successive channel bends. Reach-averaged elevation changes for the quasi-uniform, transitional, and backwater reaches for point bars are 0.7 m, 1.0 m, and 0.6 m respectively; and for cut banks are -2.5 m, -2.8 m, and -1.7 m, respectively. Changes in point bar averages between reaches fall within the standard deviations each zone (0.3 m, 0.4 m, and 0.4 m from upstream to downstream). Cut banks show a larger decrease in the magnitude of elevation change as well as a decrease in the reach standard deviations (0.8 m, 0.9 m, and 0.6 m) as the river approaches the coast. The negative value for the point bar in the bend at river kilometer 53 is due to erosion of an upstream portion of the bar by the upstream cut bank. Wilcoxon rank-sum tests done on point bar reach-averaged elevation change failed to distinguish between the zones at the 2% significance level. The same test done on the cut bank elevation changes shows the decrease between the transitional and backwater zones is statistically significant.

The local and downstream variability in cut bank erosion is well correlated with the measured subaerial point bar deposition (Figure 3.5). River bends with large volumes of

subaerial bar deposition also have higher volumes of material lost to outer bank erosion. Cut bank erosional polygons, unlike point bars, show a relatively minor spatial decrease in area (Figure 3.6) and a larger decrease in the magnitude of subaerial elevation change with distance downstream (Figure 3.7). Cut banks in the zone of quasi-uniform flow have a mean area of 2.0×10^4 m^2 dropping by 67% to 6.5×10^3 m^2 in the channel bends of the backwater zone, a much smaller change compared to the overall 91% decrease in subaerial point bar area. The downstream decrease in eroded volume of subaerial material (Figure 3.5) is therefore roughly equally due to the reduction in area (Figure 3.6) and a reduction in subaerial cut bank height of about 1 m throughout the survey length (Figure 3.7).

These downstream differences highlight the necessity of examining subaqueous as well as subaerial portions of point bars and cut banks. Both the inner and outer banks of channel bends become increasingly submerged as the river approaches the coast. The measured relative subaqueous portions of each bank and each bend (k_{pb} or k_{cb} values) increase with distance downstream (Figure 3.3). The single bend where the k_{cb} value is higher than the k_{pb} value is due to migration of the bend into the location of a partially filled paleochannel that left the cut bank unusually low. Error in the calculation of the k values decreases with distance downstream as the slopes of the long profiles (of the cut bank elevation, point bar top elevation, water surface, and thalweg elevation) decrease and variability around each fitted polynomial declines. Measured subaerial volumes for point bars and cut banks multiplied by their corresponding k_{pb} or k_{cb} value yields the best estimate for the total volume change (subaerial plus subaqueous) that occurred in each bend over the time period (Figure 3.8).

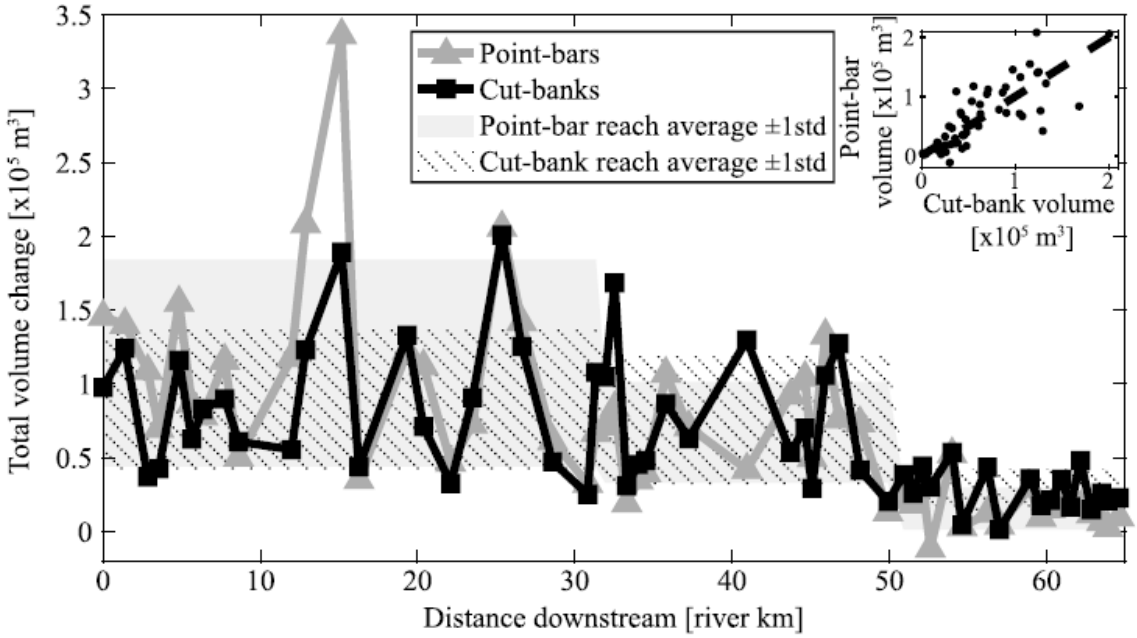

Figure 3.8: Estimated total sub-aerial plus sub-aqueous volume change for point bars and cut banks

Estimated total volume of sediment either added to or removed from each point bar (gray triangles) and cut bank (black squares). These estimated values are produced by multiplying k for each cut bank and bar in each bend (Figure 3.3) and the corresponding subaerial volume differences (Figure 3.5). Hashed and light gray filled areas denote reach means ±1 std for the quasi-uniform (point bar mean 1.1 × 10^5 m^3 and std 7.0 × 10^4 m^3, cut bank mean 1.1 × 10^5 m^3 and std 4.8 × 10^4 m^3) transitional (point bar mean 6.7 × 10^4 m^3 and std 3.4 × 10^4 m^3, cut bank mean 7.5 × 10^4 m^3 and std 4.4 × 10^4 m^3), and backwater reaches (point bar mean 1.6 × 10^4 m^3 and std 1.4 × 10^4 m^3, cut bank mean 2.8 × 10^4 m^3 and std 1.5 × 10^4 m^3; Figure 3.1). Total volumes for the inner and outer banks decrease downstream. The inset compares deposited and eroded volumes from each bend. Most bends fall near the black dashed line, which represents a one-to-one correlation (r^2 = 0.33). Wilcoxon rank-sum tests done on the reach averages show that each zone is composed of statistically distinct distributions at the 5% significance level except for the cut banks within the quasi-uniform and transitional zones, which only become distinct at 39% significance.

Spatial trends in the estimated total volumes of deposited and eroded mass (Figure 3.8) still show decreases in both cut bank and point bar volumes moving into the backwater

zone. Within each bend, volumes of cut bank erosion and point bar deposition are correlated (Figure 3.8, inset). Overall, a Wilcoxon rank-sum test showed that the erosional volumes along the outer bank and depositional volumes along the inner bank are from indistinguishable distributions at the 1% significance level. The net volume change per channel bend (difference between the amount eroded and the amount deposited) is presented in Figure 3.9a. On average, bends within the quasi-uniform reach showed net deposition (mean of 2.5×10^4 m^3), while the backwater and transitional zones were consistently erosional (Figure 9a). The reach-averaged net volume change per bend in the transitional and backwater zones is relatively similar (-7.7×10^3 m^3 and -1.2×10^4 m^3 of eroded material respectively) despite a large decrease in the magnitudes of gross depositional and erosional volumes in the backwater zone (Figure 3.8). Results of a Wilcoxon rank-sum test confirm that the distribution of values within the backwater zone is statistically different from the quasi-uniform values at the 1% significance level. In total, a net of 212,000 m^3 of material was deposited within the survey reach (with 3.8 million m^3 deposited and 3.6 million m^3 eroded).

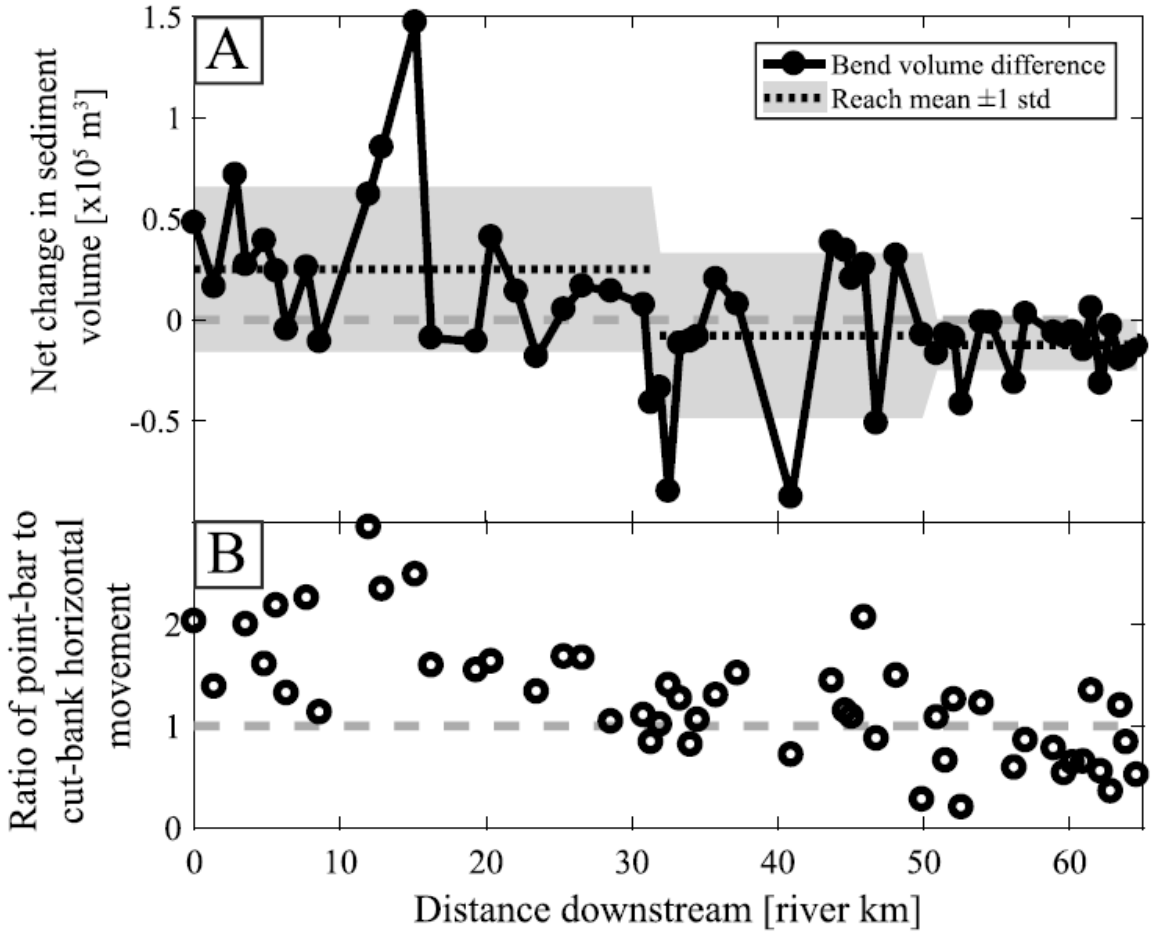

Figure 3.9: Net volume change per river bend and horizontal bank movement

Figure 3.9: Net volume change per river bend and horizontal bank movement
A) Difference between estimated volumes of sediment deposited on the point bar versus eroded from the cut bank for each bend. Dotted black lines and gray areas are averages ±1 standard deviation for the quasi-uniform (mean of 2.5 × 10^4 m^3, std of 4.1 × 10^4 m^3), transitional (mean of -7.7 × 10^3 m^3 and std of 4.1 × 10^4 m^3), and backwater reaches (mean of -1.2 × 10^4 m^3 and std of 1.3 × 10^4 m^3; Figure 1). Dashed gray line marks 0 net change. All bends with a volume difference above 0 are net depositional, and all bends below are net erosional for the 2011–2015 time interval. Upstream, bends tend to be net depositional while net erosion dominates in the transitional and backwater zones. Results of a Wilcoxon rank-sum test confirm that the distribution of values within the backwater zone is statistically different from the quasi-uniform values at the 1% significance level.
B) Ratio of point bar horizontal movement to cut bank horizontal movement for each bend. Gray dashed line represents equal movement. Horizontal motion was measured every 100 m along the channel centerline at an elevation not more than 1.5mabove the 2015 water surface and was averaged to obtain a single value for each bend. In the quasi-uniform zone, point bars tended to migrate more than the outer bank while the opposite was true within the backwater zone.

Corresponding with the change from net depositional bends upstream to net erosional bends downstream is a shift in the relative lateral motions of point bars and cut banks (Figure 3.9b). Bend-averaged point bar lateral motion ranged from -2.5 m (due to erosion of the bar) to 31 m. Bend-averaged cut bank motion ranged from 3.2 to 23 m. Upstream, bars can shift laterally as much as 3 times more than the amount of cut bank retreat. Within the backwater zone, cut banks tended to move more laterally than point bars.

Edge-to-edge widening of the channel as defined by the distance from active scroll bar to outer bank between the two survey dates was observed in all bends (Figure 3.10). In the quasi-uniform zone, an average of 22.1 m of widening was enabled through outward migration of the outer bank as well as in many cases migration of the inner bank away from the channel centerline (Figures 3.10 inset and 3.11). Widening gradually decreases downstream (a combined average of 12.8 m of widening occurred within the transitional and backwater zones) via a decrease in the lateral movement of both the inner and outer banks. Widening due to movement of the scroll bar away from the channel centerline was measured in the majority of surveyed bends (32 out of 55). A Wilcoxon rank-sum test shows that the measured distribution of inner bank movements is unique from a randomly generated normal distribution with a mean of zero and an identical standard deviation at the 10% significance level, implying that the average movement of scroll bars away from the channel centerline was statistically significant.

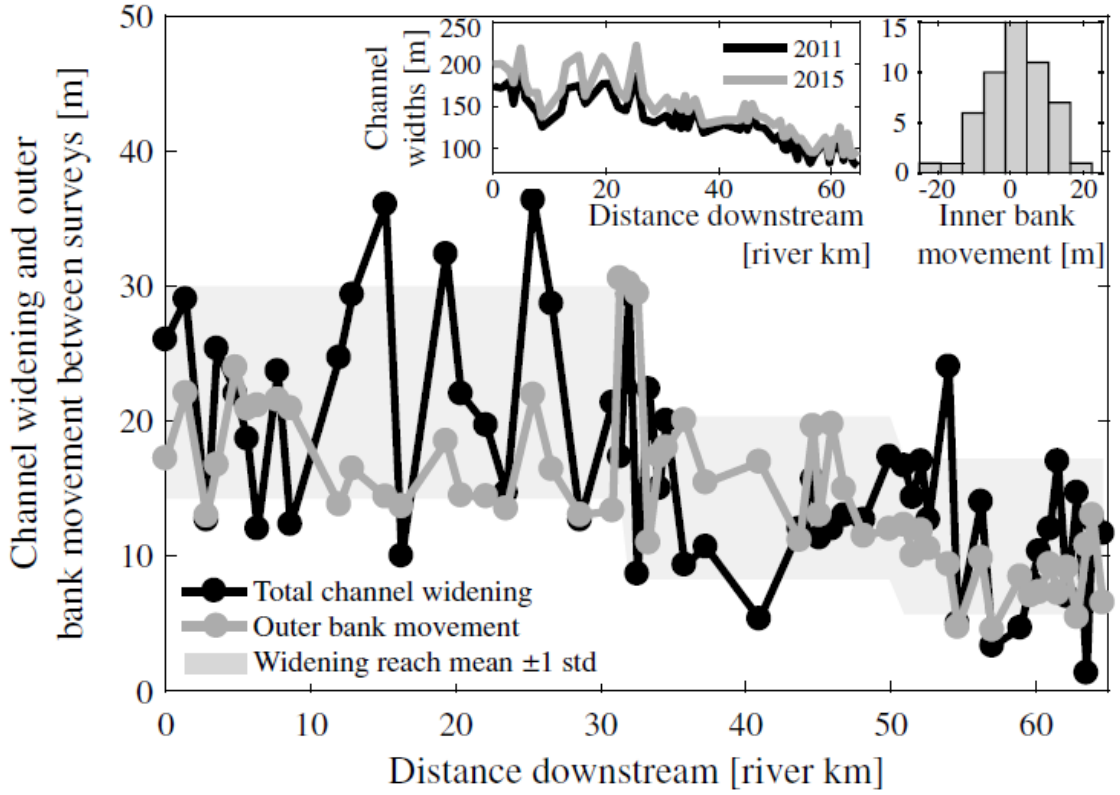

Figure 3.10: Edge-to-edge channel widening

Figure 3.10: Edge-to-edge channel widening
Edge-to-edge channel widening (black points and line, reach averages ±1 std filled in light gray) and outer bank movement (dark gray points and line) between the 2011 and 2015 lidar surveys. Reach-averaged widening was 22.1 m (std = 7.9 m), 14.3 m (std = 6.0 m), and 11.4 m (std = 5.8 m) for the quasi-uniform, transitional, and backwater zones, respectively. A Wilcoxon rank-sum test confirms that the distribution of bank-to-bank widening values in the quasi-uniform zone is distinct from the backwater distribution of values at the 2% significance level. Channel width values for both surveys (top left inset) were averaged from three separate measurements per bend. Outer bank movement was estimated using the average cut bank width measured every 100 m perpendicular to the channel centerline. All bends exhibited edge-to-edge channel widening. In 32 of 55 bends, the amount of channel widening is greater than the amount of outer bank movement due to landward migration of the inner bank as indicated by the position of the scroll bar. Top right inset shows a histogram of the inner bank movement between surveys (channel widening value minus outer bank movement value for each bend) with positive values indicating landward motion and negative values indicating channelward motion. The distribution of values is positively skewed, meaning most bends experienced scroll bar movement away from the channel centerline. Note that the inner and outer bank motions are not necessarily persistent throughout the entire length of each bend, especially because erosion of the cut bank typically does not occur along the upstream portions of bends.

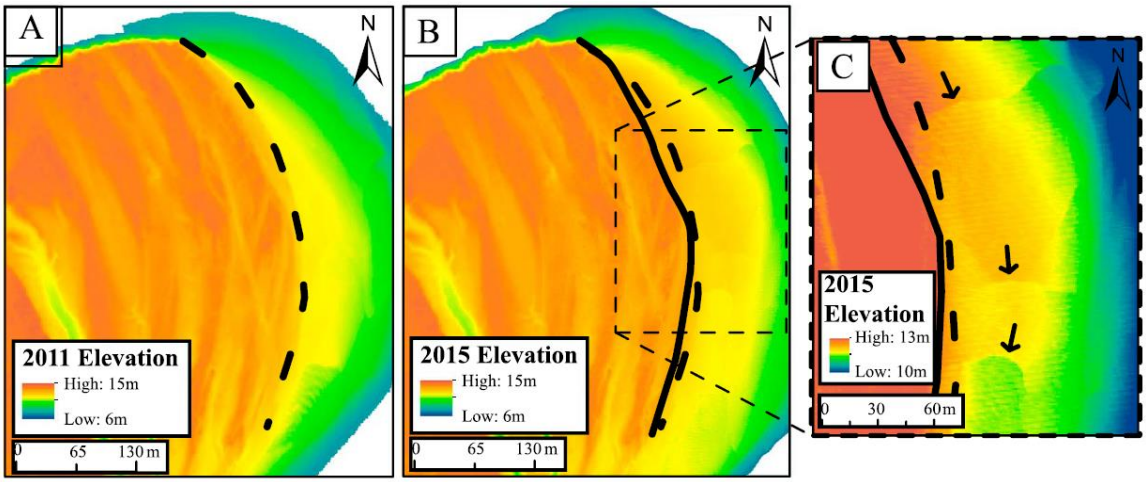

Figure 3.11: Landward motion of scroll bar marking inner edge of channel

Time-lapse lidar data showing an example of channel widening along the inner bank. The bend presented here is within the quasi-uniform flow zone. A) The 2011 elevation with the edge of the scroll bar defining the inner bank mapped in the black dashed line. B) The 2015 elevation with the edge of the scroll bar defining the inner bank mapped in the solid black line with the 2011 inner bank position in the dashed line for reference. C) A zoomed in portion of the 2015 elevation map highlighting the presence of bed forms (marked with arrows) along the previous 2011 inner bank.

DISCUSSION

The observed spatial variability in both point bar and cut bank change reveals interesting details about this system specifically, as well as fluvial morphodynamics and river-channel kinematics in general. Trends within a single bend and throughout the transition from quasi-uniform flow to backwater flow will be discussed here.

The position of greatest removal of cut bank material and outward bank shift was most likely to occur at a distance equal to about 60% of the operational bend length (Figures 3.2c and 3.4). The location of greatest sediment deposition on the point bar was typically directly across the channel from the zone of maximum erosion along the outer bank. The pattern of erosion and deposition sets the behavior of the channel migration. Meandering

rivers typically migrate via a combination of bend deformation and bend translation (bend expansion and translation of Bridge & Demicco, 2008). Pure deformation of river bends requires that erosion along the outer bank is subequal along the entire bend length (Figure 3.12), while pure bend translation requires erosion only along the downstream portions of bends. Bend extents as they are defined here typically lag downstream of the traditional definition of a bend as the distance between two centerline inflection points (see Data and methods section). Therefore, this downstream preference for erosion and deposition is amplified when using the customary definition of a bend (Figure 3.2c). This observation implies that migration in this portion of the Trinity River was dominated by bend translation within the time period captured by the two lidar surveys.

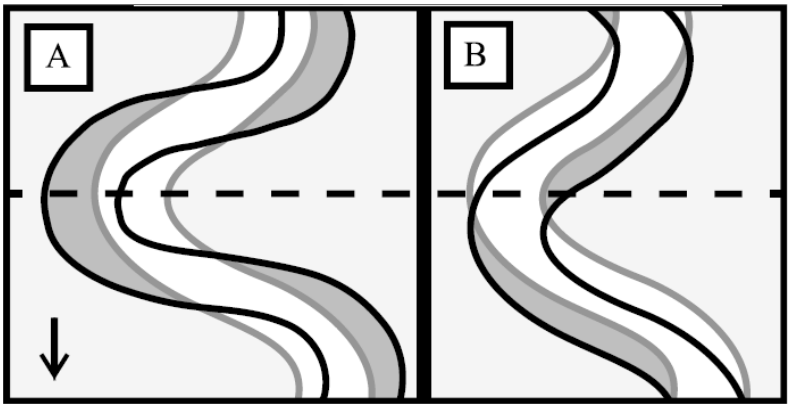

Figure 3.12: Bend deformation vs. bend translation

Idealized planform geometry of river bends at 2 times showing erosional patterns resulting from A) bend deformation and B) bend translation. Flow is from top to bottom. The initial and final positions of the channel are marked in gray and black lines, respectively. The bend apex is marked with a dashed black line. The eroded portion of the floodplain is denoted by the dark gray fill. With pure bend deformation (A), cut bank erosional width is distributed evenly above and below the bend apex. With pure bend translation (B), erosion is only present downstream of the bend apex.

The magnitude of local variability in cut bank erosion and point bar deposition changed downstream as the river transitioned into the backwater zone (as shown by a decrease in the standard deviation of net volumes in each reach; Figures 3.5, 3.8, and 3.9a). In the quasi-uniform and transitional regions, bend cutoffs are relatively commonplace. We hypothesize that the local, bend-to-bend variability in volume change is related to the amount of time that has passed since the bend has experienced cutoff. For example, bends 22 and 23 (in the transitional zone, Figure 3.2) are both low-amplitude bends that developed as a result of a ~20-year old cutoff immediately upstream. These two were some of the most highly erosional bends with outer bank migration that is actively growing bend amplitude (Figures 3.2, 3.8, 3.9a and 3.10). In the backwater zone where bend cutoffs are not observed, bend-to-bend variability in volume change is low.

While the subaerial data are useful for determining patterns of deposition and erosion within individual bends, it is insufficient for evaluating total volumes of change, especially in coastal regions where the sub-aerially exposed portions of channel decrease downstream. Because separately collected data show very little change in the slope of point bars and the long profile of the channel bottom over the duration of the flood, a single bathymetric survey combined with the lidar data are sufficient for characterizing the total volumes of change. With that said, the trend of decreasing total volumes within the backwater zone does not appear to be vastly different from the subaerial volume trends (compare Figure 3.5 to Figure 3.8). Subaerial point bars show a 91% decrease in reach-averaged volumes from upstream to downstream while the estimated total volume shows an 83% decrease. Cut banks decrease in subaerial volume by 77% while total volumes decrease by 69%. However, using the k values becomes important when estimating total net volumes (Figure 3.9a). Since cut banks are higher in elevation than the tops of point

bars, solely looking at subaerial net volumes will consistently overestimate the amount of erosion that occurred within the bend.

The estimated total net volume changes for each bend show compelling spatial trends (Figure 3.9a). On average, bends in the zone of quasi-uniform flow are strongly depositional with a net gain of 2.5×10^4 m^3 per bend (Figure 3.9a). Net volumes decrease through the transitional zone until they reach a mean of 1.2×10^4 m^3 of material eroded within each bend of the backwater zone. This shift from net depositional bends to net erosional bends is accompanied by a decrease in the relative lateral motion of point bars compared to the outer banks (Figure 3.9b). In the quasi-uniform zone, the combination of net deposition and increased lateral movement of point bars compared to cut banks points toward the importance of bar push. The large point bars in this zone obstruct the flow and topographically steer the high velocity core of the flow toward the outer bank, enhancing erosion (Dietrich & Smith, 1983; Eke et al., 2014).

The connection between edge-to-edge channel widening and overall erosion is more nuanced than expected, as highlighted by the quasi-uniform flow zone. The channel in this reach widens along its edges by about twice as much as the transitional and backwater zone (22 m as opposed to 14 m and 11 m; Figure 3.10) despite being net depositional on average (Figure 3.9a). This apparent paradox is explained by the movement of the inner banks of bends (defined by the position of the scroll bars) away from the channel centerline (Figure 3.11). During the flood, a widened swath of bed-material transport either removed and/or buried the 2011 scroll bars in the majority of bends. In addition, significant suspended sediment deposition defining the proximal overbank built new scroll bars at positions further away from the channel centerline. Thus, the widening of these bends was not solely associated with increased erosion, as the outward movement of the inner bend was primarily defined by widening of the point bar, a depositional

process. While widening along the inner bank still occurred in the transitional and backwater reaches, it was greatly decreased. The majority of channel widening within these two zones was due to erosion of the cut bank (on average for these regions, inner banks moved just 0.1 m outward while the outer banks moved 12.7 m outward). The overall prevalence of erosion in the transitional and backwater portions of the survey (Figure 3.9a) combined with edge-to-edge channel widening (Figure 3.11) and increased lateral motion of cut banks compared to point bars (Figure 3.9b) suggests that during this large, sustained flooding event, lateral channel migration in this region was driven mainly by bank pull as opposed to bar push (Dietrich & Smith, 1983; Eke et al., 2014).

Subaerial point bar area decreases with distance downstream (Figure 3.6). This is expected given the decrease in the range of river stages that occur along the backwater portion of the river. At the Romayor U. S. Geological Survey station (USGS station 08066500, 29 km upstream of the lidar start), the difference in water surface elevation between low discharge and the peak flood discharge in 2015 was 7.6 m. At the downstream extent of the survey area, the difference in stage was 3.9 m (this value includes the rise in water surface associated with storm surge). Bars can build up to the water surface, making them higher and larger in the upstream zone where the stage range is greatest, while bar growth in the backwater zone is restricted due to the limited increase in water depth during floods. The measured decrease in area of the point bars is accompanied by a change in the geometry of the bars, as noted by Smith (2012). Bars in the backwater zone have higher lateral slopes compared to their upstream counterparts (Smith, 2012) and take up a smaller fraction of channel width. The 83% decrease in total depositional volumes between the quasi-uniform flow zone and the backwater zone (Figure 3.8) is therefore more or less due to the diminishing surface area of point bars on which the sediment was able to be deposited.

The average depth of sediment added to each point bar stays relatively constant at 0.8 m (± 0.4 m) throughout the entire survey reach (Figure 3.7). This observation implies that sediment deposition rates on point bars during the flood were comparatively similar throughout the whole survey and stands in stark contrast to the hypothesized sediment deposition rates associated with low to moderate flows. During these discharges, the wetted cross-sectional area of the channel increases as the river approaches its outlet (Nittrouer et al., 2012; Smith, 2012). This change leads to a spatial deceleration in the flow, which drives a spatial convergence in bed-material load and higher deposition rates at the upstream end of the transition into backwater flow with low to negligible deposition rates inside of the backwater zone (Allen, 1985; Nittrouer et al., 2012; Smith, 2012).

The area of the eroded cut banks does not decrease as significantly as the point bar area does (Figure 3.6). However, the elevation associated with each cut bank polygon decreases with distance downstream (Figure 3.7). Again, this is expected due to the downstream trend in stage variation. Upstream, where the water height changes drastically between low and flood discharge, cut banks are higher and more material is lost per meter of lateral erosion. In the backwater zone, the height of the cut banks is smaller and so less material is eroded per meter of lateral movement of the channel. It is the combination of a small change in cut bank erosional area and a decrease in cut bank height with distance downstream that allows the volume of sediment removed to considerably decrease as the river approaches the coast (Figures 3.5 and 3.8).

CONCLUSIONS

Over the 4-year time span between lidar surveys, the coastal Trinity River in east Texas has undergone significant measureable changes, the magnitudes of which vary with

distance downstream and from bend to bend (Figures 3.3 and 3.4–3.10). The pattern of deposition and erosion within each bend remains relatively consistent throughout the entire survey reach. The greatest outward movement of the outer bank is located about 60% of the way along the operational bend length, with deposition on the point bar focused directly across the channel from it (Figures 3.2 and 3.4). This leads to a component of downstream translation of the bends themselves. Future modeling efforts that focus on how this phase-lag responds to varying discharges would be greatly beneficial to the community.

As the river approaches the coast, both the total volume of deposit that is added to point bars and the total volume of deposit that is eroded from cut banks decrease drastically (Figure 3.8). Accurate estimates of these reductions require combining subaerial data with bathymetric data to properly estimate change for the entire channel. This study marks the first observation of net erosion within the backwater zone during flood. This behavior is not due to an increase in the amount of outer bank erosion (the magnitude of eroded cut bank is much lower in the backwater zone than it is in the quasi-uniform flow zone; Figure 3.8), but instead to the extremely limited deposition of sediment onto point bars near the coast.

Edge-to-edge widening especially within the quasi-uniform reach was in many cases partially due to point bar widening and depositional processes driving the inner bank landward (Figures 3.10 and 3.11). The overall preference toward deposition (Figures 3.8 and 3.9a) and the high ratio of point bar to cut bank horizontal motion (Figure 3.9b) all imply that in this portion of the river, bar push is the mechanism that drives overall channel migration. In the transitional and backwater reaches, however, the dominance of erosion over deposition (Figures 3.8 and 3.9a) combined with the limited lateral movement of point bars (Figure 3.9b) and the dominance of cut bank erosion in widening the channel (Figure 3.10) suggests that bank pull initiates channel migration in this region during flood.

Lastly, the outward migration of scroll bars is a novel and exciting observation (Figure 3.11). Historically, scroll bars have been used to reconstruct the previous positions of river channels and it has been suggested that they can be used as indicators of overall river lateral migration rate (Hickin & Nanson, 1975; van de Lageweg et al., 2014). The results of this study show that the behavior of scroll bars and the patterns they leave behind are more complex than simple ridges marching out unidirectionally.

ACKNOWLEDGMENTS

The authors would like to thank Paola Passalacqua, Hima Hassenruck-Gudipati, Timothy Goudge, and Alicia Sendrowski. We would like to acknowledge Jim Pizutto and the remaining Journal of Geophysical Research: Earth Surface reviewers and Editors whose thoughtful and thorough suggestions improved the paper. Support was provided by the Jackson School of Geosciences and the National Science Foundation through the OCE/EAR-1135427 and EAR 1547200. The 2011 lidar is available from the TNRIS website and the 2015 lidar will be available from the NCALM website beginning in December 2017.

REFERENCES

Allen, J. R. (1963). The classification of cross-stratified units with notes on their origin. Sedimentology, 2(2), 93–114. https://doi.org/10.1111/j.1365-3091.1963.tb01204.x

Allen, J. R. L. (1985). Principles of physical sedimentology (272 pp.). London: Allen&Unwin.

Bevington, P. R. (1969). Data reduction and error analysis for the physical. Sciences, 164–176.

Bridge, J., & Demicco, R. (2008). Earth surface processes, landforms and sediment deposits (815 pp.). Cambridge, UK: Cambridge University Press. https://doi.org/10.1017/CBO9780511805516

Bridge, J. S., Alexander, J. A. N., Collier, R. E., Gawthorpe, R. L., & Jarvis, J. (1995). Ground-penetrating radar and coring used to study the large-scale structure of point-bar deposits in three dimensions. Sedimentology, 42(6), 839–852. https://doi.org/10.1111/j.1365-3091.1995.tb00413.x

Chatanantavet, P., Lamb, M. P., & Nittrouer, J. A. (2012). Backwater controls of avulsion location on deltas. Geophysical Research Letters, 39, L01402. https://doi.org/10.1029/2011GL050197

Chow, V. (1959). Open channel hydraulics. New York: McGraw-Hill Book Company, Inc.

Dietrich, W. E., & Smith, J. D. (1983). Influence of the point bar on flow through curved channels. Water Resources Research, 19(5), 1173–1192. https://doi.org/10.1029/WR019i005p01173

Edmonds, D. A., Hoyal, D. C., Sheets, B. A., & Slingerland, R. L. (2009). Predicting delta avulsions: Implications for coastal wetland restoration. Geology, 37(8), 759–762. https://doi.org/10.1130/G25743A.1

Eke, E., Parker, G., & Shimizu, Y. (2014). Numerical modeling of erosional and depositional bank processes in migrating river bends with self-formed width:Morphodynamics of bar push and bank pull. Journal of Geophysical Research: Earth Surface, 119, 1455–1483. https://doi.org/10.1002/2013JF003020

Engelund, F. (1974). Flow and bed topography in channel bends. Journal of the Hydraulics Division, 100(11), 1631–1648.

Fernandes, A. M., Törnqvist, T. E., Straub, K. M., & Mohrig, D. (2016). Connecting the backwater hydraulics of coastal rivers to fluvio-deltaic sedimentology and stratigraphy. Geology, 44(12), 979–982.

Frazier, D. E., & Osanik, A. (1961). Point-bar deposits. Louisiana: Old River Locksite.

Ghinassi, M., Ielpi, A., Aldinucci, M., & Fustic, M. (2016). Downstream-migrating fluvial point bars in the rock record. Sedimentary Geology, 334, 66–96. https://doi.org/10.1016/j.sedgeo.2016.01.005

Hickin, E. J., & Nanson, G. C. (1975). The character of channel migration on the Beatton River, Northeast British Columbia, Canada. Geological Society of America Bulletin, 86(4), 487–494. https://doi.org/10.1130/0016-7606(1975)86%3C487:TCOCMO%3E2.0.CO;2

Hoyal, D. C. J. D., & Sheets, B. A. (2009). Morphodynamic evolution of experimental cohesive deltas. Journal of Geophysical Research, 114, F02009. https://doi.org/10.1029/2007JF000882

Hudson, P. F., & Kesel, R. H. (2000). Channel migration and meander-bend curvature in the lower Mississippi River prior to major human modification. Geology, 28(6), 531–534. https://doi.org/10.1130/0091-7613(2000)28%3C531:CMAMCI%3E2.0.CO;2

Kikkawa, H., Ikeda, S., & Kitagawa, A. (1976). Flow and bed topography in curved open channels. Journal of the Hydraulics Division, 102(9), 1327–1342.

Lamb, M. P., Nittrouer, J. A., Mohrig, D., & Shaw, J. (2012). Backwater and river plume controls on scour upstreamof river mouths: Implications for fluvio-deltaic morphodynamics. Journal of Geophysical Research, 117, F01002. https://doi.org/10.1029/2011JF002079

Lane, E. W. (1957). A study of the shape of channels formed by natural streams flowing in erodible material. US Army Corps of Engineers. Missouri River Division, Omaha, Sediment series, 9.

Leeder, M. R., & Bridges, P. H. (1975). Flow separation in meander bends. Nature, 253(5490), 338–339. https://doi.org/10.1038/253338a0

Nanson, G. C. (1980). Point bar and floodplain formation of the meandering Beatton River, northeastern British Columbia, Canada. Sedimentology, 27(1), 3–29. https://doi.org/10.1111/j.1365-3091.1980.tb01155.x

Nittrouer, J. A., Mohrig, D., & Allison, M. (2011). Punctuated sand transport in the lowermost Mississippi River. Journal of Geophysical Research, 116, F04025, 1914–1934. https://doi.org/10.1029/2011JF002026

Nittrouer, J. A., Shaw, J., Lamb, M. P., & Mohrig, D. (2012). Spatial and temporal trends for water-flow velocity and bed-material sediment transport in the lower Mississippi River. Geological Society of America Bulletin, 124(3–4), 400–414. https://doi.org/10.1130/B30497.1

Parker, G., Shimizu, Y., Wilkerson, G. V., Eke, E. C., Abad, J. D., Lauer, J. W., et al. (2011). A new framework for modeling the migration of meandering rivers. Earth Surface Processes and Landforms, 36(1), 70–86.

Smith, D. G., Hubbard, S., Leckie, D., & Fustic, M. (2009). Counter point bars in modern meandering rivers: Recognition of morphology, lithofacies and reservoir significance, examples from Peace River, AB, Canada. Sedimentology, 56(6), 1655–1669. https://doi.org/10.1111/j.1365-3091.2009.01050.x

Smith, V. B. (2012). Geomorphology of a coastal sand-bed river: Lower Trinity River, Texas (PhD dissertation).

van de Lageweg, W. I., van Dijk, W. M., Baar, A. W., Rutten, J., & Kleinhans, M. G. (2014). Bank pull or bar push: What drives scroll-bar formation in meandering rivers? Geology, 42(4), 319–322.

Chapter 4: Compensational river bank migration[3]

ABSTRACT

Comparison of three bare-earth lidar data sets show that migration of the inner and outer banks of 30 consecutive river bends on the Trinity River in Texas, USA, is compensational. Two difference maps created from lidar flown in 2011, 2015, and 2017 capture this temporal variability in the amounts of inner versus outer bank migration. In twenty of the studied river bends, channel narrowing during the first time interval was counterbalanced by widening during the second interval, or vice versa. Six of the remaining ten bends underwent nearly compensational bank migration, with <1% width change during one of the time intervals. The remaining four bends narrowed during both measurement periods, facilitated by floodplain complexity associated with past bend cutoffs or tributaries. Sub-aerial volumes of sediment deposited on inner banks of bends was smaller for 2015-2017 than for 2011-2015 while erosional volumes were similar for the two intervals, despite 2015-2017 having had almost twice the number of days under flood conditions (and a decreased exceedance probability for the maximum flood discharge). This implies that the response of the channel to a flooding event is highly dependent on the duration of the flood as well as the state of the channel at the initiation

[3] This chapter was submitted by authors Jasmine Mason and David Mohrig for publication in Geology on November 16, 2018. As first author, I was responsible for designing the project, collecting the field data, data processing and analysis, and writing and submitting the paper. David Mohrig provided project guidance and edits.

of the flood. Results demonstrate that hydraulic radius approximations defining the equilibrium channel geometry in fact represent a statistical steady state that is consistently overshot and undershot by the natural system. Channel width for the river appears roughly constant through time because differences in outer- and inner-bank migration at one time are counterbalanced by compensating differences at a later time. For the Trinity River this compensation happened over time spans of 2-3 years and would lead to the appearance of invariant channel width at the decadal scale.

INTRODUCTION

Line models describing the evolution of meandering channels in both time and space represent one of the earliest and most successful morphodynamic models in geomorphology (Howard and Knutson, 1984; Sun et al., 1996). A key assumption of these models is that the left and right banks of bends (or inner and outer banks) are linked and move in equal amounts at all times. Observations from natural channels and preserved point bar deposits clearly demonstrate that inner and outer banks move different amounts at the flood to annual scale (Gupta et al., 1974; Brice, 1982; Lagasse, 2004; Mason and Mohrig, 2018). This has led to a new generation of models that treat the motions of each bank as being independent from each other (Darby et al., 2002; Asahi et al., 2013; Eke et al., 2014), and has focused attention on the intriguing question as to the relative importance of bar push versus bank pull in moving bends (Dietrich and Smith, 1983). Channel migration has variably been attributed to both cases (Van de Lageweg et al., 2012; Constantine et al., 2014; Eke et al., 2014).

All of this has led to our current paradox that centerline migration line-models perform well over many years, but the instantaneous change between banks is unequal. This paper uses multiple time-lapse lidar surveys to rationalize this inconsistency and to assess the handoff between unequal bank displacements over short times to a time-averaged roughly equal motion of a channel's margins. Results have implications for the readjustment of river channels following large perturbations, the debate on relative contributions of bank pull versus bar push, as well as for accurate interpretation of variability observed in point-bar deposits.

METHODS

This study compared three lidar data sets (from 2011, 2015, and 2017) to observe changes in patterns of deposition and erosion along a 32 km long portion of the lower Trinity River containing 30 river bends. Stage and discharge data was taken from the USGS survey station at Liberty, Texas (station ID 08067000). The annual maximum discharge at Liberty over 76 years was used to calculate the exceedance probability associated with each flood captured by the lidar data. The first lidar survey was collected in 2011 with a Leica ALS60 lidar system with a reported vertical accuracy within 15 cm of the known elevation and 1 m horizontal resolution. The 2015 bare earth lidar data set was collected by the National Center for Airborne Laser Mapping using an Optech Titan with a vertical accuracy within 5-15 cm of the known elevation and rasterized to 1 m horizontal resolution. The 2017 lidar data set was collected by the Texas Water Development Board and the Trinity River Authority. A Leica ALS70 Lidar was used to

collect data with a reported vertical accuracy of 1.7 cm and a horizontal accuracy of 3 cm. River stage was at its highest during collection of the 2015 data set, but was still no more than 0.5 m above the stage during either the 2011 or 2017 survey collection dates. These three data sets were differenced in ArcMap 10.5.1 to create two time-lapse maps, the first of which was used extensively by and is detailed within Mason & Mohrig's 2018 Journal of Geophysical Research article. Despite an estimated *maximum* uncertainty in vertical elevation for the 2011-2015 and 2015-2017 difference maps of ±30 cm and ±17 cm, respectively, there is very little net elevation change observed amongst widely distributed infrastructure. This indicates that the accuracy of the maps is relatively high and reported uncertainties in volume measurements are likely exaggerated.

For each time-lapse map, polygonal areas of elevation change were measured separately for the inner and outer banks of each river bend within the survey area. Point bars were mapped as the combined area between the landward edge and the channel-ward shoreline for both survey dates. Cut banks were defined as the area of erosion between the outer banks at the two separate times. Volumes were measured by summing the change in elevation for each pixel within each polygon. Uncertainty in volume measurements were calculated by multiplying the maximum uncertainty for each time-lapse map by the area of the polygon (areas were measured by counting the number of 1 m pixels within each polygon). Wilcoxon rank sum tests were done on resulting distributions to determine whether differences in values between time-lapse maps was statistically significant at the 5% significance level.

Channel centerlines were created by collapsing the positions of the inner and outer banks (mapped as the landward edge of the point bar and the outer bank) for all three surveys. To estimate the amount of centerline migration between survey dates, the area between two centerlines was calculated and divided by the mean length of the two centerlines. Bar-to-bank channel width was measured from the edge of the point bar to the outer bank every 100 m perpendicularly to the 2015 centerline. The bar-to-bank widths were measured at consistent elevations between surveys, as defined by the 2015 stage (the highest of the three surveys). The radius of curvature for each bend was measured by fitting a circle to the points defining the river bend using the Pratt method (Pratt 1987).

RESULTS

Between 2011 and 2015 there were a total of 76 days of flood (defined by a stage of 7.9 m at Liberty, TX) spread out over five events. Four of the contained events lasted less than 6 days on average, while the last continued for over 55 days. The maximum discharge of the single large flood was associated with a .12 exceedance probability. The duration of this magnitude of flood had not been observed on the Trinity River since the installation of the gaging station at Liberty in 1938. Between 2015 and 2017, an additional 146 days of flooding occurred spread out over 6 similarly long events (mean duration of 24 days). These shorter flooding events had exceedance probabilities that ranged from .35 to .11, with an average of .23.

Figure 1 shows a single bend contained within the survey at three different times (top row; figs. 4.1a, 4.1b, 4.1c) as well as the change in elevation between them (bottom row; figs. 4.1d, 4.1e, and 4.1f). Qualitatively, the styles of deposition and erosion varied between time intervals. Between 2011 and 2015, the flatter tops of point bars (indicated by the yellow-green area in 4.1a) grew vertically by as much as 1.5 m. In addition, the bar extended laterally. Between 2015 and 2017, the top of the point bar was eroded and the deposition that did happen was focused along the channel-ward, downstream edge of the bar. On average, erosion occurred across 36% of every point bar surface in the studied area during this interval. When considering the entire period between 2011 and 2017, the net deposition along the point bar was minimal along the top of the bar and was instead focused along the downstream edge. The pattern of cut bank erosion is similar between the two difference maps (4.1d and 4.1e).

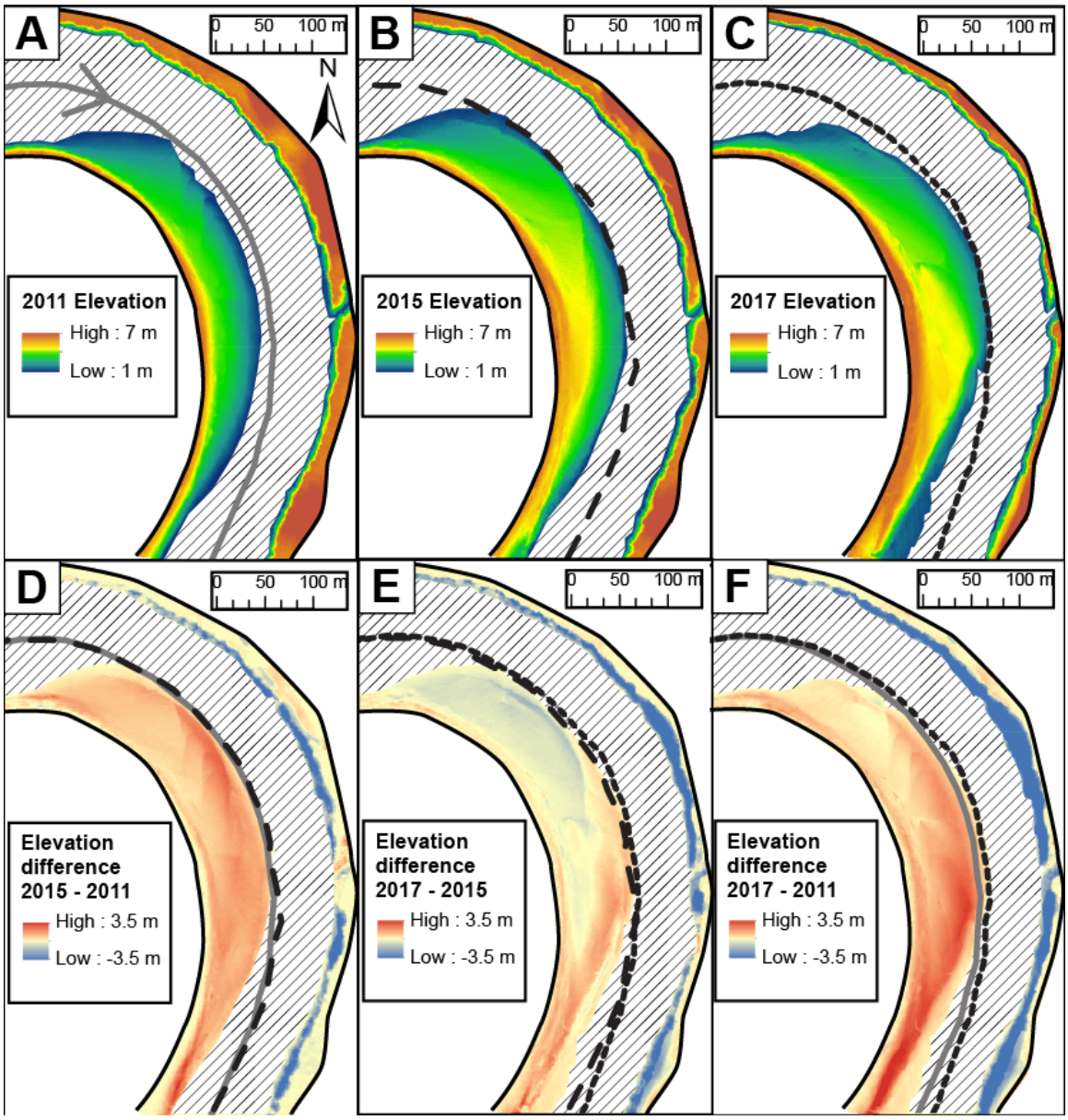

Figure 4.1: Bare earth digital elevation models for a portion of a river bend at three times and associated difference maps

Figure 4.1: Bare earth digital elevation models for a portion of a river bend at three times and associated difference maps
Pictured river bend is located at kilometer 14 in Figures 2 and 3. For all maps, north is up, flow is from top to bottom, and the water surface is denoted by the hatched line. 1a) Elevation of the point bar and outer bank in 2011. 1b) Elevation of the point bar and outer bank in 2015. Notice the lateral extent of the point bar has increased and the position of the outer bank has moved. 1c) Elevation of the point bar and outer bank in 2017. Notice the movement of the outer bank. 1d) Difference map between 2011 and 2015 with areas of deposition denoted in red and areas of erosion in blue. Deposition dominates the entire surface of the point bar. 1e) Difference map between 2015 and 2017 with areas of deposition denoted in red and areas of erosion in blue. Notice the erosional surface on the top of the point bar. 1f) Difference map between the entire study period, 2011 and 2017, showing areas of deposition in red and areas of erosion in blue. The portion of the point bar with the highest aggradation is along the downstream, channel-ward edge of the bar.

Sub-aerial volumes measured from each bar and bank polygon on each difference map quantify the difference in behavior between the two time steps (Fig. 4.2). For the period associated with a single long duration flood, volumes of deposition along point bars were almost as large as volumes of erosion along the outer banks of bends. During the period dominated by multiple intermediate-length floods, both deposition along point bars and erosion of cut banks were less than that for the previous time step despite this period having nearly double the number of total flooded days and a higher maximum discharge. Deposition on point bars was significantly reduced compared to the previous difference map, with more bars experiencing net erosion as a result of the planing off of the tops of bars (Fig. 4.1). A Wilcoxon rank sum test confirms that the depositional volumes from each time step are statistically distinct at the 5% significance level, but fails to distinguish the difference in the outer bank erosional volumes. In addition, the channel centerlines show an average of 6.5 m of lateral migration for the time period between 2011 and 2015 and 4.2 m between 2015 and 2017, again despite an almost doubling of the number of days under flood conditions (and a decrease in the exceedance probability for the highest-magnitude flood) in the latter time period (Fig. 4.1).

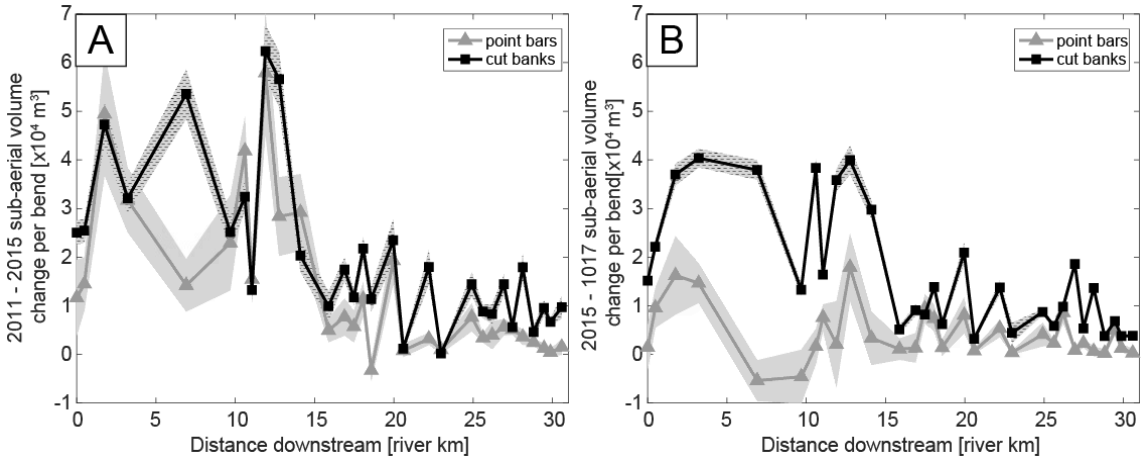

Figure 4.2: Sub-aerial volume change for each bank in every channel bend for both time intervals

Volumes were measured by summing the elevation difference in each 1x1 m pixel for each point bar (grey triangles and lines) and cut bank (black squares and lines) polygon in both difference maps. Uncertainty is shown by the grey and hatched grey areas and was estimated by multiplying the difference map's vertical uncertainty by the area of each polygon. 1a) Sub-aerial volume change between 2011 and 2015. 1b) Sub-aerial volume change between 2015 and 2017. Depositional volumes on point bars are significantly lower for the second interval, while cut bank erosional volumes for the two periods are statistically indistinguishable.

In addition to the changes in sub-aerial volumes of eroded or deposited material between time steps, there were also differences in the amount of horizontal movement of the inner and outer banks. Between 2011 and 2015, inner banks tended to move laterally more than the outer banks for 70% of the surveyed river bends, causing a local narrowing in the bar-to-bank width (Fig. 3). The remaining 30% of bends experienced relative bar-to-bank widening due to increased motion of the outer bank compared to the point bar. Between 2015 and 2017, there was a reversal in this previously observed behavior. Bends that had experienced bar-to-bank narrowing switched so that the outer bank eroded much

more than the point bar grew in the time between 2015 and 2017, or vice versa. 67% (20 of 30) of the observed river bends exhibited this reversal in behavior between time steps. Out of the remaining 10 river bends, 6 migrated nearly-compensationally, with one of the time intervals showing <1% width change. The four river bends whose banks did not migrate compensationally all narrowed throughout both intervals. Each of these river bends is complicated by an adjacent bend cutoff or in one case, the confluence of a tributary along the outer bank. Figure 4 shows the ranked radii of curvature for each river bend with the four bends that exhibited non-compensational migration highlighted. The bends with banks that did not migrate compensationally had higher than average radii of curvature.

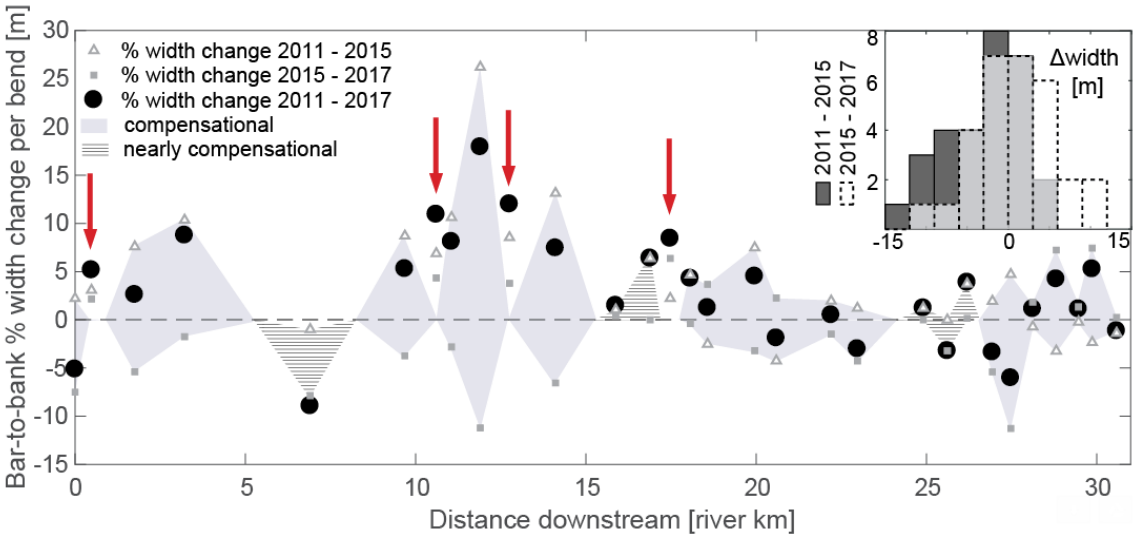

Figure 4.3: Percent change in bar-to-bank width averaged over each bend for both time intervals and overall

Bar-to-bank width changes for 2011 to 2015 are shown in triangles, 2015 to 2017 in squares, and 2011 to 2017 in black circles. Positive values (above black dashed line) indicate increased inner bank motion compared to outer bank motion, i.e. bar-to-bank narrowing. Negative values indicate bar-to-bank widening. The grey compensational area highlights bends that exhibited a reversal in bank migration behavior between the two time steps. 67% of the studied river bends demonstrated this compensational bank migration. The hatched area represents bends that migrated nearly-compensationally, with <1% width change for one of the intervals. The red arrows indicate the four bends whose bank migration was non-compensational, all of which narrowed during both time periods. The inset histograms show the distribution in width changes for each survey (dark grey for period between 2011 and 2015, white area for 2015 – 2017 interval, with the overlap between the two shown in light grey). Positive values indicate widening, negative values indicate narrowing.

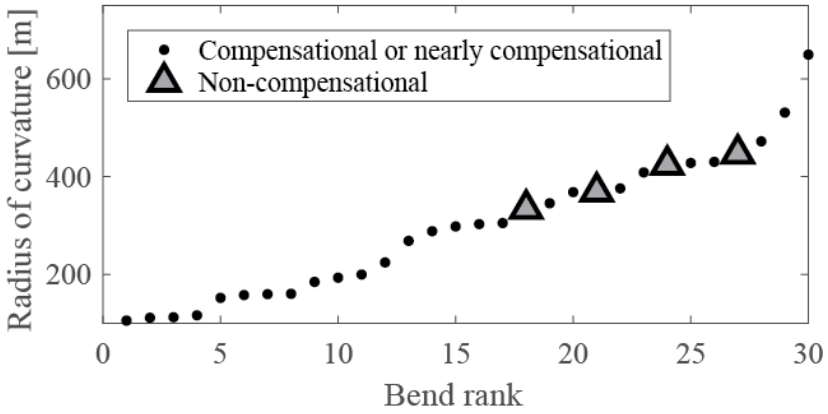

Figure 4.4: River bend radius of curvature and associated bend ranking highlighting the tendency for non-compensational banks to be associated with bends having higher radii of curvature.

DISCUSSION

Between 2015 and 2017 the tops of the point bars did not experience the same level of vertical aggradation as the previous 2011 to 2015 interval despite an additional 70 days of flood with similar (or even decreased) maximum discharge exceedance probabilities. While point bars were still net depositional in the second interval (save for two bends, Fig. 4.2b), the average bar had erosion occur across 36% of its sub-aerial surface, leading to lower depositional values compared to the previous interval (Fig. 4.2a). This could be related to the narrowing of the channel during the previous interval, or to the duration of the floods. The tendency for most bends to experience excessive growth of the point bars and narrowing during the period between 2011 and 2015 could have acted to spatially accelerate the flow through the channel during the later period, leading to less deposition. In addition, longer floods with more consecutive days of

overbank flow likely have some control over the level of aggradation along point bar tops. Even though there was a higher number of total flooded days between 2015 and 2017, the duration of the floods did not match the single event that was captured within the first time-lapse data set. Coincident with the decreases in the volumes of deposited material in the second time step is a 35% decrease in the amount of centerline migration. Altogether, these systematic decreases in the amount of change for the second studied time interval imply that an increase in the number of flooded days and a decrease in the maximum discharge exceedance probability does not necessarily correspond with a comparable response by the river channel.

Comparison of the three difference maps (Fig. 4.1d, 4.1e, 4.1f) indicates that the occurrence of bar deformation over shorter time scales can be obscured over longer periods of observation. The overall change (Fig. 4.1f) shows relatively little aggradation along the top of the point bar, with most of the change happening along the channel-ward, downstream edge of the bar; consistent with lateral bar migration and translation. However, looking at the two constituent difference maps show that the top of the bar experienced aggradation over the initial time interval followed by erosion during the second interval. Deposition along the downstream, channel-ward edge of the bar is consistently occurring despite the deformation along the flattened top of the bar. Therefore, this portion of the bar is interpreted as a more faithful recorder of the conditions that lead to its deposition.

Between 2015 and 2017, the changes in bar-to-bank channel width occurred in such a way that they acted to cancel out much of the bar-to-bank width changes between

the 2011 to 2015 interval (Fig. 4.3). Bends that narrowed between 2011 and 2015 tended to subsequently widen during the second interval, and vice versa. Of the ten bends that didn't experience this compensational bank migration, 6 were very nearly compensational, with less than 1% width change for one of the surveys. This surprising observation reinforces the idea that over long time scales, river channels maintain a characteristic geometry despite large perturbations over shorter periods. Only four bends had banks that migrated non-compensationally, with repeated narrowing during both time periods. These river bends had a higher than average radius of curvature (Figure 4.4) and were correlated with focused interaction between the floodplain and the main channel. Three bends were associated with an adjacent bend cutoff that delivered additional sediment to either the point bar or the outer bank as the oxbow lake drained. The remaining bend shows very little outer bank migration due to a small floodplain tributary that connected directly to the outer bank.

This study was limited by the amount of available data; additional lidar data sets spread out over a finer temporal resolution might have allowed the observation of compensational river bank migration occurring over shorter time intervals. However, these results suggest that the independent movements of the inner and outer banks of a river bend are compensational over 2-3 years. Observations of invariant channel width over longer timescales (Smith 2012) imply that through time, these discrete periods of widening and narrowing are averaged to maintain a constant value at the decadal scale. This implies that centerline migration models are likely most useful if they are being used

to predict change over decades or longer. Shorter timescale changes are unlikely to be captured accurately by these types of models.

CONCLUSIONS

In 2015, a large and prolonged flood perturbed the Trinity River fluvial system and led to deviations from the mean channel shape. The reversal that we observed in the behavior of the river between the two observed time intervals is interpreted as the system's readjustment to the perturbation caused by the 2015 flooding event.

One interesting repercussion of this work is the observation that, depending on the time interval at which the river channel is observed, varying conclusions can be drawn about the representative behavior of the system. There is a striking disparity in the amount of centerline migration, the patterns of sediment deposition (Fig. 1), the volumes of sediment eroded and deposited (Fig. 2), and the bar-to-bank width changes (Fig. 3) between the two studied intervals. Any extrapolation about the long term behavior of the system would be hugely skewed if only a single time interval were used for the analysis. In addition, our data suggest that an increase in the number of flooded days doesn't necessarily induce a proportional response by the river channel, as the observed decreases in volumetric change and bank migration occurred despite an almost doubling in the number of days under flood conditions whose maximum discharges were often associated with a lower exceedance probability. This result indicates that the simple use of a flood intermittency when modeling meandering rivers might not adequately capture a system's morphodynamic behavior.

Our data show that the behavior of the river channel is constantly changing and is highly dependent on the state of the channel at the initiation of the observation period. The bar-to-bank width of a river bend widens and narrows in discrete steps over periods of years. The idea of an "equilibrium" river channel geometry and bank migration rate is best thought of as a statistical steady state. In addition, this work has implications for the use of hydraulic radius approximations. We have demonstrated that the effective width of the channel can change over relatively short time scales. When averaged over longer time intervals however, the rapid adjustment of the channel makes it such that these hydraulic radius relationships can be considered adequate.

ACKNOWLEDGEMENTS

The authors would like to thank the Mohrig research group, Paola Passalacqua, Hima Hassenruck-Gudipati. Support was provided by the Jackson School of Geosciences and the National Science Foundation through the OCE/EAR-1135427 and EAR 1547200.

REFERENCES

Asahi, K., Shimizu, Y., Nelson, J., & Parker, G. (2013). Numerical simulation of river meandering with self-evolving banks. Journal of Geophysical Research: Earth Surface, 118(4), 2208-2229.

Brice, J.C., (1982). Stream channel stability assessment. No. FHWA/RD-82/021. United States. Federal Highway Administration.

Constantine, J. A., Dunne, T., Ahmed, J., Legleiter, C., & Lazarus, E. D. (2014). Sediment supply as a driver of river meandering and floodplain evolution in the Amazon Basin. Nature Geoscience, 7(12), 899.

Darby, S. E., Alabyan, A. M., & Van de Wiel, M. J. (2002). Numerical simulation of bank erosion and channel migration in meandering rivers. Water Resources Research, 38(9), 2-1.

Dietrich, W. E., & Smith, J. D., (1983). Influence of the point bar on flow through curved channels. Water Resources Research, 19(5), 1173-1192.

Eke, E., Parker, G., & Shimizu, Y. (2014). Numerical modeling of erosional and depositional bank processes in migrating river bends with self-formed width: Morphodynamics of bar push and bank pull. Journal of Geophysical Research: Earth Surface, 119(7), 1455-1483.

Gupta, A., and Fox H., (1974). "Effects of high-magnitude floods on channel form: a case study in Maryland Piedmont." Water Resources Research 10.3.

Howard, A.D., and Knutson T.R., (1984). "Sufficient conditions for river meandering: A simulation approach." Water Resources Research 20.11.

Lagasse, P.F., (2004). Handbook for predicting stream meander migration. No. 533. Transportation Research Board.

Mason, J., & Mohrig, D., (2018). Using time-lapse lidar to quantify river bend evolution on the meandering coastal Trinity River, Texas, USA. Journal of Geophysical Research: Earth Surface, 123(5), 1133-1144.

Pratt, V. (1987). Direct least-squares fitting of algebraic surfaces. In ACM SIGGRAPH 707 computer graphics (Vol. 21, No. 4, pp. 145-152). ACM.

Sun, T., Meakin, P., Jøssang, T., & Schwarz, K. (1996). A simulation model for meandering rivers. Water resources research, 32(9), 2937-2954.

van de Lageweg, W. I., van Dijk, W. M., Baar, A. W., Rutten, J., & Kleinhans, M. G (2012). Bank pull or bar push: What drives scroll-bar formation in meandering rivers?. Geology, 42(4), 319-322.

Chapter 5: Bedform groups during flood on the Trinity River—a new scale of self-organization in river bottom topography

ABSTRACT

Long wavelength (12 km) groups of bedforms were observed migrating down a 25 km stretch of the Trinity River in Texas during a prolonged flood event. These bedform groups spanned an average of 12 river bends, a scale of bed self-organization that has not previously been recognized in these types of systems. Eight separate surveys were conducted that spanned the time before, during, and after a historically large flood on the Trinity River in 2015. Peaks in bedform groups are not associated with increased topography or differences in channel bed grain size. Measurements of dune geometries, sizes, and migration rates combined with flow velocity and grain size data taken during one flood survey suggest that this bed self-organization is a result of preferential wash-out of smaller dunes. Larger dunes are able to persist and migrate downstream for the majority of the flood. Once sediment supply was cut off, even the larger dunes became sediment-starved and washed out. The final survey was taken after the flood receded and transport and supply conditions had equalized, and shows bedforms that are on average 34% larger than the washed out forms associated with the final flood survey. Results from this study offer a conceptual model for a new, extremely large scale of bed topographic self-organization, as well as suggest that measuring bedform metrics may not be an accurate method for interpreting flow conditions.

INTRODUCTION

Pulses of increased bed-material load transport have been identified as common occurrences in many rivers. As a result, much research has been completed using flume experiments, natural systems, and numerical models to understand where these sediment pulses originate and how they evolve through time. In natural systems, landslides, debris flows, bank failures, and bend cutoffs can all introduce discrete pulses of sediment into the channel that can migrate downstream as a coherent wave (Gilbert 1917; Griffiths 1979; Nicholas et al. 1995; Madej and Ozaki 1996; Benda and Dunne 1997; Cui et al. 2003; Zinger et al. 2011). Several studies have focused on the evolution and migration of these sediment pulses through time, with most agreeing that they migrate via a combination of translation and dispersion (Ashmore 1991; Lisle et al. 1997; Cui et al. 2003;). 1D numerical modelling results from Lanzoni et al. (2006) suggest that sediment waves within a channel can also steepen through time. While some of the pulses have been observed to manifest as migrating groups of bedforms (e.g., Meade 1985), most are observed as a relative increase in bed elevation or as rapid growth and migration of bar forms (e.g., Nicholas et al. 1995).

Much of the research into discrete pulses of moving sediment has been done in braided-channel networks, with several authors indicating that the interaction between multiple thalwegs is necessary for the formation of the pulses (Hoey and Sutherland 1991; Hoey 1992; Bertoldi et al. 2010). Alternatively, several studies have shown that longitudinal grain size sorting in flumes under constant discharge and sediment feed conditions can cause differences in bed-material load transport rate (Iseya and Ikeda

1987). In all of these previously documented cases of bed-material pulses, the pulses are associated with a change in the geometry or topography of the bed (e.g., an increase in the average channel bed elevation, or a change in the slope of the bed).

Historically, bedforms are understood to be critical in building larger scale bar forms (Allen 1963; Bridge and Demicco 2008) which then act to define the geometry of the channel as well as affect the kinematics of the river bends themselves (Dietrich and Smith 1983). Bedforms along the channel bed of rivers are often used as important indicators of the sediment transport conditions within the flow (e.g. Southard 1971; Karim 1995; Venditti et al. 2016). Recently, studies have shown that a surprising range of bedform geometries (size and shape) can be stable within similar flow conditions (Kostaschuk and Villard 1996; Jerolmack and Mohrig 2005; Venditti et al. 2005; Bradley and Venditti 2017). The following research compliments and expands on these studies by providing evidence that a large range of bedform geometries can coexist within a reach of a river during a single event.

This chapter will discuss the observation of migrating long-wavelength groups of bedforms within the channel of the Trinity River, TX, during a historically large flooding event in 2015. The studied reach of the river is a 25 km long stretch of channel located where the average elevation of the river bottom drops below mean sea level (Figures 5.1, 5.2). This area is of particular interest because large-scale changes in the geomorphology of the river have been connected with this transition to the backwater zone (Fernandes et al. 2016; Hudson & Kesel 2000; Lamb et al. 2012; Nittrouer et al., 2011; Nittrouer et al. 2012; Smith 2012; Mason and Mohrig 2018). We utilized commercially available sonar

instruments and a multibeam echosounder to acoustically image and survey the elevation of the bed of the channel. High and low frequency changes in bed elevation were analyzed in order to resolve any large-scale aggradation or erosion or the channel bottom and any changes in bedform size or geometry. Repeat surveys (8 total; Fig. 5.3) taken before, throughout, and following a historically large flooding event on the Trinity River have revealed usual and unprecedented bedform behavior.

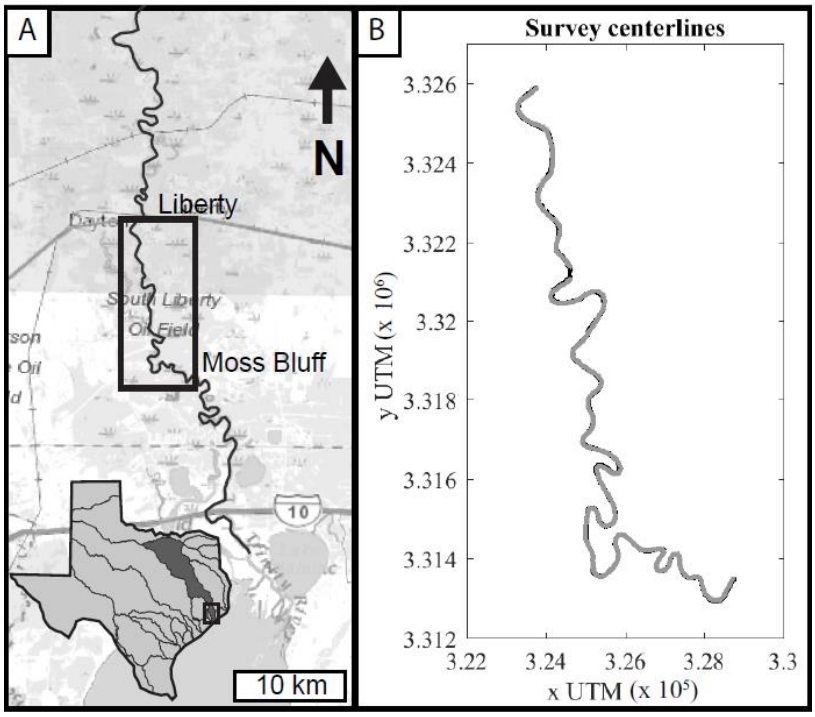

Figure 5.1: Location map of the study area.

A) Relative location of the 25 km stretch of river that was surveyed (within the black rectangle) with respect to the location of the Trinity Bay. Inset map of Texas shows the watershed for the Trinity River with the lower Trinity encased within the small black rectangle. B) All survey lines for the 8 total surveys that were completed. Note that there is very little divergence between survey lines.

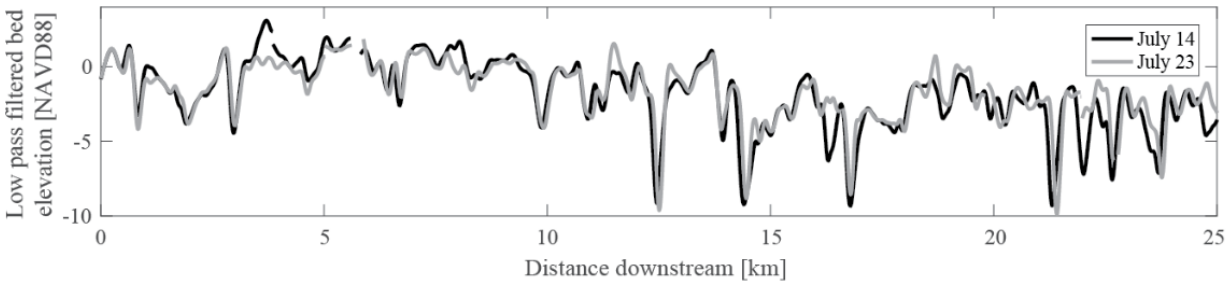

Figure 5.2. Low-pass filtered river-bottom topography for the studied river reach.

The bed elevation for two flood surveys is shown (July 14 and July 23). These long profiles were generated by filtering out all topographic fluctuations < 2 channel widths (220 m) in wavelength. The sequential surveys reveal no systematic changes in bed elevation between survey dates. The small, non-systematic differences in bed elevation and scour-pool position are likely due to slight differences between the positioning of the sequential survey lines.

Beginning in May of 2015, the greater part of Texas experienced record precipitation. The Trinity River at Liberty, TX (USGS gage station 08067000, approximately 60 river km upstream of the Trinity Bay) was flooded above the National Weather Service flood stage (defined by a discharge of 850 m^3/s at Liberty) for 55 days, an unprecedented event since the installation of the stream gage station in 1938 (Figure 5.3). Large and infrequent events like these likely have an outsized effect in terms of sediment transport to deltas and erosion and deposition within the river channel (Costa and O'Connor 1995; Shaw and Mohrig 2014). Five of eight surveys were taken during this exceptional flooding event in an attempt to understand exactly how and when bed-material load is transported through this dynamic river zone.

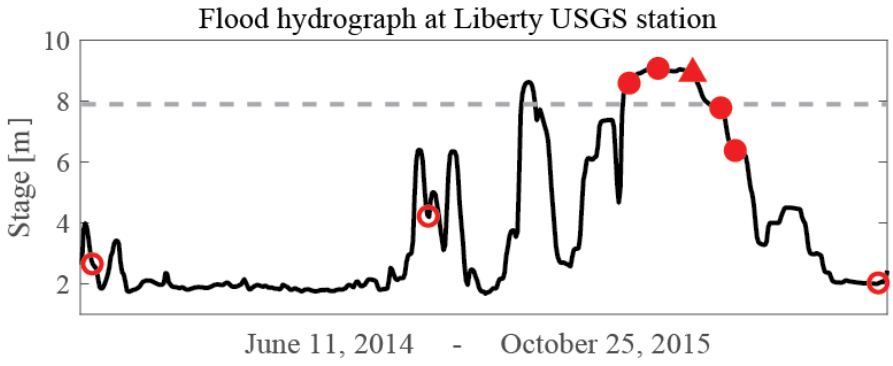

Figure 5.3: Hydrograph with superimposed survey dates

Stage data taken from the Liberty USGS station along the Trinity River (the upstream end of the survey area). The National Weather Service flood stage (7.9 m) is defined by the dashed grey line. Filled markers indicate surveys associated with the main flooding event. Red circles indicate Humminbird survey dates. The survey indicated by the triangle represents the single multibeam bathymetry, ADCP, and grain size data collection survey. Eight total surveys were taken, 2 before the major flood, five during, and one after the stage returned to low flow conditions.

METHODS

The 25 kilometer stretch between the Liberty USGS station (ID 08067000) and the Moss Bluff USGS station (ID 08067100; Figure 5.1) was chosen as the main survey area as it captures the hydraulic transition from quasi-uniform flow into gradually varying or backwater flow (defined as the approximate location where the mean channel bottom elevation drops below sea level; Figures 5.1, 5.2). The data included in this study is comprised of eight separate surveys that were completed at different times before, throughout, and following the major flooding event (Figure 3). During seven of the surveys, acoustic images and depth profiles of the channel bed were acquired using an 898c High Definition Side Imaging combo Humminbird fishfinder, a commercially available sonar instrument. The Humminbird sonar operated at 455 kHz frequency.

Navigation and depth data were recorded at 1 second intervals, translating to an average of 12 cm horizontal distance between points for those seven surveys. Vertical resolution of depth data was variable due to differences in water depth, turbidity, and suspended sediment load, but was typically around 1 cm and never worse than 5 cm. A single multibeam bathymetry survey was conducted during the peak of the flood using a Reson 7101 SeaBat multibeam echo sounder. A 210 degree swath of data was collected at 240 kHz with 12.5 mm depth resolution. Repeat measurements of the survey line taken during the multibeam survey allowed for bedform migration rates to be measured. The multibeam survey was accompanied by Acoustic Doppler Current Profiler data taken with a DR Instruments River Ray 600.

Stage data and discharge data (discharge data unavailable for the three non-flood surveys) were taken from the Liberty (08067000) and Moss Bluff (08067100) USGS stations, which are located at the upstream and downstream limits of the survey reach (Fig. 5.1). Water surface elevations at both stations were reported using the NAVD88 datum. Water surface elevations at all centerline positions were estimated by linearly interpolating between these two, reach-bounding stage elevations. Linear interpolation was sufficient as all water surface slopes were very small (the highest calculated slope was 1.4×10^{-4} which corresponded to less than a 3.5 m drop over 24.8 km; Figure 5.4). River-bottom elevation was then calculated by subtracting the measured water depth at each point from the interpolated water-surface elevation at that point. Gage data at Moss Bluff (Figure 5.1) was unavailable on June 26, so the appropriate water surface slope was

estimated based on the discharge at Liberty and the measured slopes for the other survey dates (grey star in Figure 5.4).

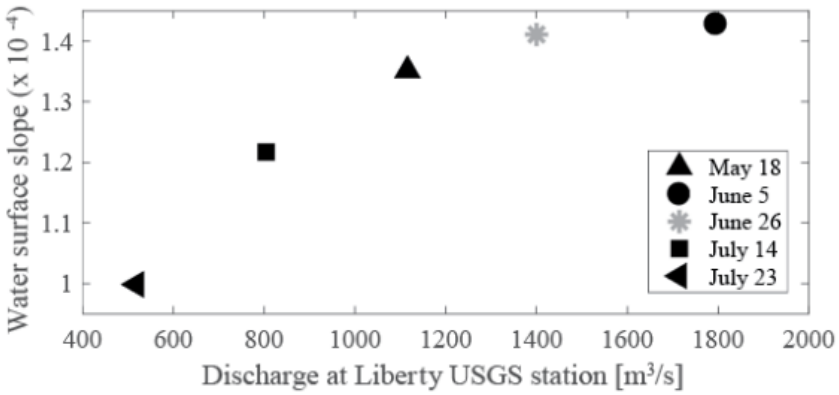

Figure 5.4: Discharge vs. water surface slope

Discharge data from the Liberty USGS station (upstream end of survey) vs. the water surface slope (estimated from interpolating a line between stage elevations at either end of the survey). The single grey star for the June 26 survey was interpolated based on the discharge at Liberty and the slopes of the other four surveys due to missing stage data from the downstream end of the survey reach.

Two bathymetric surveys were taken at low to moderate river discharge during the 11 months leading up to the flood (June 18, 2014 and January 13, 2015; Figure 5.3). Five surveys were taken at flood conditions (May 18, June 5, June 26, July 14, and July 23 2015; the first of which, taken on May 18, has a portion of the reach missing due to instrument failure). The final survey was taken after the stage returned to low flow conditions (October 20, 2015). Each survey was taken from as close to the centerline of the channel as possible (Figure 5.1b). Reaches where survey track lines diverged significantly from each other were removed in order to co-register each survey as closely as possible. Total distance downstream was calculated as the sum of the absolute distance

between navigation points. Each survey begins 1.1 km downstream of the Liberty USGS station and ends at the Moss Bluff USGS station, a total of 24.8 km of river channel.

The Humminbird fishfinder provided a depth profile along the nadir of the survey as well as sidescan sonar imaging of the bed. This combination allowed for the unambiguous identification of dunes and the manual measurement of dune heights and wavelengths of bedforms along the channel centerline. The multibeam data was manually cleaned using SonarWiz7 and a depth profile along the channel centerline was extracted and used to measure bedform geometry. Bedform heights were measured as the vertical distance between a crest and its downstream trough. Moving averages of bedform heights were calculated using a window of 10 channel widths (1100 m). For the single multibeam survey, bedform migration rates for individual dunes were measured as the horizontal distance between successive crest positions divided by the amount of elapsed time. Bedform group velocity between flood surveys was measured by shifting the entire profile laterally by the distance needed to best match the peaks and dividing by the elapsed time. This was possible because spacing between group peaks stayed constant despite deformation of the group shape.

Depth profiles were splined at 10 cm intervals to allow for subsequent frequency filtering. Each spline was manually checked against the raw depth profiles and corrected for any errors. A low pass Butterworth filter with a maximum threshold of two average channel widths (220 m) defined the river's long profile (Fig. 5.2) and facilitated inspection of any large-scale patterns of channel-bed aggradation or erosion as a result of the flooding event. Net elevation differences between successive profiles were also

calculated to provide a quantitative estimate of temporal change. A high pass Butterworth filter with a minimum threshold of one average channel width (110 m) was applied to each bathymetric survey to produce data series highlighting any spatial trends in dune topography.

Four samples of bed material were collected during the June 16 flood survey (Figure 5.5). Each of these samples was collected along a straight portion of channel spread out along the length of the study reach. Grain size analysis on these samples was completed on a Retsch Camsizer P4 particle analyzer, which uses dynamic image analysis to determine grain size. Flood conditions made collection of samples during the other surveys impossible.

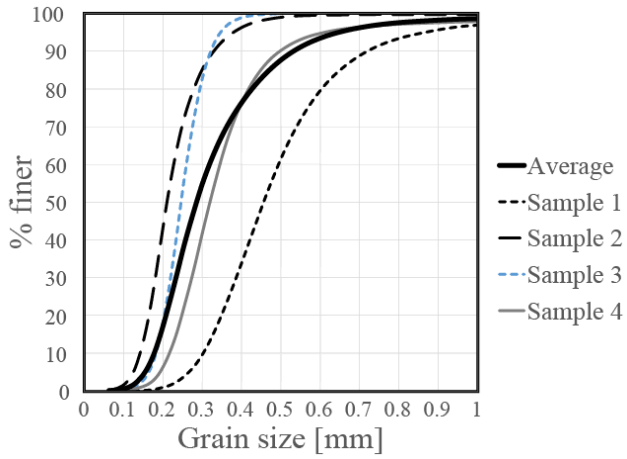

Figure 5.5: Cumulative grain size distribution for the four samples collected during the flood survey on June 26

Samples were collected from areas with small and large bedforms along the entire survey reach. The d50 of the average cumulative distribution was used for calculations of total volumetric sand flux as there was no evident spatial trend or pattern in grain size.

OBSERVATIONS AND RESULTS

Estimations of water surface slope range from about 1.4×10^{-4} for the highest flood discharge survey to 9.9×10^{-5} for the lowest flood discharge (Figure 5.4). Slopes associated with the non-flood surveys range from 2.4×10^{-5} to 6.4×10^{-5}. Water surface slope increases logarithmically with increasing discharge for the four flood surveys that have available discharge data. Pre- and post- flood survey discharges fall below the discharge detection threshold (283 m^3/s) for the Liberty USGS station.

Using a low pass filter on the bed elevation data allows for the observation of large scale bed topography without the scatter caused by the presence of bedforms and/or large woody debris on the channel bottom (Figure 5.2). Multiple scales of patterns in the low wavelength data (i.e. bend scale, reach scale, time series) have been recognized. Segments between bends, measured from one bend apex to the next, were an average of 1 km long with a range of 3 km. As expected, within each survey there is a gradual decrease in bed elevation between the upstream end and the downstream end (Figure 5.2). An average bend typically consists of a stretch of relatively high bed elevation followed by a deep scoured pool and another stretch of relative high elevation. These scour pools are located close to bend apexes, which are flanked both upstream and downstream by the higher crossings that connect consecutive bend apexes. Scour pools in the backwater zone tend to be deeper compared to upstream pools. Stream-wise locations and depths of scour pools persist between surveys, with slight differences small enough to be entirely accounted for by navigation differences between survey tracks.

There is no evidence for extensive aggradation or erosion of the channel bed between individual surveys or throughout the entire duration of the study period. The low pass filtered bed profiles more or less stack on top of each other through time (see Figure 5.2 for an example). Differencing the bed elevation data between all surveys and then summing up all of the differences leads to a mean net vertical change at any specific location along the survey profile of 10 cm, a value that is lower than the average bedform height for any of the surveys.

Using a high pass frequency filter on the bed elevation data allows for spatial changes in high frequency bed elevation to be highlighted. These small wavelength changes are due either to the presence of bedforms or in some cases debris along the base of the channel. Patterns in this filtered bed elevation are present both at the bend scale and at the reach scale. At the bend scale, the largest bedforms were consistently located at the higher elevation thalweg crossings and dunes were limited-to-absent in scour pools at bend apexes. For the remainder of the chapter, I will focus on reach-scale or multi-bend patterns found in the higher frequency topography as well as its change through time.

Figure 5.6 shows an example of the spatial variability in bedform heights that can be present along a survey long profile. Each individual bedform height and the moving average (window is 10 channel widths, 1100 m) along the 25 kilometer stretch of river is shown for the flood survey taken on July 14. There are areas with bedforms that are consistently < 50 cm tall (near km 0) that grade into regions where bedforms can be greater than 1.5 m in height (near km 8). The bedforms become smaller downstream, and begin to increase in height yet again near km 20. We define a group as the packet of

bedforms that make up the spatial pattern from small to large to small again (km 3 to km 15 in Figure 5.6). Multibeam data from July 26 (Figure 5.7) shows what the dunes comprising one of these groups look like along the base of the channel. Bedform groups have a wavelength that is consistent at 12 km long, which spans an average of 12 river bends. The groups are also visible by the increase and decrease in the envelope of the high pass filtered bed elevation (Figures 5.10-5.13). For each survey, a moving average of measured bed form heights (see Figure 5.6 for an example) is plotted on top of the high pass filtered bed elevation to show the correlation between spatial trends in high frequency bed elevation and bedform heights (Figures 5.8-5.15).

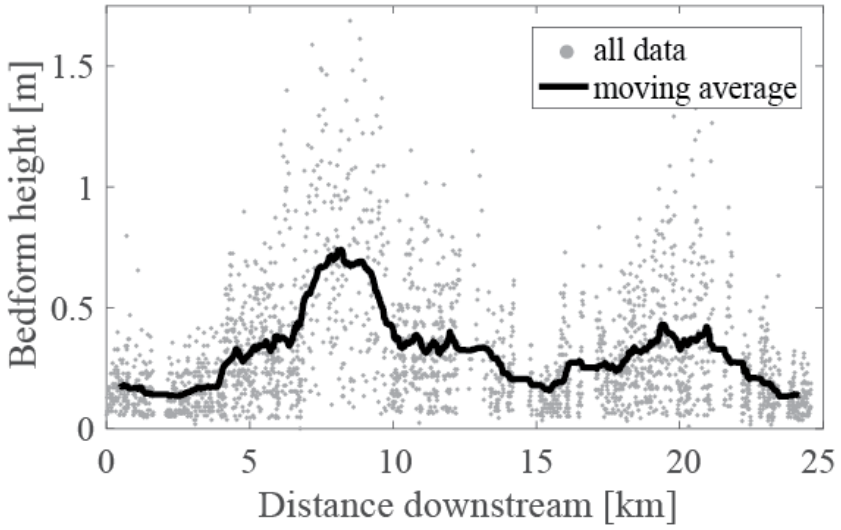

Figure 5.6: Individual bedform height measurements and moving average

Bedform heights measured from depth profile collected on July 14. The moving average window was 10 channel widths (1100m).

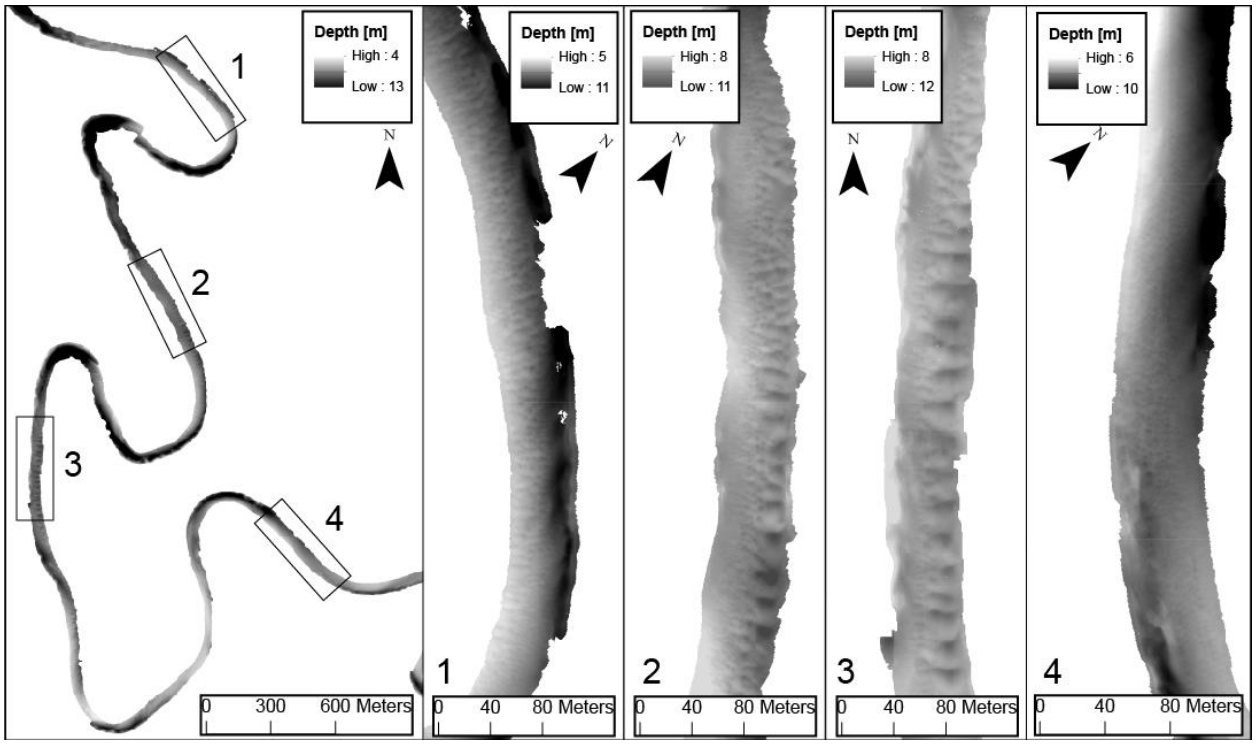

Figure 5.7: Multibeam data collected on June 26, 2015

Multibeam data collected from the straight portions of channels shows the scale of the spatial trend in bedform sizes. The scale of the four inset boxes is the same. Box 1 shows small bedforms upstream, 2 shows medium bedforms, 3 shows large bedforms, and 4 shows essentially no bedforms present at the base of the channel. This group is the downstream group in Figure 9.

The first two surveys that were taken on June 18, 2014 and January 13, 2015 were taken during minor flood conditions (first two points in Figure 5.3). For both of these surveys, the low pass filtered bed elevation shows no spatial trend (Figures 5.8 and 5.9). Measured bedform heights are similar (about 20 cm) for both surveys and again show no trend in size along the studied reach.

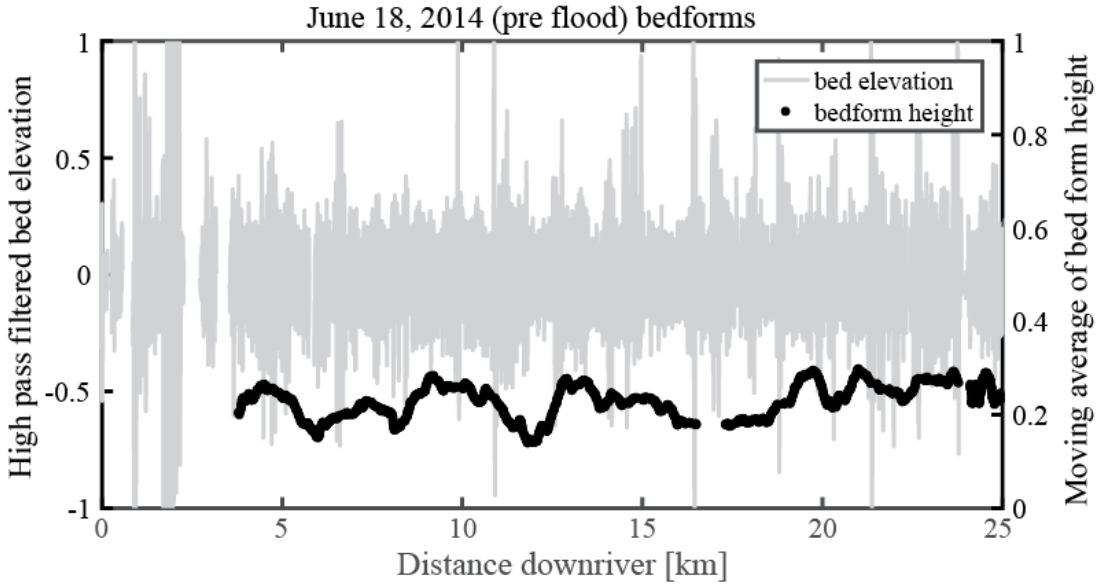

Figure 5.8: High pass filtered bed elevation and bed forms on June 18, 2014 (pre flood).

The grey line shows the bed elevation long profile with fluctuations >1 channel width (110 m) in wavelength filtered out. High frequency variability is due to either bedforms or the presence of debris along the base of the channel. A moving average of bedform heights (with a window of 10 channel widths, 1100 m) is shown with the black circles. There is no spatial trend in bedform size.

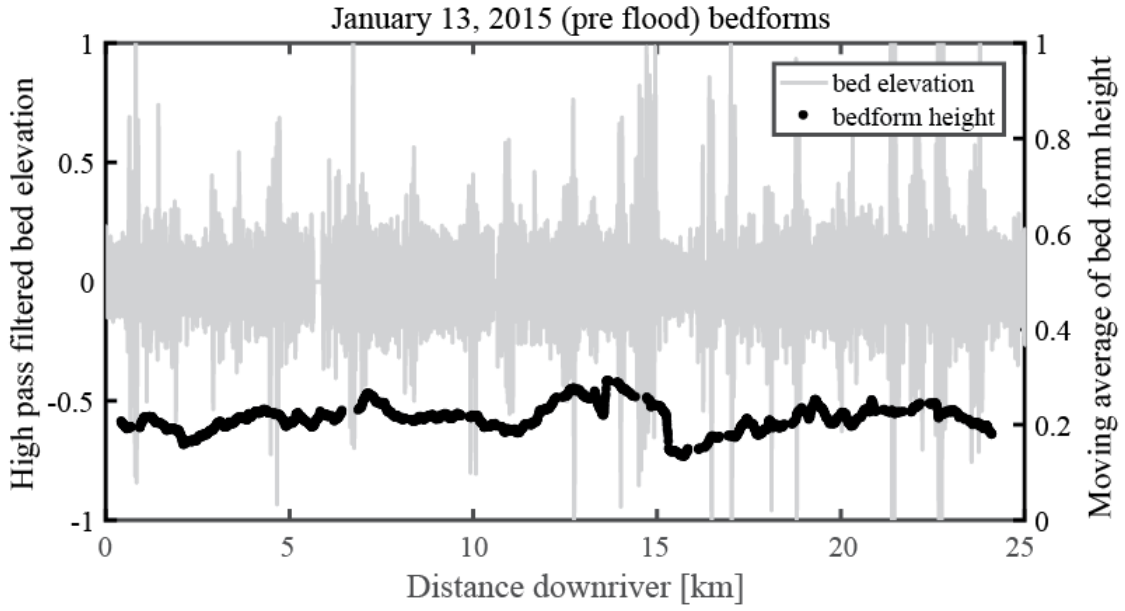

Figure 5.9: High pass filtered bed elevation and bed forms on January 13, 2015 (pre flood).

The grey line shows the bed elevation long profile with fluctuations >1 channel width (110 m) in wavelength filtered out. High frequency variability is due to either bedforms or the presence of debris along the base of the channel. A moving average of bedform heights (with a window of 10 channel widths, 1100 m) is shown with the black circles. There is no spatial trend in bedform height.

Instrument failure caused a portion of the data that was collected during the first flood survey to be lost. Despite the data loss, it is still evident that there is an emergent spatial pattern in the size of bedforms that was not present before the flood began (Figure 5.10). Bedforms at the most upstream end of the reach were up to 60 cm tall on average, decreasing to an average of about 30 cm some 12 km farther downstream. Bedform sizes begin to increase again farther downstream.

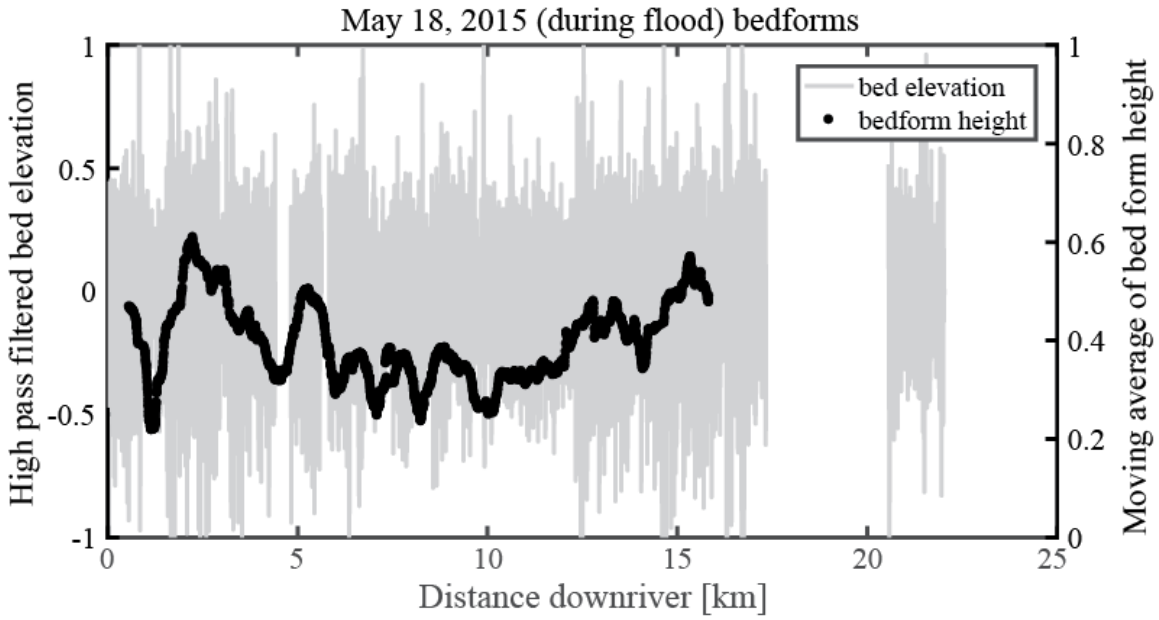

Figure 5.10: High pass filtered bed elevation and bed forms on May 18, 2015 (during flood).

The grey line shows the bed elevation long profile with fluctuations >1 channel width (110 m) in wavelength filtered out. High frequency variability is due to either bedforms or the presence of debris along the base of the channel. A moving average of bedform heights (with a window of 10 channel widths, 1100 m) is shown with the black circles. A portion of the data for this survey was lost due to instrument failure. The moving average of bedform heights show an emergent spatial trend of tall, to short, to tall bedforms along a 17 km long stretch of the river channel.

The second, third, and fourth flood surveys (collected on June 5, June 26, and July 14) reveal that the long wavelength groups of bedforms present in the first flood survey advect downstream (Figures 5.11-5.13). Each of these surveys displays two main peaks in bedform heights. The upstream group consistently has higher peak bedform heights compared to the downstream group. Between May 18 and June 5, the peaks of the bedform groups grew slightly taller and advected downstream about 1.3 km, averaging a rate of about 3 m/hr (Figure 5.11). This is coincident with an increase in river discharge

(Figures 3, 4). Between June 5 and June 26, the discharge decreased slightly and the groups again grew in height and advected downstream an additional 0.9 km, averaging a rate of about 1.8 m/hr (Figure 5.12). As the flood continued to decrease, the bedform groups during the July 14 survey reveals lower peak heights and migration totaling 3 km, averaging 6.9 m/hr throughout the interval (Figure 5.13). Finally, during the July 23 survey (conducted during the rapidly falling limb of the flood, Figure 5.2), the bedform groups have disappeared (Figure 5.14).

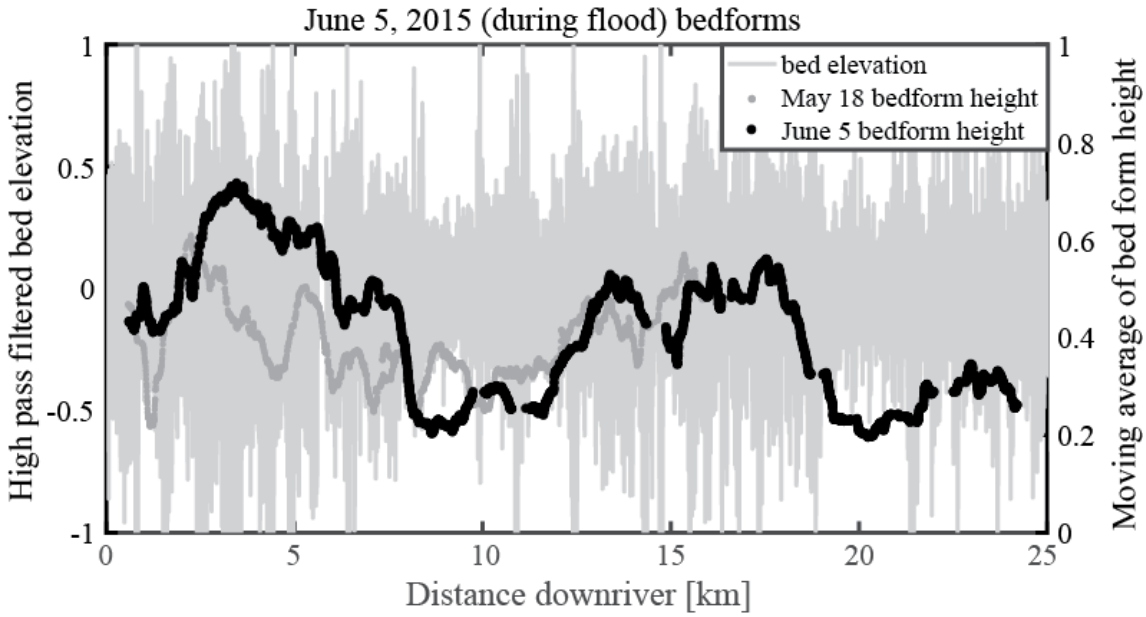

Figure 5.11: High pass filtered bed elevation and bed forms on June 5, 2015 (during flood).

The grey line shows the bed elevation long profile with fluctuations >1 channel width (110 m) in wavelength filtered out. High frequency variability is due to either bedforms or the presence of debris along the base of the channel. A moving average of bedform heights (with a window of 10 channel widths, 1100 m) is shown with the black circles. The moving average of the bedform heights associated with the previous survey is shown in the dark grey circles. The groups can be seen advecting and deforming downstream. The groups appear to become less broad.

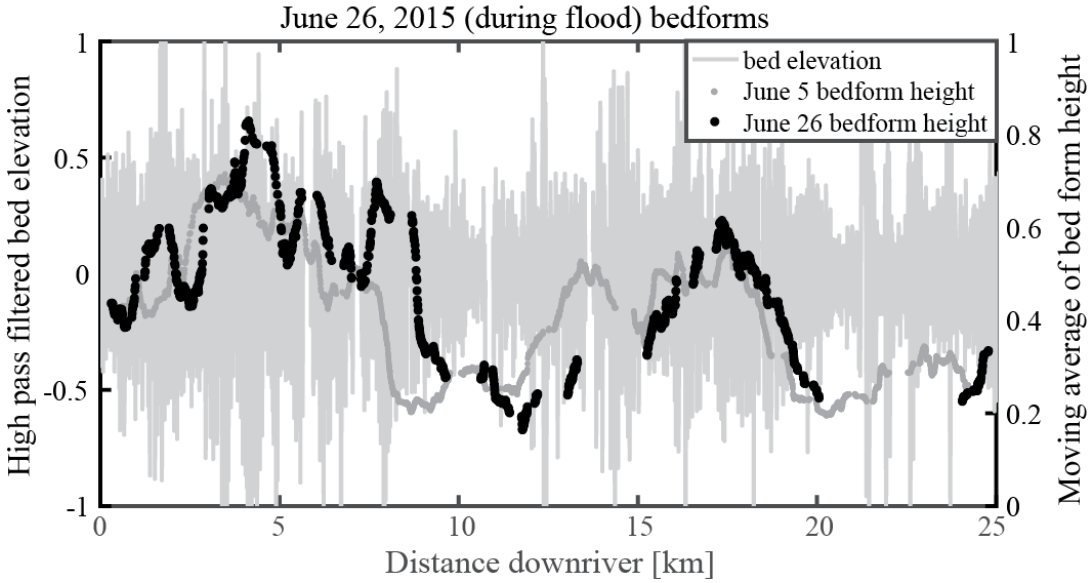

Figure 5.12: High pass filtered bed elevation and bed forms on June 26, 2015 (during flood).

The grey line shows the bed elevation long profile with fluctuations >1 channel width (110 m) in wavelength filtered out. High frequency variability is due to either bedforms or the presence of debris along the base of the channel. A moving average of bedform heights (with a window of 10 channel widths, 1100 m) is shown with the black circles. The moving average of the bedform heights associated with the previous survey is shown in the dark grey circles. The groups can be seen advecting and deforming downstream. The groups appear to become less broad.

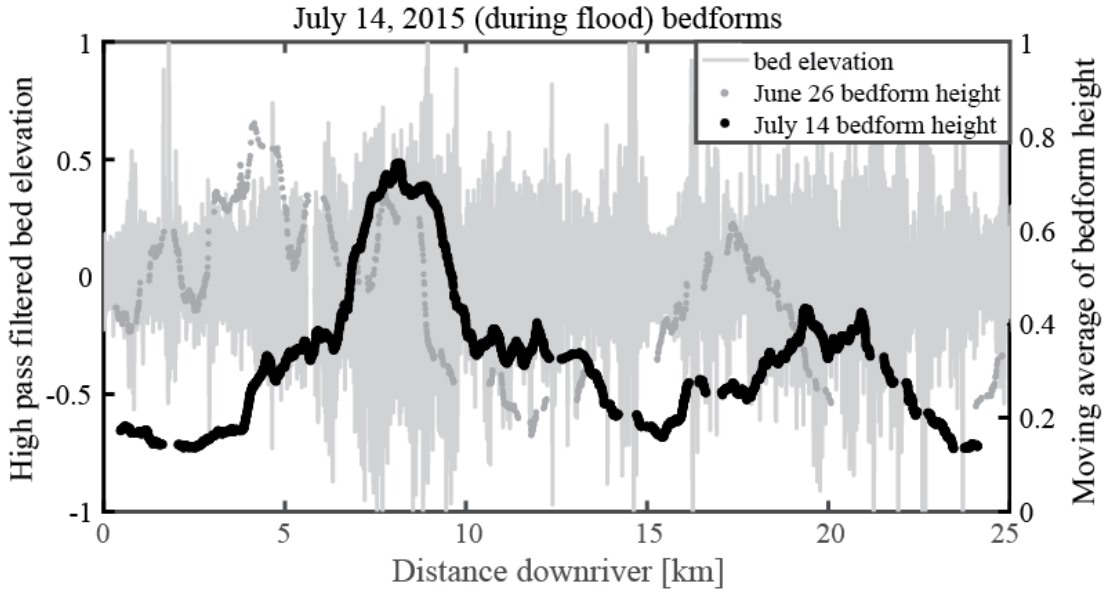

Figure 5.13: High pass filtered bed elevation and bed forms on July 14, 2015 (during flood).

The grey line shows the bed elevation long profile with fluctuations >1 channel width (110 m) in wavelength filtered out. High frequency variability is due to either bedforms or the presence of debris along the base of the channel. A moving average of bedform heights (with a window of 10 channel widths, 1100 m) is shown with the black circles. The moving average of the bedform heights associated with the previous survey is shown in the dark grey circles. The groups can be seen advecting and deforming downstream (the peaks appear to become less broad).

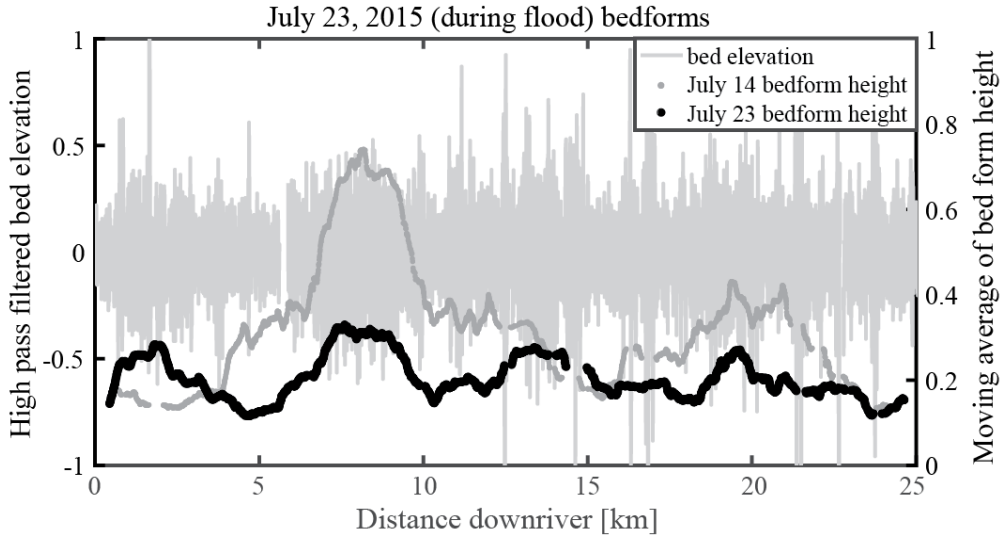

Figure 5.14: High pass filtered bed elevation and bed forms on July 23, 2015 (during flood).

The grey line shows the bed elevation long profile with fluctuations >1 channel width (110 m) in wavelength filtered out. High frequency variability is due to either bedforms or the presence of debris along the base of the channel. A moving average of bedform heights (with a window of 10 channel widths, 1100 m) is shown with the black circles. The moving average of the bedform heights associated with the previous survey is shown in the dark grey circles. Between the previous survey date and this one, the bedform groups entirely disappear.

The final survey was collected months after the flood receded and discharge had returned to low flow conditions. Bedforms along the base of the channel during this survey tended to be larger than the final flood survey bedforms despite being associated with a much lower river stage and discharge (stage was ~4 m lower; Figures 3, 15). The mean bedform height for the post-flood low flow survey (27 cm) was 34% greater than the mean bedform height for the final flood survey (20 cm).

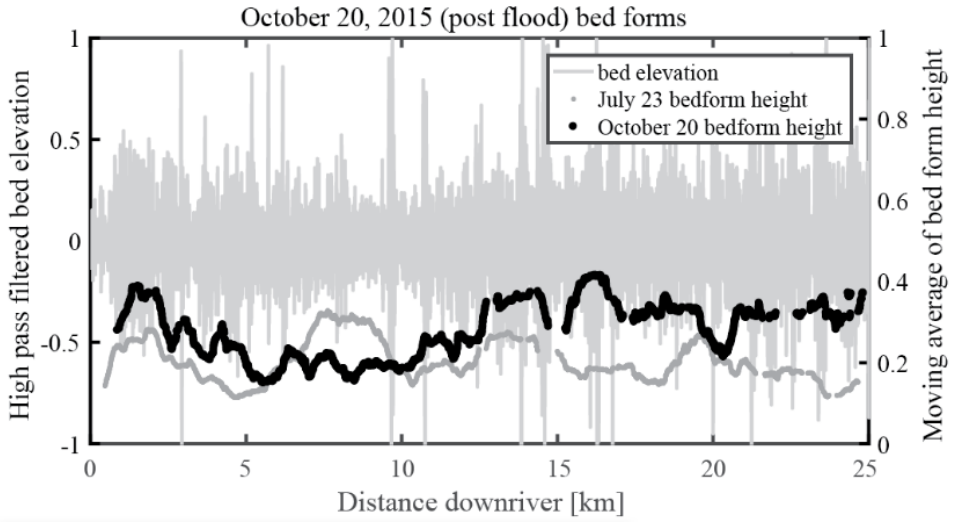

Figure 5.15: High pass filtered bed elevation and bed forms on October 20, 2015 (post flood).

The grey line shows the bed elevation long profile with fluctuations >1 channel width (110 m) in wavelength filtered out. High frequency variability is due to either bedforms or the presence of debris along the base of the channel. A moving average of bedform heights (with a window of 10 channel widths, 1100 m) is shown with the black circles. The moving average of the bedform heights associated with the previous survey is shown in the dark grey circles. The low flow bedform heights are taller on average than the bedforms that were present during the final stages of the flood.

Positions of the bedform group peaks do not correspond with noticeably higher topography along the low pass filtered bed profiles. The surveys conducted on July 14 and July 23 display the largest temporal difference in bedform group peak heights (Figure 5.14). The peaks of the bedform groups on July 14 are roughly located in 5 km long swaths centered around km 8 and km 20. These groups are entirely gone by the 23rd. The low pass filtered bed profile for these two surveys shows no obvious increase in topography associated with either of the bedform groups (Figure 5.2).

Bedform height, length, and migration rate were measured from a portion of the June 26 multibeam data. Bedform ripple indexes (length/height) appear to be constant when looking at all of the data (Figure 5.16). Migration rates appear constant despite the differences in bedform sizes (Figure 5.17). Group migration rates are on the higher end of the individual bedform migration rates. Bed-material load flux associated with the migrating dunes was calculated using the equation from Simons et al. (1965):

$$(1)\ q_{dune} = \varepsilon_{bed} C \frac{H}{2}$$

where $\varepsilon_{bed} = 0.7$ is the approximate volume concentration of the bed, C is the measured dune celerity, and H is the measured dune height. Because the migration rate was constant for dunes of all sizes, the flux varies linearly with the dune size (Figure 5.18). Figure 5.19 shows that dune sand flux appears constant with dune ripple index except for the small dunes that are associated with moving less sediment.

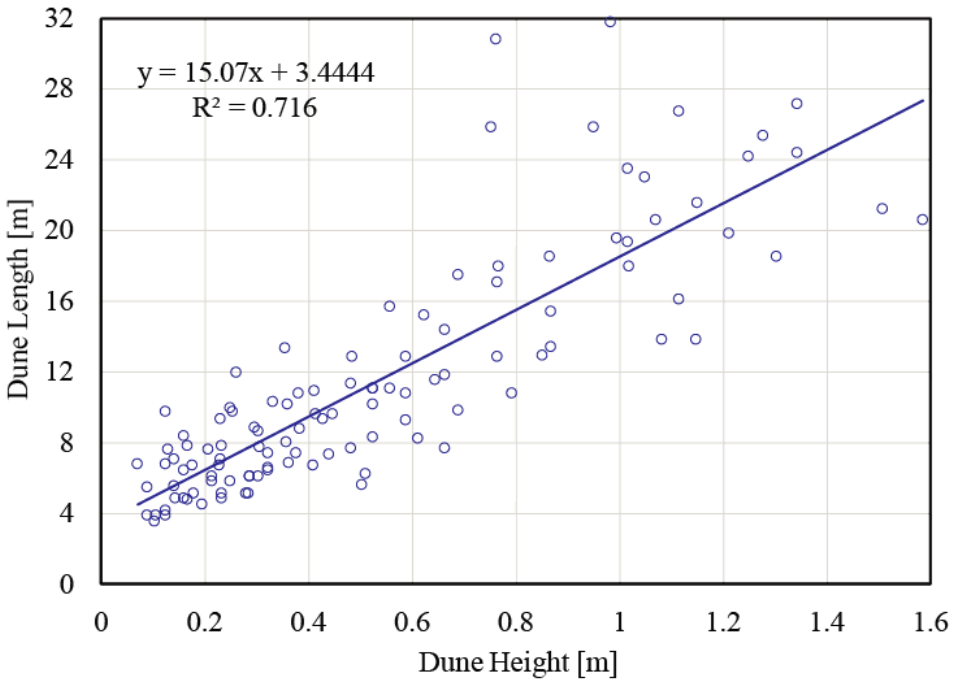

Figure 5.16: Dune heights vs. dune lengths for dunes measured on June 26, 2015

Dune measurements extracted from profile along a portion of the multibeam data. Only dunes with significant migration (because of sufficient elapsed time between multibeam passes) were measured. Dune height length varies linearly with dune height.

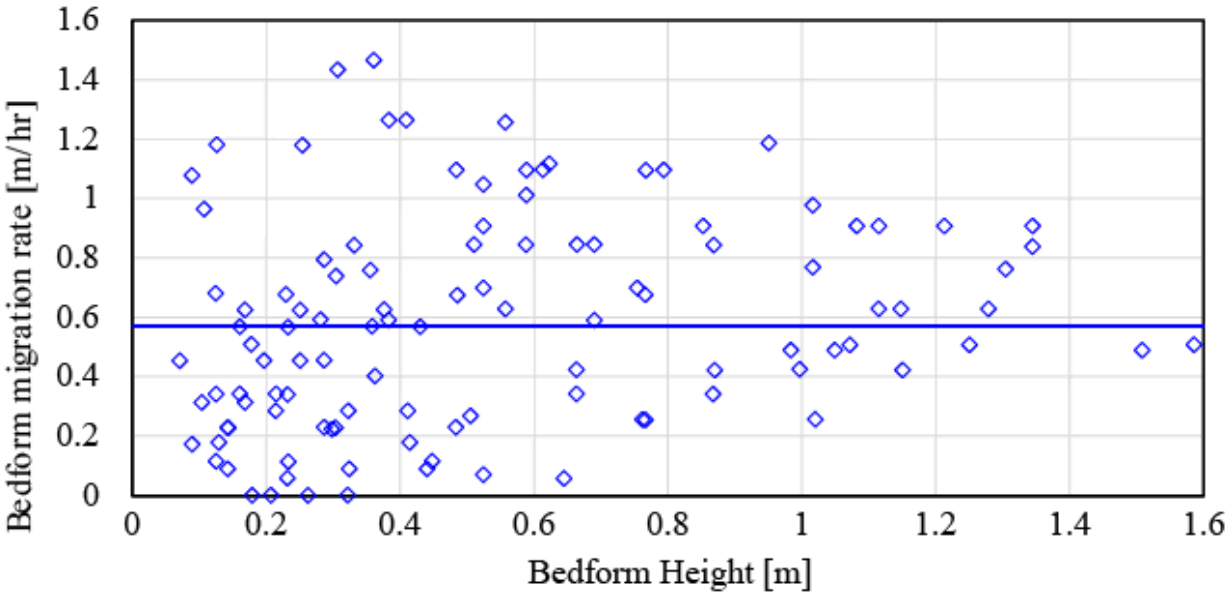

Figure 5.17: Bedform height vs. migration rate for a portion of the June 26 survey

Migration rates measured from a portion of the June 26 multibeam bathymetry data show no trend with bedform height.

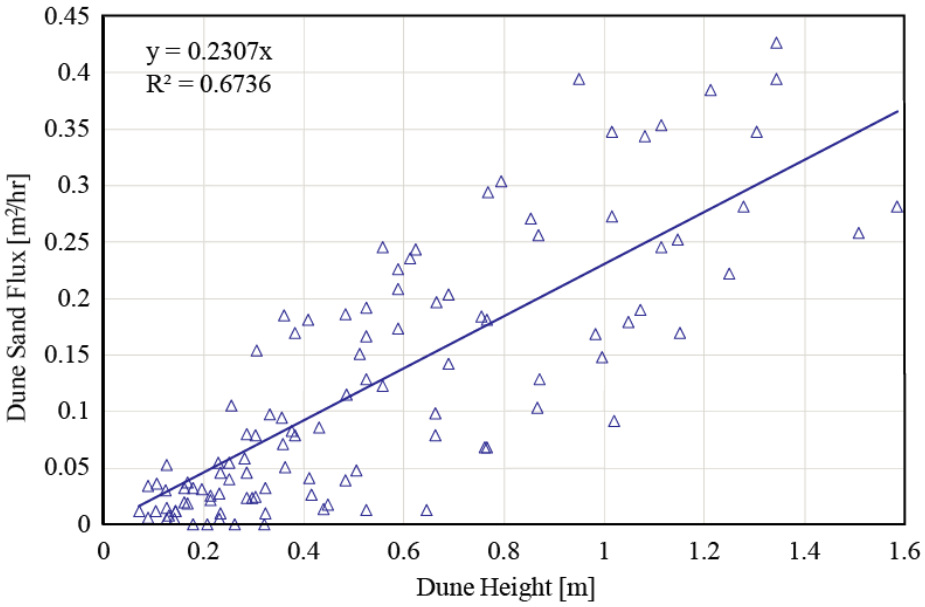

Figure 5.18: Dune height vs. associated dune sand flux

Equation (1) was used to calculate the sand flux associated with the migration of dunes. Because all sizes of dunes move at a constant rate, the flux varies linearly with the dune height.

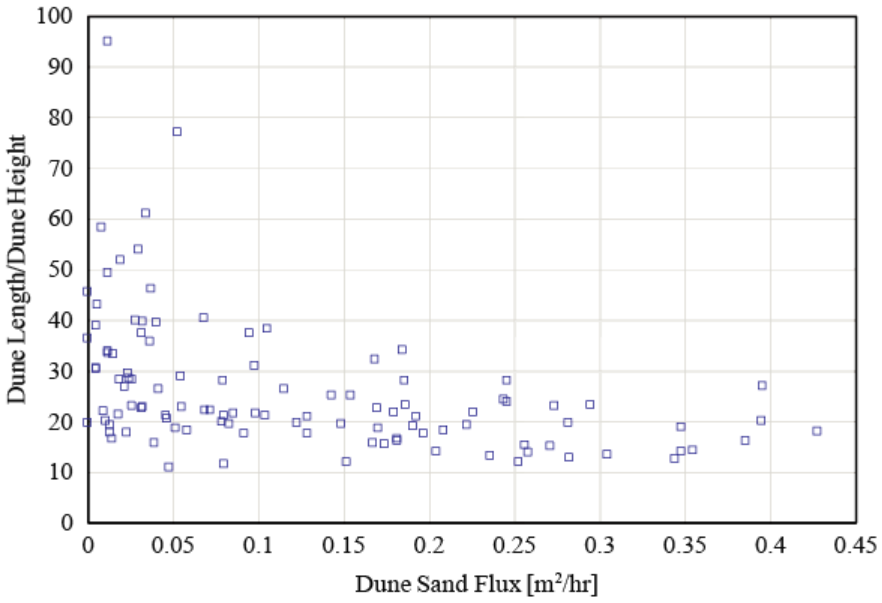

Figure 5.19: Dune sand flux vs. dune ripple index (length/height)

Ripple index varies linearly with sand flux for bedforms associated with flux >0.1 m^2/hr. Below that threshold, ripple index increases, a common expression of dunes that are nearing washout conditions. Dunes associated with these low flux values are typically quite small (Figure 16).

Acoustic Doppler Current Profiler data were noisy due to high turbidity and associated suspended sediment concentrations, but do not vary with distance downstream. Two representative vertical velocity profiles averaged over the width of the central channel are shown in Figure 5.20. Fitting a simple logarithmic velocity profile to these field data provided an estimate for shear velocity based on the slope of the trendline. This shear velocity was then used in the following equations to obtain an upper limit estimate of the total volumetric sand flux using a modified Myer-Peter Muller equation (Fernandez Luque and Van Beek 1976):

$$(2)\ \tau_{*(cr)} = \rho_f u_*^2$$

$$(3)\ \tau_* = \frac{\tau_{*(cr)}}{(\rho_s - \rho_f) g d_{50}}$$

$$(4)\ \gamma = 1.6(ln\tau_*) + 9.8$$

$$(5)\ \phi = \gamma[\tau_* - \tau_{*(cr)}]^{3/2}$$

$$(6)\ \phi = \frac{q_b}{\sqrt{\left(\frac{\rho_s}{\rho_f} - 1\right) g d_{50}^3}}$$

using d_{50}= 300 microns from the grain size samples taken during flood (Figure 5.5), ρ_s = 2.65 kg/m^3, ρ_f = 1 kg/m^3, and g = 9.81 m/s^2. Grain size samples were taken from portions of the channel with small and large bedforms (both upstream and downstream) and show no significant difference. The maximum total volumetric sand flux is calculated as **0.68 m^2/hr**, higher than any of the dune sand flux measurements (Figures 5.18 and 5.19). Here we define the bypass fraction as the difference between the maximum total volumetric sand flux and the dune sand flux. This value represents the fraction of bed-material load that is moving along the base of the channel but is not being incorporated into the dune migration. Figure 5.21 shows how this bypass fraction correlates with the ripple index of dunes for this Trinity River flood data as well as for several flume studies (Stein 1965; Guy et al. 1966). These results suggest that a significant fraction of the bed material load was bypassing the dunes during the flood.

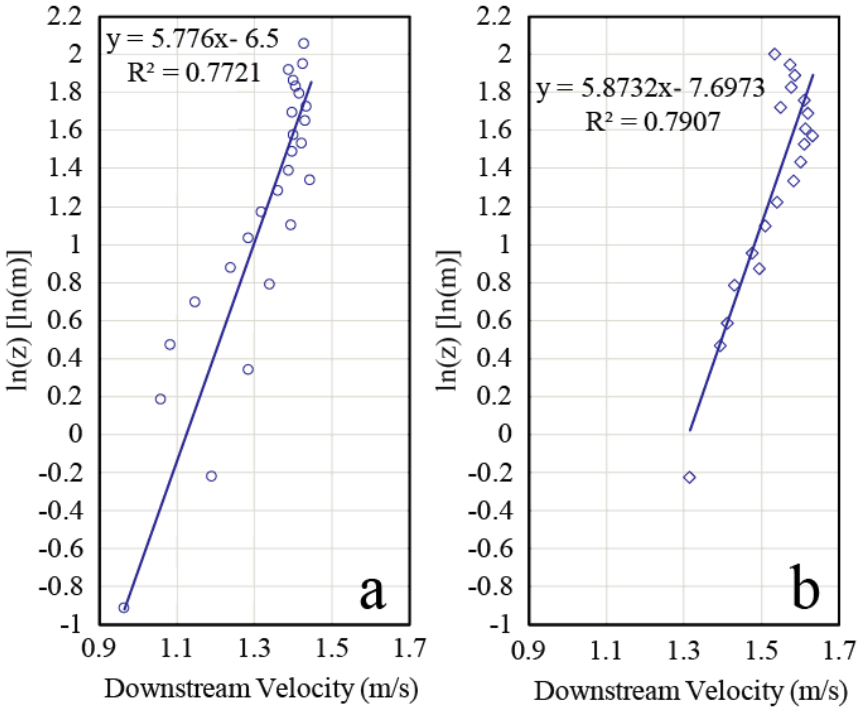

Figure 5.20: Width-averaged velocity profile for two ADCP transects

Data is noisy due to high turbidity and suspended sediment concentration. The slope of a line fit to the data was used to estimate u_*. This value for u_* was then plugged into equations 2-6 to estimate the total volumetric sand flux. a) velocity profile associated with a portion of the channel with smaller bedforms. b) velocity profile associated with a portion of the channel with larger bedforms.

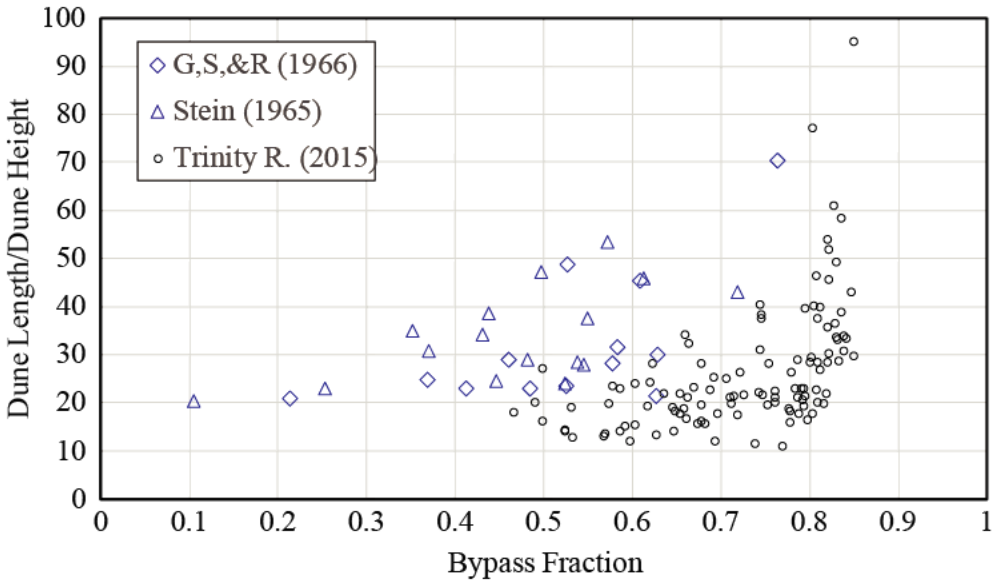

Figure 5.21: Bypass fraction vs ripple index for each measured bedform on June 26

The ripple index increases for dunes associated with a higher bypass fraction [(total volumetric sand flux – dune flux)/total volumetric sand flux]. These high ripple index, high bypass bedforms tend to be smaller dunes (Figures 5.15-5.17).

DISCUSSION

Our results suggest that the prolonged flooding event that occurred in 2015 did not result in any significant vertical aggradation of erosion of the channel bed. This is an important discovery, as previous studies have already shown a great deal of change in the same portion of river channel associated with the same flood (Mason and Mohrig 2018). The results of this analysis have shown that effectively all of the erosion and deposition that occurred within the channel during the flood was connected to lateral movement of channel bends and channel-width adjustment.

The most important outcome of this research was the observation of long wavelength groups of bedforms that translate downstream (Figures 5.10-5.13). Their

observation is especially surprising given the order of magnitude difference in scale between the relief of the high pass filtered data (Figures 5.8-5.15) versus the relief of the low pass filtered data (Figure 5.2). One might expect that the topographic slopes present along the channel bed (e.g., associated with moving from a crossing into a scour) might drown out the smaller wavelength changes in topography, but that is not the case here. These groups of bedforms are distinct from any previously studied pulses in bed-material load because of three main reasons: 1) the extensive spatial scale, 2) the lack of any significant topographic expression, 3) the lack of any observable longitudinal grain size trend.

These bedform groups have a peak to peak wavelength of 12 km that stays consistent as they migrate downstream throughout the duration of the flood. There are 25 bends included within the 25 km long survey reach, making the bedform groups cover an average of 12 river bends. Even the "mega-scale" pulses of Hoey and Sutherland (1991) are on the order 10 channel widths (1.1 km for the Trinity River), an order of magnitude smaller than the observed pulses here. Another distinguishing characteristic of these groups of bedforms is the lack of topographic expression. Along a bed profile, peaks in the heights of bedforms do not correlate with increases in topography. While the crests of the large bedforms are higher than the crests of the smaller bedforms, the troughs are equivalently lower, maintaining a constant average elevation within the range of bedform sizes. This implies these groups are best thought of as spatial increases and decreases in the thickness of the active layer (Parker et al. 2000). In addition, our observations of grain

size show that there is no discernable trend along the groups, implying that their presence can't be attributed to any effect of longitudinal grain size sorting.

We suggest that these reach-scale migrating bedform groups are an expression of prolonged washout. Any field of dunes within a natural system has inherent variability in bedform size and geometry. Grain excursion length is defined as the downstream distance a grain travels as it settles from a characteristic height within the flow depth (Mohrig and Smith 1996). As transport stage increased, the excursion lengths of individual grains being transported along the bed increased commensurately. If a bedform wavelength was smaller than the excursion length of the grain, it bypassed that bedform entirely. In addition, longer, taller bedforms (Figure 5.15) created more form drag compared to their smaller counterparts. Increased form drag lead to lower near-bed velocities along the base of the channel, thereby lowering the excursion lengths of grains. Thus, larger bedforms with longer wavelengths were favored to incorporate a larger portion of the total volumetric sand flux during flood. Washout of dunes occurs as the dune bypass fraction of the total volumetric flux increases to the point that insufficient sand is deposited on the lee faces of the dunes (Mohrig and Smith 1996). Our data suggest that the smaller dunes in these bedform groups were unable to capture the majority of the bed material load flux (Figures 5.16, 5.18, 5.19) and washed out as a consequence (a high dune length/height ratio is a common symptom of washout). The larger bedforms were leaking a significant amount of sediment but were still able to migrate and survive, leading to the downstream advection and deformation of the groups (notice that the groups tend to become less broad through time, Figures 5.10-5.13). Once the flood discharge lowered sufficiently to

decrease sediment supply (likely through a decrease in the amount of cut bank erosion), the dunes became sediment-starved, washing out and decreasing in height as a consequence (Figure 5.13). Months after the flood receded, dunes along the base of the channel were 34% taller than those present at the end of the flood. This implies that the transport conditions exceeded the sediment supply for the final flood survey. Once the transport and supply conditions had time to equalize, dunes could again grow to be taller.

The Trinity River bedforms appear to wash out later than the Stein (1965) and Guy et al. (1966) flume bedforms (Figure 5.21). This is because our calculation of the total volumetric sand flux provided a maximum value. For the lab data, both the total bed material flux and the dune flux were directly measured. If we had been capable of taking direct measurements of the total bed material flux it is likely the field and flume data would plot more consistently.

The downstream peak in bedform heights is consistently smaller than the upstream peak (Figures 5.6, 5.10-5.13). This implies that they are more washed out than their upstream counterparts, either due to an increase in the transport conditions, a decrease in the sediment availability, or a combination of both. ADCP data shows no spatial trend in the velocity with distance downstream, so an increase in transport conditions cannot be the source of the decrease in group peak height. Figure 5.22 shows the volume of material associated with cut bank erosion between 2011 and 2015 for the same portion of the Trinity River (includes changes due to the flood captured here; adapted from Mason and Mohrig 2018). The spatial decrease in erosional volumes is well-correlated with the decrease in bedform group peak height. Thus, the decrease in

peak height with distance downstream is in all likelihood due to the decrease in sediment availability associated with lessened cut bank erosion.

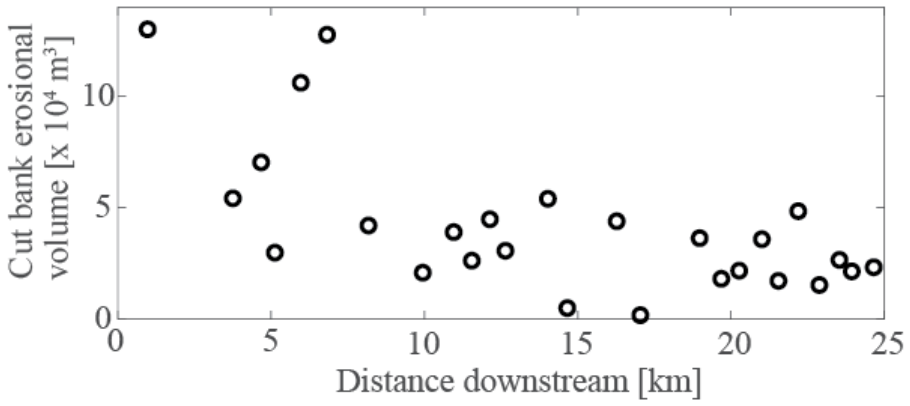

Figure 5.22: Estimated volumes of sediment released into the channel as a result of cut bank erosion

Each point represents the erosional volume of the cut bank associated with a single bend (data adapted from Mason and Mohrig 2018, https://doi.org/10.1029/2017JF004492). Lower values in cut bank erosional volumes correlate with smaller peak heights in the downstream bedform groups.

CONCLUSIONS

Our observations suggest that reach-scale patterns in bedforms can form in single thread channels in the absence of any instantaneous increase in sediment source or longitudinal grain size sorting. These groups of bedforms span an average of 12 river bends, and deform and advect downstream. We propose that they are an expression of prolonged washout that initiated on a spatially variable bedform field. During high transport conditions, larger bedforms were favored to capture a greater fraction of the total volumetric sand flux because of their increased wavelength and form drag. The

smaller dunes lose more and more sediment while the large dunes maintain their size and shape and migrate downstream. Eventually, when sediment supply is cut off, all of the dunes wash out. These observations lead to the development of a new conceptual model for an extremely large scale bedform self-organization process.

One important question that remains is related to the spacing between group peaks. We still do not understand what exactly sets up the characteristic group wavelength. It could be due to long wavelength changes in the bed topography (Figure 5.2 shows some low amplitude, high wavelength variability in the long profile topography) or potentially due local differences in cut bank erosional volumes. Future field observations as well as numerical modelling efforts aimed at better understanding this will be extremely helpful. Additionally, field observations and modelling will also allow us to better understand why group migration rates tend to be slightly higher than the individual bedform migration rates.

Bedforms are often used to interpret transport conditions within the flow. Typically, measurements of bedform geometry and migration are taken locally (often in a single location) and the interpretations of the associated flow regime are extrapolated out to the entire reach. The data presented here suggest that this practice needs to be seriously constrained. For this event on the Trinity River, even if bedform measurements had been taken across a stretch of several river bends, they would still not have captured the enormous spatial variability that existed.

Lastly, these observations suggest that throughout the duration of this unprecedented flooding event on the Trinity River, there was no net aggradation of

erosion along the base of the channel. However, previous studies (Mason & Mohrig 2018 and Chapter 4 of this dissertation) have shown a large amount of lateral adjustments along the banks of the river bends. This means that at the event scale, the long profile of the river isn't being altered and all of the change is accommodated by lateral adjustments of the channel.

ACKNOWLEDGEMENTS

The authors would like to thank the Mohrig Research Group, as well as Wayne Wagner, Max Daniller-Varghese, Corey van Dyk, Dan Duncan, Marcy Davis, Eric Prococki, and Travis Swanson. Funding was provided by the Jackson School of Geosciences.

REFERENCES

Allen, J. R. (1963). The classification of cross-stratified units with notes on their origin. Sedimentology, 2(2), 93–114.

Ashmore, P. (1991). Channel morphology and bed load pulses in braided, gravel-bed streams. Geografiska Annaler: Series A, Physical Geography, 73(1), 37-52.

Benda, L., & Dunne, T. (1997). Stochastic forcing of sediment routing and storage in channel networks. Water Resources Research, 33(12), 2865-2880.

Bertoldi, W., Zanoni, L., & Tubino, M. (2010). Assessment of morphological changes induced by flow and flood pulses in a gravel bed braided river: The Tagliamento River (Italy). Geomorphology, 114(3), 348-360.

Bridge, J., & Demicco, R. (2008). Earth surface processes, landforms and sediment deposits (815 pp.). Cambridge, UK: Cambridge University Press.

Bradley, R. W., & Venditti, J. G. (2017). Reevaluating dune scaling relations. Earth-science reviews, 165, 356-376.

Costa, J. E., & O'Connor, J. E. (1995). Geomorphically effective floods. Natural and anthropogenic influences in fluvial geomorphology, 89, 45-56.

Cui, Y., Parker, G., Lisle, T. E., Gott, J., Hansler-Ball, M. E., Pizzuto, J. E., ... & Reed, J. M. (2003). Sediment pulses in mountain rivers: 1. Experiments. Water Resources Research, 39(9).

Dietrich, W. E., & Smith, J. D. (1983). Influence of the point bar on flow through curved channels. Water Resources Research, 19(5), 1173–1192.

Fernandes, A. M., Törnqvist, T. E., Straub, K. M., & Mohrig, D. (2016). Connecting the backwater hydraulics of coastal rivers to fluvio-deltaic sedimentology and stratigraphy. Geology, 44(12), 979–982.

Fernandez Luque, R., & Van Beek, R. (1976). Erosion and transport of bed-load sediment. Journal of hydraulic research, 14(2), 127-144.

Gilbert, G. K. (1917). Hydraulic-mining debris in the Sierra Nevada (No. 105). US Government Printing Office.

Griffiths, G. A. (1979). Recent sedimentation history of the Waimakariri River, New Zealand. Journal of Hydrology (New Zealand), 6-28.

Guy, H. P., Simons, D. B., & Richardson, E. V. (1966). Summary of alluvial channel data from flume experiments, 1956-61. US Government Printing Office.

Hoey, T. B., & Sutherland, A. J. (1991). Channel morphology and bedload pulses in braided rivers: a laboratory study. Earth Surface Processes and Landforms, 16(5), 447-462.

Hoey, T. (1992). Temporal variations in bedload transport rates and sediment storage in gravel-bed rivers. Progress in physical geography, 16(3), 319-338.

Hudson, P. F., & Kesel, R. H. (2000). Channel migration and meander-bend curvature in the lower Mississippi River prior to major human modification. Geology, 28(6), 531–534.

Iseya, F., & Ikeda, H. (1987). Pulsations in bedload transport rates induced by a longitudinal sediment sorting: A flume study using sand and gravel mixtures. Geografiska Annaler: Series A, Physical Geography, 69(1), 15-27.

Jerolmack, D. J., and D. Mohrig (2005), A unified model for subaqueous bed form dynamics, Water Resour. Res., 41.

Karim, F. (1995). Bed configuration and hydraulic resistance in alluvial-channel flows. Journal of Hydraulic Engineering, 121(1), 15-25.

Kostaschuk, R., & Villard, P. (1996). Flow and sediment transport over large subaqueous dunes: Fraser River, Canada. Sedimentology, 43(5), 849-863.

Lamb, M. P., Nittrouer, J. A., Mohrig, D., & Shaw, J. (2012). Backwater and river plume controls on scour upstream of river mouths: Implications for fluvio-deltaic morphodynamics. Journal of Geophysical Research, 117, F01002.

Lanzoni, S., Siviglia, A., Frascati, A., & Seminara, G. (2006). Long waves in erodible channels and morphodynamic influence. Water Resources Research, 42(6).

Lisle, T. E., Pizzuto, J. E., Ikeda, H., Iseya, F., & Kodama, Y. (1997). Evolution of a sediment wave in an experimental channel. Water Resources Research, 33(8), 1971-1981.

Madej, M. A., & Ozaki, V. (1996). Channel response to sediment wave propagation and movement, Redwood Creek, California, USA. Earth Surface Processes and Landforms, 21(10), 911-927.

Mason, J., & Mohrig, D. (2018). Using time-lapse lidar to quantify river bend evolution on the meandering coastal Trinity River, Texas, USA. Journal of Geophysical Research: Earth Surface, 123(5), 1133-1144.

Meade, R. H. (1985). Wavelike movement of bedload sediment, East Fork River, Wyoming. Environmental Geology and Water Sciences, 7(4), 215-225.

Mohrig, D., & Smith, J. D. (1996). Predicting the migration rates of subaqueous dunes. Water Resources Research, 32(10), 3207-3217.

Nicholas, A. P., Ashworth, P. J., Kirkby, M. J., Macklin, M. G., & Murray, T. (1995). Sediment slugs: large-scale fluctuations in fluvial sediment transport rates and storage volumes. Progress in physical geography, 19(4), 500-519.

Nittrouer, J. A., Mohrig, D., & Allison, M. (2011). Punctuated sand transport in the lowermost Mississippi River. *Journal of Geophysical Research*, *116*, F04025, 1914–1934.

Nittrouer, J. A., Shaw, J., Lamb, M. P., & Mohrig, D. (2012). Spatial and temporal trends for water-flow velocity and bed-material sediment transport in the lower Mississippi River. *Geological Society of America Bulletin*, *124*(3–4), 400–414.

Parker, G., Paola, C., & Leclair, S. (2000). Probabilistic Exner sediment continuity equation for mixtures with no active layer. Journal of Hydraulic Engineering, 126(11), 818-826.

Shaw, J. B., & Mohrig, D. (2014). The importance of erosion in distributary channel network growth, Wax Lake Delta, Louisiana, USA. Geology, 42(1), 31-34.

Simons, D. B., Richardson, E. V., & Nordin, C. F. (1965). Bedload equation for ripples and dunes. US Government Printing Office.

Smith, V. B. (2012). Geomorphology of a coastal sand-bed river: Lower Trinity River, Texas (PhD dissertation).

Southard, J. B. (1971). Representation of bed configurations in depth-velocity-size diagrams. Journal of Sedimentary Research, 41(4), 903-915.

Stein, R. A. (1965). Laboratory studies of total load and apparent bed load. Journal of Geophysical Research, 70(8), 1831-1842.

Venditti, J. G., Church, M., & Bennett, S. J. (2005). On the transition between 2D and 3D dunes. Sedimentology, 52(6), 1343-1359.

Venditti, J. G., Lin, C. Y. M., & Kazemi, M. (2016). Variability in bedform morphology and kinematics with transport stage. Sedimentology, 63(4), 1017-1040.

Zinger, J. A., Rhoads, B. L., & Best, J. L. (2011). Extreme sediment pulses generated by bend cutoffs along a large meandering river. Nature Geoscience, 4(10), 675.

Chapter 6: Conclusions

This dissertation discusses morphodynamic change at a range of temporal and spatial scales. The first project (Chapter 2) defined the geomorphic edge of the channel by systematically measuring and observing the form and stratigraphic architecture of scroll bars and inferring processes required for their formation. All the data that were collected and analyzed (elevation and stratigraphic data) suggest that scroll bars represent proximal overbank deposits, i.e. levees. I have direct evidence that their position can be pushed both towards the channel and away from the channel, an observation that throws into question the use of scroll bar spacing as an indicator of channel migration rate. In addition, we suggest that many features qualitatively described as scroll bars in the ancient record are actually lateral accretion surfaces associated with point bars, which has potential to alter any paleo-channel reconstructions made based on the deposit. This chapter (and the corresponding manuscript submitted to Earth Surface Processes and Landforms) constrained the basic formative processes for these features. Additional future research is necessary in order to more comprehensively understand their form and function. For example, numerical modelling of the flow regime over the flattened top of point bars would be extremely helpful in determining why scroll bars form where they do. It would also likely reveal details about what controls the spacing between scroll bars, a subject that still remains unclear.

The two chapters that use time-lapse bare earth lidar data to observe bend-scale changes in deposition and erosion along the river have helped distinguish how the inner and outer banks independently move and readjust through time. In the normal flow portion of the river reach, we have shown that a large perturbation forced increased deposition along point bars relative to erosion along the outer bank, effectively narrowing the bar-to-bank width of the channel. During the following observation period, the same portion of

the channel underwent increased outer bank erosion compared to point bar deposition. Decreased values for gross point bar deposition and cut bank erosion within the backwater zone can account for the decreased lateral migration rate of this portion of the channel. This compensational bank migration behavior implies that at short time scales, river banks tend to migrate independently. However, over-widening or over-narrowing of the channel causes changes in the flow regime which then act to reverse the previous behavior. Again, future research that utilizes numerical models to distinguish when channels tend to widen versus narrow would be extremely helpful for understanding this compensational bank migration behavior. In addition, more field data sets that document how channels respond to various magnitudes of discharge events would improve our understanding of how this compensational bank migration occurs over a finer temporal resolution, as well as provide numerical models with more natural system validation.

The observation of the migrating bedform groups present along the base of the channel in chapter 5 allowed me to see a new scale of bed self-organization. While this project provides a comprehensive picture of the spatial and temporal variability in bed topography that occurred as a result of spatially variable bedform wash out, there are still several remaining questions. For example, what sets up the 12 km wavelength of these bedform groups? Is the spacing due to some change in the geometry of the reach, or is it arbitrarily set up by the bedform field that is present at the beginning of the flood? Do these bedform groups form during every flood that exceeds some discharge threshold? Numerical modelling combined with more field observations of channel beds during flood will both help immensely with understanding the initiation of this newly observed phenomenon.

This dissertation has provided field observations of sediment transport at a variety of temporal and spatial scales. These observations and the subsequent analyses have

allowed us to better understand how coastal river systems time-integrate changes in sediment transport conditions into their larger-scale geomorphology and kinematics. Results have not only illuminated much about the behavior of this particular natural system, but can also be extrapolated out to other systems as well. Particularly, the observations regarding scroll bars, compensational river bank migration, and the reduction in depositional and erosional volumes of river bank change within the backwater zone are likely applicable to the majority of meandering river systems.

All of the recorded observations imply that the various geomorphic components comprising the fluvial channel (scroll bar, point bar, and outer bank) can operate independently over short time scales. Scroll bars can grow and evolve separately from the point bars that they are attached to (as evidenced by the landward movement of the focus of scroll bar deposition concurrent with the channel-ward aggradation and movement of the point bar shoreline; Chapter 2). The inner and outer bank do not necessarily move in unison, as shown by the temporal changes in bar-to-bank width in Chapters 3 and 4. Despite the fact that these geomorphic features have been directly observed to evolve independently of one another over the event to annual time scale, there is a preponderance of evidence that suggests that the channel geometry tends to maintain a consistent mean shape over longer intervals. This intriguing disparity requires that the various elements comprising the channel geometry migrate compensationally over short intervals, consistently overshooting and undershooting the mean channel condition. This suggests that that centerline migration numerical models are only accurate over decadal timescales. Ultimately, numerical models that allow the various river bank components to evolve independently of one another may be necessary in order to predict change over shorter timescales.

Appendix

Data from each survey detailed in Chapter 5 is available as supplementary materials from the University of Texas at Austin library online repository. There are two text files providing header descriptions for the survey data and the bedform data. The additional 16 text files are the long profiles of the 8 surveys (files ending in the survey date mmddyy) and the manual bedform measurements from each survey (files ending in the survey date and "_bf"). The included files are listed:

- survey_column_headers.txt
- bf_column_headers.txt
- preflood1_061814.txt
- preflood1_061814_bf.txt
- preflood2_011315.txt
- preflood2_011315_bf.txt
- flood1_051815.txt
- flood1_051815_bf.txt
- flood2_060515.txt
- flood2_060515_bf.txt
- flood3_062615.txt
- flood3_062615_bf.txt
- flood4_071415.txt
- flood4_071415_bf.txt

- flood5_072315.txt
- flood5_072315_bf.txt
- postflood_102015.txt
- postflood_102015_bf.txt

Bibliography

Chapter 1: Introduction

Allen, J. R. L. (1985). Principles of physical sedimentology (272 pp.). London: Allen&Unwin.

Blum, M. D., & Roberts, H. H. (2009). Drowning of the Mississippi Delta due to insufficient sediment supply and global sea-level rise. Nature Geoscience, 2(7), 488.

Te Chow, V. (1959). Open-channel hydraulics (Vol. 1). New York: McGraw-Hill.

Hay, C. C., Morrow, E., Kopp, R. E., & Mitrovica, J. X. (2015). Probabilistic reanalysis of twentieth-century sea-level rise. Nature, 517(7535), 481.

Hudson, P. F., & Kesel, R. H. (2000). Channel migration and meander-bend curvature in the lower Mississippi River prior to major human modification. Geology, 28(6), 531-534.

Fernandes, A. M., Törnqvist, T. E., Straub, K. M., & Mohrig, D. (2016). Connecting the backwater hydraulics of coastal rivers to fluvio-deltaic sedimentology and stratigraphy. Geology, 44(12), 979-982.

Lamb, M. P., Nittrouer, J. A., Mohrig, D., & Shaw, J. (2012). Backwater and river plume controls on scour upstream of river mouths: Implications for fluvio-deltaic morphodynamics. Journal of Geophysical Research: Earth Surface, 117(F1).

Nanson, G. C., & Hickin, E. J. (1983). Channel migration and incision on the Beatton 694 River. Journal of Hydraulic Engineering, 109(3), 327-337.

Nittrouer, J. A., Mohrig, D., & Allison, M. (2011). Punctuated sand transport in the lowermost Mississippi River. Journal of Geophysical Research: Earth Surface, 116(F4).

Nittrouer, J. A., Shaw, J., Lamb, M. P., & Mohrig, D. (2012). Spatial and temporal trends for water-flow velocity and bed-material sediment transport in the lower Mississippi River. Bulletin, 124(3-4), 400-414.

Rodnight, H., Duller, G. A. T., Tooth, S., & Wintle, A. G. (2005). Optical dating of a 710 scroll-bar sequence on the Klip River, South Africa, to derive the lateral migration rate of 711 a meander bend. The Holocene, 15(6), 802-811.

Smith, V. B. (2012). Geomorphology of a coastal sand-bed river: Lower Trinity River, Texas. PhD dissertation.

Wassmann, R., Hien, N. X., Hoanh, C. T., & Tuong, T. P. (2004). Sea level rise affecting the Vietnamese Mekong Delta: water elevation in the flood season and implications for rice production. Climatic Change, 66(1-2), 89-107.

Chapter 2: Scroll bars are inner bank levees along bends in meandering channels

Bridge, J. S. (2009). Rivers and floodplains: forms, processes, and sedimentary record. John Wiley & Sons.

Brierley, G. J., Ferguson, R. J., & Woolfe, K. J. (1997). What is a fluvial levee? Sedimentary Geology, 114(1-4), 1-9.

Burr, D. M., Enga, M. T., Williams, R. M., Zimbelman, J. R., Howard, A. D., & Brennand, T. A. (2009). Pervasive aqueous paleoflow features in the Aeolis/Zephyria Plana region, Mars. Icarus, 200(1), 52-76.

Durkin, P. R., Hubbard, S. M., Boyd, R. L., & Leckie, D. A. (2015). Stratigraphic expression of intra-point-bar erosion and rotation. Journal of Sedimentary Research, 85(10), 1238-1257.

Durkin, P. R., Hubbard, S. M., Holbrook, J., & Boyd, R. (2017). Evolution of fluvial meander-belt deposits and implications for the completeness of the stratigraphic record. Geological Society of America Bulletin.

Fernandes, A. M., Törnqvist, T. E., Straub, K. M., & Mohrig, D. (2016). Connecting the backwater hydraulics of coastal rivers to fluvio-deltaic sedimentology and stratigraphy. Geology, 44(12), 979-982.

Hassenruck-Gudipati, H.J., Mohrig, D.C., and Passalacqua, P. Characterizing natural levee morphology for a sand-bed coastal river. Abstract 202-4, Geological Society of America Annual Meeting, Seattle, WA. October 22-25, 2017.

Hickin, E. J. (1974). The development of meanders in natural river-channels. American journal of science, 274(4), 414-442.

Hickin, E. J., & Nanson, G. C. (1975). The character of channel migration on the Beatton River, northeast British Columbia, Canada. Geological Society of America Bulletin, 86(4), 487-494.

Hudson, P. F., & Kesel, R. H. (2000). Channel migration and meander-bend curvature in the lower Mississippi River prior to major human modification. Geology, 28(6), 531-534.

Ielpi, A., & Ghinassi, M. (2014). Planform architecture, stratigraphic signature and morphodynamics of an exhumed Jurassic meander plain (Scalby Formation, Yorkshire, UK). Sedimentology, 61(7), 1923-1960.

Jackson, R.G. (1976) Large scale ripples of the lower Wabash River. Sedimentology, 23, 593-623.

Lamb, M. P., Nittrouer, J. A., Mohrig, D., & Shaw, J. (2012). Backwater and river plume controls on scour upstream of river mouths: Implications for fluvio-deltaic morphodynamics. Journal of Geophysical Research: Earth Surface, 117(F1).

Leopold, L. B., Wolman, M. G., and Miller P. (1964). Fluvial processes in geomorphology. Dover Publications.

Lewin, J., & Ashworth, P. J. (2014). The negative relief of large river floodplains. Earth-Science Reviews, 129, 1-23.

Mason, J. & Mohrig, D. (2018). Using time-lapse lidar to quantify river bend evolution on the meandering coastal Trinity River, Texas, USA. Journal of Geophysical Research: Earth Surface, 123. https://doi.org/10.1029/2017JF004492

McGowan, J. H., and L. E. Garner (1970), Physiographic features and stratification types of coarse-grained point bars: Modern and ancient examples, Sedimentology, 14, 77–111.

Moore, J. M., & Howard, A. D. (2005). Large alluvial fans on Mars. Journal of Geophysical Research: Planets, 110(E4).

Moore, J. M., A. D. Howard, W. E. Dietrich, and P. M. Schenk (2003), Martian Layered Fluvial Deposits: Implications for Noachian Climate Scenarios, Geophys. Res. Lett., 30, 2292, doi:10.1029/2003GL019002, 24.

Nanson, G. C. (1980). Point bar and floodplain formation of the meandering Beatton River, northeastern British Columbia, Canada. Sedimentology, 27(1), 3-29.

Nanson, G. C. (1981). New evidence of scroll-bar formation on the Beatton River. Sedimentology, 28(6), 889-891.

Nanson, G. C., & Croke, J. C. (1992). A genetic classification of floodplains. Geomorphology, 4(6), 459-486.

Nanson, G. C., & Hickin, E. J. (1983). Channel migration and incision on the Beatton River. Journal of Hydraulic Engineering, 109(3), 327-337.

Nilsson, G. and Martvall, S. (1972) The Ore River and its Meanders. Uppsala Univ., Dept. phys. Geugr. Urgi. Rep. 19.

Nittrouer, J. A., Allison, M. A., & Campanella, R. (2008). Bedform transport rates for the lowermost Mississippi River. Journal of Geophysical Research: Earth Surface, 113(F3).

Nittrouer, J. A., Shaw, J., Lamb, M. P., & Mohrig, D. (2012). Spatial and temporal trends for water-flow velocity and bed-material sediment transport in the lower Mississippi River. Geological Society of America Bulletin, 124(3-4), 400-414.

Pratt, V. (1987). Direct least-squares fitting of algebraic surfaces. In ACM SIGGRAPH computer graphics (Vol. 21, No. 4, pp. 145-152). ACM.

Rodnight, H., Duller, G. A. T., Tooth, S., & Wintle, A. G. (2005). Optical dating of a scroll-bar sequence on the Klip River, South Africa, to derive the lateral migration rate of a meander bend. The Holocene, 15(6), 802-811.

Schon, S. C., Head, J. W., & Fassett, C. I. (2012). An overfilled lacustrine system and progradational delta in Jezero crater, Mars: Implications for Noachian climate. Planetary and Space Science, 67(1), 28-45.

Smith, V. B. (2012). Geomorphology of a coastal sand-bed river: Lower Trinity River, Texas. PhD dissertation.

Sundborg, A. (1956). The River Klaralven, a study of fluvial processes. Geogr. Annlr, 38, 127-316.

van de Lageweg, W. I., van Dijk, W. M., Baar, A. W., Rutten, J., & Kleinhans, M. G. (2014). Bank pull or bar push: What drives scroll-bar formation in meandering rivers?. Geology, 42(4), 319-322.

Wang, J, and Bhattacharya J.P. (2017). Plan-view Paleochannel Reconstruction of Amalgamated Meander Belts, Cretaceous Ferron Sandstone, Notom Delta, South-central Utah, U.s.a.. Journal of Sedimentary Research; 88 (1): 58–74. doi: https://doi-org.ezproxy.lib.utexas.edu/10.2110/jsr.2017.77

Zen, S., Gurnell, A. M., Zolezzi, G., & Surian, N. (2017). Exploring the role of trees in the evolution of meander bends: The Tagliamento River, Italy. Water Resources Research.

Chapter 3: Using time-lapse lidar to quantify channel bend evolution

Allen, J. R. (1963). The classification of cross-stratified units with notes on their origin. Sedimentology, 2(2), 93–114. https://doi.org/10.1111/j.1365-3091.1963.tb01204.x

Allen, J. R. L. (1985). Principles of physical sedimentology (272 pp.). London: Allen&Unwin.

Bevington, P. R. (1969). Data reduction and error analysis for the physical. Sciences, 164–176.

Bridge, J., & Demicco, R. (2008). Earth surface processes, landforms and sediment deposits (815 pp.). Cambridge, UK: Cambridge University Press. https://doi.org/10.1017/CBO9780511805516

Bridge, J. S., Alexander, J. A. N., Collier, R. E., Gawthorpe, R. L., & Jarvis, J. (1995). Ground-penetrating radar and coring used to study the large-scale structure of point-bar deposits in three dimensions. Sedimentology, 42(6), 839–852. https://doi.org/10.1111/j.1365-3091.1995.tb00413.x

Chatanantavet, P., Lamb, M. P., & Nittrouer, J. A. (2012). Backwater controls of avulsion location on deltas. Geophysical Research Letters, 39, L01402. https://doi.org/10.1029/2011GL050197

Chow, V. (1959). Open channel hydraulics. New York: McGraw-Hill Book Company, Inc.

Dietrich, W. E., & Smith, J. D. (1983). Influence of the point bar on flow through curved channels. Water Resources Research, 19(5), 1173–1192. https://doi.org/10.1029/WR019i005p01173

Edmonds, D. A., Hoyal, D. C., Sheets, B. A., & Slingerland, R. L. (2009). Predicting delta avulsions: Implications for coastal wetland restoration. Geology, 37(8), 759–762. https://doi.org/10.1130/G25743A.1

Eke, E., Parker, G., & Shimizu, Y. (2014). Numerical modeling of erosional and depositional bank processes in migrating river bends with self-formed width:Morphodynamics of bar push and bank pull. Journal of Geophysical Research: Earth Surface, 119, 1455–1483. https://doi.org/10.1002/2013JF003020

Engelund, F. (1974). Flow and bed topography in channel bends. Journal of the Hydraulics Division, 100(11), 1631–1648.

Fernandes, A. M., Törnqvist, T. E., Straub, K. M., & Mohrig, D. (2016). Connecting the backwater hydraulics of coastal rivers to fluvio-deltaic sedimentology and stratigraphy. Geology, 44(12), 979–982.

Frazier, D. E., & Osanik, A. (1961). Point-bar deposits. Louisiana: Old River Locksite.

Ghinassi, M., Ielpi, A., Aldinucci, M., & Fustic, M. (2016). Downstream-migrating fluvial point bars in the rock record. Sedimentary Geology, 334, 66–96. https://doi.org/10.1016/j.sedgeo.2016.01.005

Hickin, E. J., & Nanson, G. C. (1975). The character of channel migration on the Beatton River, Northeast British Columbia, Canada. Geological Society of America Bulletin, 86(4), 487–494. https://doi.org/10.1130/0016-7606(1975)86%3C487:TCOCMO%3E2.0.CO;2

Hoyal, D. C. J. D., & Sheets, B. A. (2009). Morphodynamic evolution of experimental cohesive deltas. Journal of Geophysical Research, 114, F02009. https://doi.org/10.1029/2007JF000882

Hudson, P. F., & Kesel, R. H. (2000). Channel migration and meander-bend curvature in the lower Mississippi River prior to major human modification. Geology, 28(6), 531–534. https://doi.org/10.1130/0091-7613(2000)28%3C531:CMAMCI%3E2.0.CO;2

Kikkawa, H., Ikeda, S., & Kitagawa, A. (1976). Flow and bed topography in curved open channels. Journal of the Hydraulics Division, 102(9), 1327–1342.

Lamb, M. P., Nittrouer, J. A., Mohrig, D., & Shaw, J. (2012). Backwater and river plume controls on scour upstreamof river mouths: Implications for fluvio-deltaic morphodynamics. Journal of Geophysical Research, 117, F01002. https://doi.org/10.1029/2011JF002079

Lane, E. W. (1957). A study of the shape of channels formed by natural streams flowing in erodible material. US Army Corps of Engineers. Missouri River Division, Omaha, Sediment series, 9.

Leeder, M. R., & Bridges, P. H. (1975). Flow separation in meander bends. Nature, 253(5490), 338–339. https://doi.org/10.1038/253338a0

Nanson, G. C. (1980). Point bar and floodplain formation of the meandering Beatton River, northeastern British Columbia, Canada. Sedimentology, 27(1), 3–29. https://doi.org/10.1111/j.1365-3091.1980.tb01155.x

Nittrouer, J. A., Mohrig, D., & Allison, M. (2011). Punctuated sand transport in the lowermost Mississippi River. Journal of Geophysical Research, 116, F04025, 1914–1934. https://doi.org/10.1029/2011JF002026

Nittrouer, J. A., Shaw, J., Lamb, M. P., & Mohrig, D. (2012). Spatial and temporal trends for water-flow velocity and bed-material sediment transport in the lower Mississippi River. Geological Society of America Bulletin, 124(3–4), 400–414. https://doi.org/10.1130/B30497.1

Parker, G., Shimizu, Y., Wilkerson, G. V., Eke, E. C., Abad, J. D., Lauer, J. W., et al. (2011). A new framework for modeling the migration of meandering rivers. Earth Surface Processes and Landforms, 36(1), 70–86.

Smith, D. G., Hubbard, S., Leckie, D., & Fustic, M. (2009). Counter point bars in modern meandering rivers: Recognition of morphology, lithofacies and reservoir significance, examples from Peace River, AB, Canada. Sedimentology, 56(6), 1655–1669. https://doi.org/10.1111/j.1365-3091.2009.01050.x

Smith, V. B. (2012). Geomorphology of a coastal sand-bed river: Lower Trinity River, Texas (PhD dissertation).

van de Lageweg, W. I., van Dijk, W. M., Baar, A. W., Rutten, J., & Kleinhans, M. G. (2014). Bank pull or bar push: What drives scroll-bar formation in meandering rivers? Geology, 42(4), 319–322.

Chapter 4: Compensational river bank migration

Asahi, K., Shimizu, Y., Nelson, J., & Parker, G. (2013). Numerical simulation of river meandering with self-evolving banks. Journal of Geophysical Research: Earth Surface, 118(4), 2208-2229.

Brice, J.C., (1982). Stream channel stability assessment. No. FHWA/RD-82/021. United States. Federal Highway Administration.

Constantine, J. A., Dunne, T., Ahmed, J., Legleiter, C., & Lazarus, E. D. (2014). Sediment supply as a driver of river meandering and floodplain evolution in the Amazon Basin. Nature Geoscience, 7(12), 899.

Darby, S. E., Alabyan, A. M., & Van de Wiel, M. J. (2002). Numerical simulation of bank erosion and channel migration in meandering rivers. Water Resources Research, 38(9), 2-1.

Dietrich, W. E., & Smith, J. D., (1983). Influence of the point bar on flow through curved channels. Water Resources Research, 19(5), 1173-1192.

Eke, E., Parker, G., & Shimizu, Y. (2014). Numerical modeling of erosional and depositional bank processes in migrating river bends with self-formed width: Morphodynamics of bar push and bank pull. Journal of Geophysical Research: Earth Surface, 119(7), 1455-1483.

Gupta, A., and Fox H., (1974). "Effects of high-magnitude floods on channel form: a case study in Maryland Piedmont." Water Resources Research 10.3.

Howard, A.D., and Knutson T.R., (1984). "Sufficient conditions for river meandering: A simulation approach." Water Resources Research 20.11.

Lagasse, P.F., (2004). Handbook for predicting stream meander migration. No. 533. Transportation Research Board.

Mason, J., & Mohrig, D., (2018). Using time-lapse lidar to quantify river bend evolution on the meandering coastal Trinity River, Texas, USA. Journal of Geophysical Research: Earth Surface, 123(5), 1133-1144.

Pratt, V. (1987). Direct least-squares fitting of algebraic surfaces. In ACM SIGGRAPH 707 computer graphics (Vol. 21, No. 4, pp. 145-152). ACM.

Sun, T., Meakin, P., Jøssang, T., & Schwarz, K. (1996). A simulation model for meandering rivers. Water resources research, 32(9), 2937-2954.

van de Lageweg, W. I., van Dijk, W. M., Baar, A. W., Rutten, J., & Kleinhans, M. G (2012). Bank pull or bar push: What drives scroll-bar formation in meandering rivers?. Geology, 42(4), 319-322.

Chapter 5: Bedform groups during flood on the Trinity River—a new scale of self-organization in river bottom topography

Allen, J. R. (1963). The classification of cross-stratified units with notes on their origin. Sedimentology, 2(2), 93–114.

Ashmore, P. (1991). Channel morphology and bed load pulses in braided, gravel-bed streams. Geografiska Annaler: Series A, Physical Geography, 73(1), 37-52.

Benda, L., & Dunne, T. (1997). Stochastic forcing of sediment routing and storage in channel networks. Water Resources Research, 33(12), 2865-2880.

Bertoldi, W., Zanoni, L., & Tubino, M. (2010). Assessment of morphological changes induced by flow and flood pulses in a gravel bed braided river: The Tagliamento River (Italy). Geomorphology, 114(3), 348-360.

Bridge, J., & Demicco, R. (2008). Earth surface processes, landforms and sediment deposits (815 pp.). Cambridge, UK: Cambridge University Press.

Bradley, R. W., & Venditti, J. G. (2017). Reevaluating dune scaling relations. Earth-science reviews, 165, 356-376.

Costa, J. E., & O'Connor, J. E. (1995). Geomorphically effective floods. Natural and anthropogenic influences in fluvial geomorphology, 89, 45-56.

Cui, Y., Parker, G., Lisle, T. E., Gott, J., Hansler-Ball, M. E., Pizzuto, J. E., ... & Reed, J. M. (2003). Sediment pulses in mountain rivers: 1. Experiments. Water Resources Research, 39(9).

Dietrich, W. E., & Smith, J. D. (1983). Influence of the point bar on flow through curved channels. Water Resources Research, 19(5), 1173–1192.

Fernandes, A. M., Törnqvist, T. E., Straub, K. M., & Mohrig, D. (2016). Connecting the backwater hydraulics of coastal rivers to fluvio-deltaic sedimentology and stratigraphy. Geology, 44(12), 979–982.

Fernandez Luque, R., & Van Beek, R. (1976). Erosion and transport of bed-load sediment. Journal of hydraulic research, 14(2), 127-144.

Gilbert, G. K. (1917). Hydraulic-mining debris in the Sierra Nevada (No. 105). US Government Printing Office.

Griffiths, G. A. (1979). Recent sedimentation history of the Waimakariri River, New Zealand. Journal of Hydrology (New Zealand), 6-28.

Guy, H. P., Simons, D. B., & Richardson, E. V. (1966). Summary of alluvial channel data from flume experiments, 1956-61. US Government Printing Office.

Hoey, T. B., & Sutherland, A. J. (1991). Channel morphology and bedload pulses in braided rivers: a laboratory study. Earth Surface Processes and Landforms, 16(5), 447-462.

Hoey, T. (1992). Temporal variations in bedload transport rates and sediment storage in gravel-bed rivers. Progress in physical geography, 16(3), 319-338.

Hudson, P. F., & Kesel, R. H. (2000). Channel migration and meander-bend curvature in the lower Mississippi River prior to major human modification. Geology, 28(6), 531–534.

Iseya, F., & Ikeda, H. (1987). Pulsations in bedload transport rates induced by a longitudinal sediment sorting: A flume study using sand and gravel mixtures. Geografiska Annaler: Series A, Physical Geography, 69(1), 15-27.

Jerolmack, D. J., and D. Mohrig (2005), A unified model for subaqueous bed form dynamics, Water Resour. Res., 41.

Karim, F. (1995). Bed configuration and hydraulic resistance in alluvial-channel flows. Journal of Hydraulic Engineering, 121(1), 15-25.

Kostaschuk, R., & Villard, P. (1996). Flow and sediment transport over large subaqueous dunes: Fraser River, Canada. Sedimentology, 43(5), 849-863.

Lamb, M. P., Nittrouer, J. A., Mohrig, D., & Shaw, J. (2012). Backwater and river plume controls on scour upstream of river mouths: Implications for fluvio-deltaic morphodynamics. Journal of Geophysical Research, 117, F01002.

Lanzoni, S., Siviglia, A., Frascati, A., & Seminara, G. (2006). Long waves in erodible channels and morphodynamic influence. Water Resources Research, 42(6).

Lisle, T. E., Pizzuto, J. E., Ikeda, H., Iseya, F., & Kodama, Y. (1997). Evolution of a sediment wave in an experimental channel. Water Resources Research, 33(8), 1971-1981.

Madej, M. A., & Ozaki, V. (1996). Channel response to sediment wave propagation and movement, Redwood Creek, California, USA. Earth Surface Processes and Landforms, 21(10), 911-927.

Mason, J., & Mohrig, D. (2018). Using time-lapse lidar to quantify river bend evolution on the meandering coastal Trinity River, Texas, USA. Journal of Geophysical Research: Earth Surface, 123(5), 1133-1144.

Meade, R. H. (1985). Wavelike movement of bedload sediment, East Fork River, Wyoming. Environmental Geology and Water Sciences, 7(4), 215-225.

Mohrig, D., & Smith, J. D. (1996). Predicting the migration rates of subaqueous dunes. Water Resources Research, 32(10), 3207-3217.

Nicholas, A. P., Ashworth, P. J., Kirkby, M. J., Macklin, M. G., & Murray, T. (1995). Sediment slugs: large-scale fluctuations in fluvial sediment transport rates and storage volumes. Progress in physical geography, 19(4), 500-519.

Nittrouer, J. A., Mohrig, D., & Allison, M. (2011). Punctuated sand transport in the lowermost Mississippi River. *Journal of Geophysical Research*, *116*, F04025, 1914–1934.

Nittrouer, J. A., Shaw, J., Lamb, M. P., & Mohrig, D. (2012). Spatial and temporal trends for water-flow velocity and bed-material sediment transport in the lower Mississippi River. *Geological Society of America Bulletin*, *124*(3–4), 400–414.

Parker, G., Paola, C., & Leclair, S. (2000). Probabilistic Exner sediment continuity equation for mixtures with no active layer. Journal of Hydraulic Engineering, 126(11), 818-826.

Shaw, J. B., & Mohrig, D. (2014). The importance of erosion in distributary channel network growth, Wax Lake Delta, Louisiana, USA. Geology, 42(1), 31-34.

Simons, D. B., Richardson, E. V., & Nordin, C. F. (1965). Bedload equation for ripples and dunes. US Government Printing Office.

Smith, V. B. (2012). Geomorphology of a coastal sand-bed river: Lower Trinity River, Texas (PhD dissertation).

Southard, J. B. (1971). Representation of bed configurations in depth-velocity-size diagrams. Journal of Sedimentary Research, 41(4), 903-915.

Stein, R. A. (1965). Laboratory studies of total load and apparent bed load. Journal of Geophysical Research, 70(8), 1831-1842.

Venditti, J. G., Church, M., & Bennett, S. J. (2005). On the transition between 2D and 3D dunes. Sedimentology, 52(6), 1343-1359.

Venditti, J. G., Lin, C. Y. M., & Kazemi, M. (2016). Variability in bedform morphology and kinematics with transport stage. Sedimentology, 63(4), 1017-1040.

Zinger, J. A., Rhoads, B. L., & Best, J. L. (2011). Extreme sediment pulses generated by bend cutoffs along a large meandering river. Nature Geoscience, 4(10), 675.